TEXAS INSTRUMENTS
INCORPORATED

HEAT STERILIZABLE AND IMPACT RESISTANT Ni-Cd BATTERY DEVELOPMENT

SECTION II.
TASK X. BATTERY ENGINEERING DEVELOPMENT

Jet Propulsion Laboratory
Contract No. 951972, Modification No. 14

Final Report, Volume II
January 1969 -- January 1970

AUTHOR: E. J. Rubin

PROJECT MANAGER: P. V. Popat

TEXAS INSTRUMENTS INC.
Research and Development Laboratories
Attleboro, Massachusetts

TI Report No. 51-70-8

This work was performed for the Jet Propulsion Laboratory, California Institute of Technology, sponsored by the National Aeronautics and Space Administration under Contract NAS-7-100; Task Order No. RD-26.

NOTICE

This report was prepared as an account of government-sponsored work. Neither the United States, nor the National Aeronautics and Space Administration (NASA), nor any person acting on behalf of NASA:

(a) makes warranty of representation, expressed or implied with respect to the accuracy, completeness, or usefulness of the information contained in this report, or that the use of any information, apparatus, method, or process disclosed in this report may not infringe privately owned rights;

(b) assumes any liabilities with respect to the use of, or for damages resulting from the use of any information, apparatus, method or process disclosed in this report.

As used above, "person acting on behalf of NASA" includes any employees or contractor of NASA, or employee of such contractor to the extent that such contractor prepares, disseminates, or provides access to any information pursuant to his employment with such contractor.

Requests for copies of this report should be referred to:

National Aeronautics and Space Administration
Office of Scientific and Technical Information
Attention: AFSS-A

SECTION II.

ENGINEERING DESIGN AND EVALUATION

TABLE OF CONTENTS

SECTION II.

ENGINEERING DESIGN AND EVALUATION

1. Introduction

The engineering effort in this program was concerned with the design, construction and testing of heat-sterilizable nickel-cadmium cells. This investigation involved the study of higher energy density plate materials and evaluation of hermetic seals, other structural components and fabrication techniques. The stability of these components in the cells' internal environment and their effects on cell performance were used as measurement criteria. Particular attention and effort were devoted to seal evaluation.

Other engineering tasks included manufacture and evaluation of sintered nickel plaque for use as high energy density plates capable of delivering a capacity density of 11 ampere hours per cubic inch.

2. Hermetic Seal Development

Three seal designs were used in the development and testing of the heat-sterilizable nickel-cadmium cells. They were: (1) glass-to-metal; (2) ceramic-to-metal; and (3) plastic-to-metal (crimped polymeric seal). This phase of the engineering program was primarily concerned with the development of the crimped polymeric seal. However, the other seals mentioned

were used in the program and are therefore discussed.

The glass-to-metal seals used were of the compression type where the fused glass insulator is held under compression by a metal sleeve. Since the glass will react with KOH in the cell, the portion of the seal exposed to the cell interior must be protected from corrosion. This was accomplished by using an impervious KEL-F film. Since the glass insulator is brittle, it is not recommended for general hardware use but was used successfully as a research vehicle.

The ceramic-to-metal seals were also used successfully on heat-sterilizable nickel-cadmium cells. These seals are commonly used on aerospace flight hardware and are composed of a high alumina body, metallized and brazed to a "strain relief collar." The hermeticity of these seals was maintained during and after heat sterilization.

The performance of glass-to-metal and ceramic-to-metal seals was shown to be acceptable. Both seal designs, however, have disadvantages. The sensitivity of glass to attack by alkaline solutions and its relative fragility preclude its use for long-range missions especially those involving heat sterilization and shock and vibration spectra associated with rocket launching and pyrotechnic firing. Ceramic-to-metal seals, however, resist these conditions. Under the original goals of this contract, cells capable of withstanding shocks

up to 4000 g were required. It was believed that the ceramic-to-metal seals commonly used for space missions would not survive this shock level (impact test results for cell components are reported in Volume III, Section III). In addition, the common types of brazing alloys used for the ceramic-to-metal and metal-to-metal joints of these seals are subject to a slow attack by alkaline solutions. There have been reports of seal failure after three to five years of continuous testing. Based on these conditions the plastic-to-metal seal was chosen for evaluation and development. Its main advantages are lack of brittle members and ability to withstand prolonged exposure to alkaline solutions.

The seal is constructed using a center conductor which is insulated from a thick outer metal sleeve by chemically-resistant, high-dielectric, polymeric materials. The outer metal sleeve is threaded along its inside diameter with a thread size and form which matches the thread on the outside diameter of the polymeric insulator. The center conductor is inserted in a smooth hole in the center of the polymeric insulator. The seals can then be produced by either extruding or crimping the assembly. Both of these methods were investigated. Initially, several seals were fabricated by assembling the components and then drawing the assemblies through various dies.

These first samples consisted of a 1/4 inch outside diameter

sleeve with a 5/32 P-32 BSW thread, a matching KEL-F 300 polymer insulator and a 1/16 inch diameter conductor pin. The seals were completed by drawing the assemblies through various dies as shown in Table II-1. The seals were then tested for leaks using an NCR 925 mass spectrometer.

The seven polymeric compression seal samples were subjected to heat sterilization at 135°C for 72 hours, then retested on the NCR 925 mass spectrometer. These data are also shown in Table II-1. All samples tested exhibited an increase in leak rate after heat sterilization. Three of the six initially acceptable seals tested became gross leakers and were considered failures.

Due to the nature of the thread form and the less than optimum machinability of the KEL-F material the match between the threads on these initial samples was suspected to be imperfect. An x-ray examination of these seals indicated an axial distortion (axis of center conductor not parallel with axis of outer sleeve) caused by the extrusion method of seal manufacture. Since the insulator was transparent to x-ray the thread mating could not be examined in this manner. Therefore three of the seven seals were encapsulated in a resin and metallurgically sectioned for further study.

Microscopic examination of the seals indicated that the thread form of the polymeric insulator was less than ideal. This

allowed a helical leak path to develop which was aggravated by the expansion and contraction of the seal members during heat sterilization. Since the machinability of the polymeric insulator is poor especially when fabricating small components and since larger conductors are required to withstand large currents from the 25 ampere hour cell, the next group of seals manufactured had center conductors of 0.187" thick and correspondingly larger plastic insulators.

In addition to the problem of axial distortion, cell top assembly methods (i.e. attachment of seal assembly to cell top) favored the use of an "in situ" radial crimping method of seal fabrication. To use this fabrication technique, the outer sleeve is welded to the cell top; then the seal is assembled and crimped to a split die which reduces the seal diameter uniformity.

A number of these seals were manufactured and tested. These data are presented in Table II-2. Prior to heat sterilization the seals were leak-tight as noted. After heat sterlization (135°C for 72 hours) all seals were gross leakers with the exception of seal Number 4.

Examination of these seals (including cross-sectioning) reveals an extrusion of the KEL-F insulator leaving a leak path along the thread as shown in Figure II-A. Four of these leakers were recrimped on dies that were ground an additional 0.010".

This allowed additional reduction of the seal diameter and increased hydrostatic pressure which should improve the seal. One of these assemblies was resealed during this operation and showed a leak rate in the same order of magnitude ($1x10^{-8}$ std cc He/sec/atm) as before. The other three assemblies did not reseal to the same degree; however, their leak rate was measurably reduced. These tests indicate that the thread form of the KEL-F is not destroyed during the heat sterilization process and loss of hermeticity is caused by the flow of material out of the seal area. This flow decreases the hydrostatic pressures produced during the crimping process and the seal loses its hermeticity.

To determine if this effect could be eliminated or reduced by prior heat treatment of the polymer, these same assemblies were heat treated for a second time. Again the seals became leakers. It was therefore surmised that the flow of KEL-F material is caused by the heating during sterilization which softens the material and is aided by the hydrostatic forces generated within the seal during the radial crimping process.

The next seal design provided a tapered top to restrict the movement of KEL-F out of the seal during the heat sterilization process. Ten seal assemblies of this type were manufactured. A photo of the cross-section of one of these seals is shown in Figure II-B. Prior to heat sterilization the seals had leak rates, as before, in the 10^{-8} std cc He/sec/atm range.

Several of these seals were welded in conventional "D" size (4 AH cylindrical) cells and placed on charge. These cells were overcharged for a period of six months. During this time the seals were checked for leakage by visually observing the seal for carbonate deposits and using the phenolphthalein test. No leaks were observed.

Six of these seal assemblies that, were crimped on the ends as well as along the axis, were found to be gross leakers (e.g. pump down to 10μ only) after heat sterilization. Visual examination of the assemblies revealed that the end crimp retention design was only partially effective. A cross-sectioned view of a seal (shown in Figure II-B) showed a narrow but full-length leak path along the threaded portion of the seal.

Other design changes were then made. These included: (1) a reduction in the cross-section of the polymeric insulator designed to reduce material flow; (2) a rolled outer sleeve lip designed to further restrict polymer flow out of the seal area and (3) a blind thread at the bottom of the outer sleeve to restrict polymer flow in that direction. A schematic diagram of this seal is shown in Figure II-C. Also included in this new design was the use of polypropylene as an alternate material of construction.

Eight of these seals were fabricated and tested. There were

no detectable leaks down to 1 x 10^{-10} std cc He/sec/atm, the limit of the mass spectrometer device used. After heat sterilization at 135°C, all seals leaked to the extent that the vacuum system in the NCR 925 could only maintain a pressure of 25 μ. Examination of the seals showed that in spite of the mechanical design and material design changes the polymers used still flow sufficiently during heat sterilization to cause the seals to leak.

This study has shown that hermetic plastic-to-metal seals can be manufactured and used as isolated feedthroughs for nickel-cadmium cells. Further development is indicated, however, for seals used in applications requiring heat-sterilizable components. In spite of the mechanical design changes, most seals manufactured did not survive heat sterilization. It appears that the materials used and tested have too low a glass transition temperature and therefore flow at the sterilization temperature of 135°C. It is recommended that other materials be selected based on chemical stability and glass transition temperature in future investigations.

3. Design, Fabrication and Testing of Prismatic Cells

Two cell designs were evaluated during this contract, namely, the prismatic and cylindrical cells. Each design has its particular advantages and disadvantages which are described and evaluated. The two cell designs are reported separately.

The cell plates were comprised of a sintered nickel plaque supported by nickel wire mesh and impregnated with nickel or cadmium hydroxides. To minimize the possibility of exposed wires or loose active materials the edges of all electrodes were coined. Also, the plate corners were rounded to further reduce the chance of separator penetration caused by sharp edges. The tabs used were two 1/2 inch x 0.005 inch strips welded to both sides of the plates directly to the nickel wire substrate.

Initially the collection and heliarc welding of the tabs into comb-like collectors resulted in heat flowing into the plates via the tabs. This caused oxidation of the plates and melting of the separator in spite of the use of rather intricate water-cooled chills. A redesign of the comb and the use of resistance welding minimized this difficulty. A sample of the weldment achieved using resistance welding was subjected to an oxidizing environment in KOH. There was no evidence of degradation of the weld after sixty days of testing. Microscopic inspection of cross-section samples revealed that each tab had melted during the welding operation resulting in a metallurgical bond. A typical cross-section is shown in Figure II-D.

The cells were assembled using the conventional interleaving technique. The separator-plate package was assembled prior to tab collection and welding thus avoiding any repeated

bending and forming of tabs. This technique also allowed accurate alignment of the plates thereby minimizing nonuniformity in cell core packaging.

To establish a cell design and evaluate the effects of heat sterilization on these larger, 25 ampere hour cells, a number of model cells were constructed and tested. The performance data of these cells are graphically presented in Figures II-E through II-G with design characteristics presented in Table II-3.

The performance of the cell containing polyamide separator is shown in Figure II-E. This cell was used as a control standard to which other cells are compared. Another model of this cell design was built which eventually became negative limited on charge after a few test cycles. This cell was considered atypical since no other cells of this type behaved similarly. At the 10 ampere discharge rate at ~70°F the cell has a specific energy of 15.5 watt-hours per pound.

The performance data of non-heat-sterilized cells containing polypropylene separator are shown in Figure II-F. The delivered capacity is similar to cells containing polyamide separator and did not show any appreciable capacity loss with continued cycling. The end-of-charge pressure was somewhat higher than cells with polyamide separator and reflected the smaller recombination rate constant associated with the

polypropylene separator. The slightly lower discharge voltage believed caused by an increase in cell impedence ascribed to the separator resulted in a lower specific energy of 14.5 watt-hours per pound.

The performance data of the heat-sterilized cell containing polypropylene separator are shown in Figure II-G. Preheat-sterilization data were comparable to the non-heat-sterilized cell excepting the cell pressure. This was caused by an excessive electrolyte fill level. Post heat sterilization was characterized by a decrease in cell capacity and an increase in cell end-of-charge voltage.

The small loss in cell capacity was not clearly understood at that time. However, experimental data obtained since that time show that some 4 AH prismatic cells become negative-limited during discharge after being heat sterilized. Other data show that a considerable quantity of oxygen gas is evolved during heat sterilization. It is hypothesized that the evolved oxygen gas reacts with the residual cadmium metal, thus removing the "charge adjust" or free cadmium metal used to assure positive limitation during discharge. The effect of negative limitation during discharge is to reduce the cell capacity deliverable to 1.00 volts.

The increase in end-of-charge voltage of the cell is associated withthe positive electrode and is not an indicator of

hydrogen evolution. This was verified by analyzing the cell atmosphere with a gas chromatograph. After the first post sterilization charge cycle, these cells contained approximately two mole percent hydrogen. Similar analyses performed after subsequent cycles showed no change in the hydrogen content.

Based on the data of the previously discussed cells, a number of prismatic cells were built. The design characteristics of these cells are presented in Table II-4. These cells served as a means of evaluating the prismatic cell design as well as being used for the long-range testing program described in a subsequent section.

A total of twenty prismatic cells were built and tested. The test results from ten of these cells are plotted in Figure II-H. Preheat sterilization data were comparable to model cell performance with the cell delivering, at the $^{C}/10$ discharge rate, 16 watt-hours per pound. The atypical behavior of the cells after heat sterilization resulted from high rate cycling performed in agreement with JPL, NASA Langley and Martin-Marietta. This testing included discharging these cells as rapidly as the 4C rate to a 1.00 volt per cell cut-off point. This test routine resulted in an incomplete cell discharge and therefore a greater degree of overcharge. Combined with a C/5 recharge (6 amperes for eight hours), higher end-of-charge voltages and pressures resulted.

Subsequent post sterilization data (after high rate cycling) were as expected. The cells exhibited a loss in capacity (~ 2-3 ampere hours) and a higher end-of-charge voltage. Similar results were obtained from the other ten cells tested. These cells, however, were not subjected to repetitive post sterilization cycling. At the $^{C}/10$ discharge rate the cells delivered 13 watt-hours per pound. The entire group of twenty cells was then used for the long-range testing program.

4. Design, Fabrication and Testing of Cylindrical Cells

Large cylindrical cells are not found in common usage in aerospace applications. The reasons though are not clear but those commonly mentioned by workers in the field are difficulty in producing a cylindrical core, cracking and spalling of the active materials and supporting plaque and need for unconventional battery packaging. A careful evaluation of these "difficulties" shows that they can be overcome.

To establish the design for a 25 ampere-hour, heat-sterilizable cylindrical cell a number of model cells were constructed. The basic cell design includes four negative and three positive plates interleaved with separator and rolled in a "jelly roll" or "Swiss roll" to form a right circular cylinder. The advantages of this design include: (1) the use of fewer and larger electrodes which minimizes "edges" and their characteristic

problem of loose wires or burrs; (2) the spiral design of the cell core in combination with Texas Instruments' plate (supporting substrate is on one side of the plaque which is kept on the outside of "jelly rolls") which maintains a compressive force on the active material and therefore reduces the tendency for active material cracking and spalling; (3) a high (>1.5) negative to positive ratio without the use of heavily loaded negative plates (the four negative plates and three positive plates provide at least a 1.3 geometric ratio); and (4) no need for cell or battery restraining plates.

The engineering design effort was concerned with evaluation of selected plate materials and electrolyte levels. The effects of core concentricity and tab size and location were then determined. Initial models were fabricated with polyamide separator. The data shown in Figure II-I and Figure II-J is representative of this cell type. After 110 deep discharge cycles the cell operating parameters remained quite stable. There were fluctuations in capacity; however they were a result of deviations from the indicated cycling regime as well as ambient temperature excursions. The middle of discharge voltage was nearly fifty millivolts lower than normal and was caused by a high cell resistance. The tabbing arrangement, which was an expedient to allow evaluation of electrode materials, consisted of one 1/4" tab per plate and was the source of the high internal impedance. The specific energy exhibited

by the cell was 14 watt-hours per pound. This value improved when the tabbing arrangement which will be discussed later was redesigned.

Concurrently, cells of similar design with polypropylene separator were built and evaluated. The performance data from cells of this design are presented in Figure II-K. They show depressed discharge voltage which is a result of a high cell impedance caused by the same tabbing arrangement previously described. The lower cell capacity was believed caused by the higher cell impedance and the eccentricity of the cell core. The higher cell impedance reduced the capacity deliverable to 1.00 volts which may in part result from the core eccentricity which causes uneven compression and nonuniform electrolyte distribution.

The performance of the previously discussed cells with polyamide or polypropylene separators, proved the feasibility of the cylindrical design although there was need for improvement. Firstly, the current collection was improved by changing to four 1/2 inch by 0.005 inch nickel tabs per plate. Also, the concentricity of the cell core was improved. Performance of cells incorporating these changes are shown in Figures II-L and II-M. The performance of the cell with polyamide separator is characterized by an improved discharge voltage profile and a stable capacity. The end-of-charge pressure is

slightly higher than expected and may have resulted from a high electrolyte fill level. (The increased concentricity of the cell core may reduce the electrolyte fill level due to a more uniform compression of the separator). The specific energy of the cell increased to 15.5 watt-hours per pound.

Preheat sterilization performance of the cells with polypropylene separator included an improved discharge profile. Cell capacity was slightly lower than cells with polyamide separator. However, this has been a consistent effect exhibited by cells with polypropylene separator. The post heat sterilization cell behavior is characterized by an increased end-of-charge voltage, a similar effect exhibited by heat-sterilized prismatic cells. There were no other observed effects resulting from the heat sterilization process. After eighty deep-discharge cycles the capacity remained unchanged. The specific energy was 14.5 watt-hours per pound.

Based on the behavior of the previously discussed cells a group of twenty cylindrical cells were built. The design characteristics are presented in Table II-5. Also, the core concentricity was improved by altering the mandrel used in shaping the "jelly roll." As a result cell cores with a total indicator reading of less than 0.030 inches were produced. These cells were used to evaluate the performance characteristics of 25 AH heat-sterilizable, cylindrical cells as well as being used in the long-range testing program described in a subsequent section.

The test results obtained from ten of these cells are shown in Figure II-N. The preheat sterilization cell performance is comparable to data obtained from the model cell testing. The cell behavior immediately after heat sterilization resulted from the previously mentioned high-rate testing. Data generated during subsequent testing showed little or no change in cell pressure, discharge voltage and capacity. As expected, the end-of-charge voltage rose after heat sterilization and as usual was not associated with hydrogen evoluation. At the C/10 discharge rate the cells delivered 14 watt-hours per pound. The entire group of twenty cells was then used for the long-range testing program.

5. Design Review, Analysis and Fabrication of Interim and Final Design Cells

During July 1969, a design review meeting was held with JPL representatives to discuss the various design parameters investigated and their effect on cell performance. It was determined that the characteristics of cylindrical and prismatic cells presented in Tables II-4 and II-5 represented satisfactory designs. The attributes of the prismatic vs. the cylindrical designs were discussed. The design parameters are presented in Table II-6.

One of the basic differences between the behavior of the two designs is that the cylindrical cells do not exhibit any appreciable capacity loss after heat sterilization. Experimental

data obtained while performing the electrochemical investigations show that 4 AH prismatic cells are negative limited during discharge after being subjected to a heat sterilization cycle. Other data indicate that a considerable quantity of oxygen gas is evolved during heat sterilization. It is hypothesized that this evolved oxygen reacts with the residual cadmium thus removing the "charge adjust" or free cadmium used to assure positive limitation during discharge. Since the cylindrical cell has a larger amount of free cadmium metal compared to the prismatic cell, which results from a larger negative to positive ratio (i.e. 1.65 vs 1.40), all the free cadmium metal is not consumed. Therefore, the cylindrical cell remains positive limited after sterilization. To increase the negative to positive ratio of the prismatic cells to those higher levels to allow for more free cadmium metal would require the use of more heavily loaded negative plates. Other studies show that cadmium plates loaded to the level necessary to attain this ratio do not perform well electrochemically. They show higher polarization during charge and discharge, and lower efficiency of active material utilization.

Based on these considerations as well as those presented in Table II-6, the cylindrical cell design was selected for the interim as well as final design.

The interim cell design characteristics are shown in Table II-7. These cells were built and tested for capacity prior to heat sterilization. These test data are presented in Table II-8. The final cell design was similar to the interim cell design excepting the seals which were ceramic-to-metal in place of the glass-to-metal seals. These cells were also tested prior to heat sterilization. Typical test data are presented in Table II-9.

Neither these cells nor the interim model cells were heat sterilized or tested further prior to termination of this contract.

6. Long-Range Testing Program

It was the purpose of this program to evaluate the proper storage methods (wet stand) and cycling conditions to allow power system designers to more accurately determine the capacity, durability and other physical and electrical parameters of heat-sterilizable, nickel-cadmium systems. In addition, the data provided by this test program would allow for a proper selection of storage (wet stand) conditions consistent with mission requirements.

The test conditions are outlined in Table II-10. Under Part A, the performance of cells for various duty cycles and temperatures was determined. In a parallel test, the various charge maintenance regimes were tested in Part B to determine

the optimum conditions for long-stand times. These various conditions for wet stand were selected since they will affect the chemistry and morphology of the cell as previously described. It was planned that in Part C the cells tested under Part B would be subjected to the cycling regime selected as optimum under Part A of this testing program. However, due to the premature termination of this phase of the contract, the latter part of the program (i.e. Part C) was not undertaken.

Cell parameters listed below were measured and tabulated daily for the first 14 days of testing then at 7 day intervals throughout the testing program.

1. End-of-Charge Voltage;
2. End-of-Charge Resistance;
3. End-of-Charge Pressure;
4. Cell Capacity;
5. End-of-Discharge Voltage;
6. End-of-Discharge Resistance;
7. End-of-Discharge Pressure.

All tests were conducted in temperature controlled environmental chambers with accuracies of $\pm 1^{\circ}F$. Charging and discharging were performed using constant current power supplies except as noted in Table II-10.

The cells used for this program were the initial forty cells constructed under Task X of this contract. Twenty of these

cells were the prismatic configuration and twenty the cylindrical configuration, both rated to deliver 25 ampere-hours at the C/2 rate after a 16-hour charge at the 10-hour rate. These cells were characterized for parameters listed above, as well as discharge profile (i.e. cell voltage at 25, 50, 75% depth-of-discharge prior to and after heat sterilization at 135°F for 72 hours). Prismatic cells were constrained by plates during the testing period to prevent cell case distortion due to unusual pressures which exceed ambient pressure. Cylindrical cells were not restrained.

Cells were cycled, as outlined, for 24 to 30 cycles at which time the testing was stopped due to termination of this phase of the contract. During this time there were no cell failures, although some erratic results are evident; however, these are a result of test equipment and/or power failures. The test outline and the cycling data gathered are presented in Appendix II-B. Due to the short duration of the testing, sufficient data for factorial analysis could not be collected. Also, the effect of the various charge maintenance regimes could not be evaluated.

7. Fabrication and Evaluation of High Energy Density Plaque and Plates

Another goal of this contractual effort was to build heat-sterilizable, nickel-cadmium cells with specific energies approaching 20 watt-hours per pound. This task was approached

by providing a selected series of plaques and plates of varied thicknesses and porosities and characterizing them. Subsequently, a number of these plates were chosen for study in a factorial designed experiment. The effects of porosity, pore ratio and electrolyte quantity on plate efficiency (specific energy) were measured.

Thus, the experimental work was divided into two phases. Initially, a series of plaques were prepared. During the first plaque run, sinter weight as well as gauge were controlled in order to maintain favorable porosity and pore size distribution. It was expected that by maintaining a favorable pore size distribution, and experimenting with the pore structure produced, a higher electrochemical loading might be obtained.

Table II-11 identifies the plaque produced and the physical attributes obtained.

During the production of plaque, sufficient material is applied to the screen to produce a certain gauge at a given temperature, while still maintaining constant porosity and pore size.

If insufficient material is applied, the correct gauge cannot be achieved. If excess material is applied it is possible to achieve the desired gauge, through compaction. However, total porosity decreases. The plaque produced for these experiments is considered the optimum with respect to the gauge, sinter weight and porosity interrelationship. Plaque gauge was not

controlled by rolling or other compaction techniques. These data are presented in Figure II-O.

Of the plaque identified in Table II-11, those lots which are asterisked were selected for impregnation with active material.

The long holding tabs used on the plates restricted the growth and movement of the plates during impregnation and conversion, resulting in distorted and buckled plates. Many were damaged to such an extent that they were discarded. Due to the malformed condition of the plates from the first positive impregnation run, no formation was performed on these plates. Only analytical data and certain physical attributes were determined and are presented in Table II-12.

Using identical plaque material, the impregnation was repeated, this time using shorter holding tabs. Impregnation parameters remained the same except that metal ion concentration in the impregnation bath was reduced. No problems were experienced, no plate distortion occurred. All plates were available for analysis and subsequent formation. The plates from positive Impregnation II were formed, in groups of three. Each three-plate group represented a particular plaque type and gauge and a certain impregnation routine. To determine the capacity of the formed plates, the following test cycle was chosen:

Charge -- 3-hour rate for 6 hours (100% overcharge).

Discharge -- $^{C}/_{2}$ rate to the knee of the discharge curve.

Flooded capacity data are tabulated in Table II-13.

With very few exceptions the electrochemical efficiency of the plates exceeded 90%.

Plates exceeding .035" in gauge warped during formation and cracked under restraint.

An analysis of the impregnation data shows a direct relationship of gauge to weight of active material introduced into the pore structure by impregnation and conversion.

Since the relationship is a linear function, it is a useful tool for anticipating the chemical loading during impregnation or for determining the process parameter changes required to produce a certain plate loading and/or for determining the plaque attributes required to achieve a certain plate loading.

The relationship of active material to gauge for various types of plaque material is illustrated in Figures II-P, II-Q, II-R, and II-S.

The same relationship exists with respect to flooded delivered capacity vs gauge.

Figure II-T exhibits corrosion of plaque produced at various sintering temperatures, during 3, 4 and 5 cycles of positive impregnation.

From the data accumulated, the following facts are evident

concerning corrosion of the plaque during the impregnation process.

1. More corrosion occurs with low-temperature, sintered plaque;
2. Corrosion increases with the number of impregnation cycles;
3. The higher the gauge, the more corrosion.

Negative Plate Manufacture -- In order to provide matching negative plate for the high capacity positive previously impregnated, high capacity negative plates were impregnated. The plaque used for this impregnation was identical to that used for the high capacity positive. Three sample plates from each plaque lot were removed from the impregnation and analyzed prior to formation. The appearance of all the plates after impregnation was excellent. No distortion, shedding or cracking was apparent.

Table II-14 lists the analytical data for the impregnated negative material.

The plates from the negative impregnation were formed in groups of three. Each group represented a given plaque type, plaque gauge and impregnation routine. Plate capacities were determined in the flooded condition based on the following cycle:

Charge: $C/3$ rate for 6 hours (100% overcharge).

Discharge: $C/2$ rate to the knee of the discharge curve.

where C is the capacity of the plates based on chemical analysis. These data are also presented in Table II-14.

Analysis of Negative Impregnation Results -- Unlike the positive impregnation, the negative data does not exhibit the straight line relationship between gauge and active material pickup. The straight line relationship exists up to a gauge of .035". At gauges greater than .035" there is a tapering off of active material pickup.

This phenomenon might be attributed to any or a combination of the following:

1. Higher gauge plates require more rinsing to effectively remove caustic residues from previous impregnation and conversion cycles.
2. Higher gauge plates require more nitrate diffusion cycles to give efficient loading.
3. Higher gauge plates require longer conversion time.

From the data presented in this section it is apparent that plate materials having capacity densities greater than nine ampere-hours per cubic inch are possible.

Since cell components have various weights, the specific energy of cell is a function of its

capacity. Using data from present cell designs and previously discussed plate capacities the specific energies described in Figure II-U are achievable. The plates having a higher energy density are thicker than can presently be accommodated in the cylindrical design, therefore, prismatic designs are presented.

Although prepared in a controlled systematic manner the loading capabilities (chemical capacity) of the plaques could not be predicted in advance. Also, the behavior of the plates under varied conditions of electrolyte starvation and operating current density could not be predicted. Qualitatively, one can surmise more heavily loaded plates may not perform efficiently due to filling of pores leading to increased concentration polarization.

Obviously, the size and number of pores and the electrolyte level will also affect the ability of plaque and subsequently plate materials to perform. Therefore, a factorial experiment was designed to specifically measure the effect of plaque porosity, pore ratio*, electrolyte quantity, and duty cycle. The plaques prepared were divided by median values into ranges of porosity and pore ratios*, and classified into these four catagories:

1. High porosity, high pore ratio;

---

* Ratio = $\frac{\text{Pore Volume of 10}\mu\text{ to 15}\mu\text{ size pores}}{\text{Pore Volume of 15}\mu\text{ to 20}\mu\text{ size pores}}$

2. High porosity, low pore ratio;
3. Low porosity, high pore ratio;
4. Low porosity, low pore ratio.

These data are tabulated in Table II-15. The designation of low and high indicates lower than or higher than median values.

Selections of plate materials were made within each pore size distribution group on the basis of the availability of the plate specimen, the plate's suitability as a typical example of its group with respect to its porosity and pore ratio values, and the structural integrity of the plate material. The properties of these materials are shown in Table II-16.

A test program was devised to subject both positively and negatively limited sealed cells to a number of charge and discharge rates. Since the results of these tests were to be used in a factorial analysis, the factors evaluated for their effect on sealed cell performance were determined in advance of the test. These factors are porosity, pore size ratio, and electrolyte fill (Table II-V).

Uniformity of critical cell construction parameters such as plate separation and electrolyte fill level is an assumption in attributing validity to the factorial analysis.

The positive limited cells employed one NiOOH and four Cd plates to maintain a minimum 2.5 to 1 ratio of negative to

positive flooded capacity. Layers of Pellon were interleaved to separate the plates within the nickel steel clamping fixture of the test cell. The thickness of each plate was determined to an accuracy of $^{+.001"}_{-0}$ and the package of plates and separator was clamped to the degree necessary to compress the pellon layers to .005 inches. The thickness of this clamped package was adjusted by screws to within $^{+0}_{-.001"}$ of the pre-determined value. Negative limited cells used one Cd electrode and two NiOOH electrodes with interleaved Pellon layers. Similar clamping procedures were followed.

One hundred percent saturation levels were determined for each positive and negative limited cell. The figures obtained were used to calculate 60, 70 and 80% fill levels for each test cell. Electrolyte was introduced into the cells within 3% of the pre-determined value.

After their test program was completed, the 60% saturated cells of both the limited positive and negative limited types were refilled to the 70% level and the 80% level and run through an identical test program.

The efficiency graphs (Figures II-W, II-X, II-Y) indicate that the best positive plate performance is achieved at the 80% electrolyte fill level as expected. The low porosity, low pore ratio plaque delivered between 70 and 80% efficiency at C/2 discharge and 50% efficiency at 3C discharge. Note

the performance change of the high porosity, low pore ratio plaque at the 80% fill level as discharge rates increased to 3C and decreased to C/2 at the end of the test series. Its efficiency (~70%) is among the lowest of the four samples at the C/2 rate, but it attains the highest efficiency (53%) at the 3C rate. This high efficiency at high discharge rate also appears in the 70% fill level test.

At the 60% fill level the low porosity, low pore ratio plaque is the best performer at all discharge rates.

An examination of the negative limited cell efficiencies indicates that the high performance plaques have high porosity with low pore ratio and low porosity with high pore ratio respectively. This implies that some factor other than porosity and pore ratio favors high efficiency in negative plate.

Results of the factorial analysis for both positive and negative plate indicate that the effect of electrolyte fill level is most significant while the pore size distribution of the plaque prior to impregnation is of lesser significance. Of least statistical significance is the plaque porosity prior to impregnation within the range studied. The higher performance obtained by lighter loading may indicate that active material loading is a limiting factor to negative plate efficiency. Therefore, an evaluation of the porosity and pore size distribution of plate material after impregnation as well

as loading level may yield more useful data.

Internal resistance in the positive limited cells declined by 30% as the electrolyte fill level was increased from 60 to 80%. Significantly, the positive limited cell with the low porosity and low pore ratio showed internal resistances 10 to 20% less than the other cells at all electrolyte fill levels.

Internal resistances in the negative limited fluctuated greatly with no noticeable trends except the gradual increase in resistance of each cell as the number of cycles increased.

Cell pressures in the 80% fill level, positive limited condition reached a high of 56 psi for the cell corresponding to low porosity, low pore ratio plaque. Pressures for the other cells at this fill level were generally half this value.

A considerable amount of further development and optimization work remains to be performed before these heavily loaded, positive and negative plates can be used in sealed, heat-sterilizable cells.

APPENDIX TO SECTION II

ENGINEERING DESIGN AND EVALUATION

Contract Number 951972

Performed by Texas Instruments Incorporated

APPENDIX II-A

LIST OF TABLES IN APPENDIX II-A

TABLE II-1

CHARACTERISTICS OF DRAWN POLYMERIC SEALS

Sample No.	Leak Rate (std cc He/sec/atm) As Assembled	Leak Rate (std cc He/sec/atm) After 72 Hrs @ 135°C	Assembly Method
1a	25μ (gross leaker)	160μ *	Drawn through a 0.246" die
1b	2.0×10^{-8}	2μ *	Drawn through a 0.246" die
1c	1.5×10^{-8}	1.8×10^{-6}	Drawn through a 0.246" die
1d	0.7×10^{-8}	5μ *	Drawn through a 0.246" die
2	0.4×10^{-8}	5μ *	Drawn through a tapered die (0.250"/0.236")
3	1.0×10^{-8}	3.8×10^{-6}	Drawn through a 0.246" die
4	0.8×10^{-8}	6.0×10^{-6}	Drawn through 3 dies progressively (0.246", 0.242", 0.238")

* During the pump-down operation this minimum pressure was achieved, after which the safety switches on the mass spectrometer leak detector were automatically tripped indicating a large leak had developed.

TABLE II-2

CHARACTERISTICS OF CRIMPED POLYMERIC SEALS

	Crimp		Pre Heat Sterilization Leak Rate std cc/sec/atm		Post Heat Sterilization Leak Rate
No	PSI	Dia	air	He	std cc He/sec/atm
1	1300	.427	2.5×10^{-8}	1.4×10^{-7}	70μ
2	1300	.427	2.6×10^{-8}	9.6×10^{-7}	100μ
3	1300	.427	3.2×10^{-8}	3.2×10^{-8}	------
4	1000	.434	3.5×10^{-8}	3.5×10^{-8}	1×10^{-6}
5	1000	.434	3.9×10^{-8}	3.9×10^{-8}	90μ
6	1000	.434	4.3×10^{-8}	4.3×10^{-8}	------
7	1300	.503	2.9×10^{-8}	3.1×10^{-8}	90μ
8	1300	.503	4.2×10^{-8}	4.2×10^{-8}	80μ
9	1300	.503	5.0×10^{-8}	5.0×10^{-8}	------
10	1000	.509	4.4×10^{-8}	4.4×10^{-8}	70μ
11	1000	.509	4.6×10^{-8}	4.6×10^{-8}	70μ
12	1000	.509	5.2×10^{-8}	5.2×10^{-8}	------
A	1000	.509	----------	----------	∿10μ gross leak
B	1000	.509	----------	----------	∿ 8μ gross leak

Before heat sterilization the seals were generally leak tight as noted. After heat sterilization (135°C for 72 hours) all seals were gross leakers excepting Seal number 4.

TABLE II-3

DESIGN CHARACTERISTICS
OF
ENGINEERING MODEL PRISMATIC CELLS

	CELL DATA IN FIGURE II-E	CELL DATA IN FIGURE II-F	CELL DATA IN FIGURE II-G
SEPARATOR	POLYAMIDE PELLON 2505K[I]	POLYPROPYLENE PELLON FT2140	POLYPROPYLENE PELLON FT2140
NO. OF POSITIVE PLATES	12	12	12
NO. OF NEGATIVE PLATES	13	13	13
TAB ATTACHMENT	HELIARC WELD	HELIARC WELD	RESISTANCE WELD
SEAL TYPE	O-RING COMPRESSION	O-RING COMPRESSION	GLASS-TO-METAL
ELECTROLYTE	100cc - 30% KOH	99cc - 30% KOH	99cc - 30% KOH
CELL WEIGHT	1125 gr	1126 gr	1110 gr
NEGATIVE/POSITIVE RATIO	1.4	1.4	1.4

TABLE II-4

DESIGN CHARACTERISTICS
25 AH HEAT STERILIZABLE
PRISMATIC CELLS

PLATES:	
POSITIVE	12
NEGATIVE	13
RATIO (Delivered negative capacity to positive capacity)	1.4
SEPARATOR	PELLON FT2140 NONWOVEN POLYPROPYLENE
ELECTROLYTE	
QUANTITY	78cc
CONCENTRATION	30% KOH
WEIGHT	1080 grams
SEAL	CERAMIC-TO-METAL
CASE	304L SS WELDED CONSTRUCTION

TABLE II-5

DESIGN CHARACTERISTICS
25 AH HEAT STERILIZABLE
CYLINDRICAL CELLS

PLATES	
POSITIVE	3
NEGATIVE	4
RATIO (Delivered negative to positive capacity)	1.65
SEPARATOR	PELLON FT2140 NONWOVEN POLYPROPYLENE
ELECTROLYTE	
QUANTITY	90cc
CONCENTRATION	30% KOH
WEIGHT	1155 grams
SEALS	GLASS-TO-METAL
CASE	Ni PLATED STEEL DEEP DRAWN CASE

TABLE II-6

DESIGN CONSIDERATIONS FOR INTERIM AND FINAL DESIGNS

I. Prismatic Cell

A. Mechanical

1. Cell packaging is more conventional
2. Physical restaints required for packaging cells
3. Thermal transport - 64 in^2 of surface
4. Cell weights = 1080 grams

B. Electrochemical

1. Limited geometric plate ratio (using conventional cross sections)
   i.e. N positives, N+1 negatives
2. Limited practical negative to positive ratio
3. Operating pressure controlled by electrolyte content and plate loading

C. Effect of Sterilization

1. Higher end-of-charge voltage (than prior to sterilization)
2. 10-20% loss in capacity

II. Cylindrical Cell

A. Mechanical

1. Cell packaging is less conventional
2. Cell self-containing -- no restraints required
3. Thermal transport -- 50 in^2 of surface
4. Fewer internal welds (14 vs 25 for prismatic cell)
5. Cell weight = 1155 grams
6. Fewer plate edges which act as a potential cutting edge (310 in^2 vs 670 in^2)

B. Electrochemical

1. Wider range of geometric plate ratio
2. Wider range of negative to positive ratio
3. Intrinsically lower operating pressure (due to coreless design)

C. Effect of Sterilization

1. Higher end-of-charge voltage (than prior to sterilization)
2. Negligible capacity loss

TABLE II-7

DESIGN CHARACTERISTICS, INTERIM CELL DESIGN

25 AMPERE-HOUR HEAT-STERILIZABLE CYLINDRICAL CELLS

PLATES	
POSITIVE	3
NEGATIVE	4
RATIO (Negative to positive formation capacity)	1.8
SEPARATOR	NONWOVEN POLYPROPYLENE PELLON FT2140
ELECTROLYTE	
TYPE	KOH
CONCENTRATION	30%
QUANTITY	90cc
WEIGHT	1155 gr
SEALS	GLASS-TO-METAL

TABLE II-18

PERFORMANCE DATA FOR INTERIM MODEL CELLS

Charging Conditions 3.0 Amperes for 16 hours
Discharging Conditions 10 Amperes to 1.00 volt cut off
Cycle Number 3

Cell No.	ECV (volt)	OCV (volt)	V @ 50% (volt)	ECR (mΩ)	ECP (psia)	ECC (Ah)
C250	1.435	1.389	1.263	5.6	32	32.88
C251	1.429	1.388	1.264	4.2	35	33.45
C252	1.427	1.386	1.262	4.4	33	32.78
C253	1.427	1.387	1.263	4.2	31	33.15
C254	1.422	1.382	1.263	3.9	29	33.03
C255	1.426	1.386	1.262	4.2	31	32.48
C256	1.423	1.383	1.263	3.8	32	32.60
C257	1.423	1.385	1.267	3.7	28	33.48
C258	1.437	1.389	1.258	6.6	28	33.23
C259	1.436	1.391	1.267	3.8	29	32.63
C260	1.438	1.394	1.270	3.8	32	32.65
C261	1.432	1.390	1.267	4.4	28	32.75
C262	1.437	1.392	1.264	4.0	30	33.33
C263	1.428	1.385	1.262	4.4	30	32.65
C264	1.424	1.381	1.263	3.8	15	32.15
C265	1.426	1.384	1.256	3.8	33	31.28
C266	1.427	1.385	1.265	3.6	31	32.30
C268	1.430	1.387	1.262	3.7	27	32.98
C269	1.437	1.391	1.261	4.0	15	32.60
C270	1.441	1.393	1.258	5.1	28	33.08
AVG.	1.430	1.387	1.263	4.2	30	32.56
STD. DEV.	0.006	0.003	0.003	0.7	5	0.49

TABLE II-9

PERFORMANCE DATA FOR TYPICAL FINAL MODEL CELLS

Charging Conditions: 3.0 Amperes for 16 Hours

Discharging Conditions: 10 Amperes to 1.00 Volt Cut-Off

Cell No.	ECV (Volts)	OCV (Volts)	V @ 50% (Volts)	ECR (mΩ)	ECP (psia)	ECC (ah)
C294	1.406	1.368	1.258	2.4	24	32.34
C295	1.402	1.367	1.258	2.5	24	32.04
C296	1.403	1.368	1.258	2.5	27	32.12
C297	1.510	1.366	1.218	3.7	24	31.77
C298	1.637	1.360	1.247	3.4	26	31.52
C299	1.397	1.362	1.256	2.7	17	31.72
C300	1.392	1.358	1.257	2.5	24	31.32
C301	1.401	1.364	1.256	2.7	32	32.02
C302	1.395	1.363	1.258	2.4	28	31.70
C303	1.412	1.375	1.256	2.6	14	31.50
C304	1.407	1.373	1.260	2.4	24	31.42
C305	1.402	1.367	1.257	2.4	24	31.27
C306	1.404	1.369	1.259	2.4	24	31.20
C307	1.405	1.371	1.259	2.3	14	32.27
C308	1.405	1.371	1.258	2.4	26	31.42
C309	1.431	1.370	1.209	4.0	24	31.52
C310	1.401	1.367	1.258	2.4	23	31.92
C311	1.397	1.365	1.256	2.5	24	30.45
C312	1.404	1.368	1.256	3.0	26	31.25
C313	1.416	1.373	1.250	5.0	24	31.20
C314	1.407	1.372	1.258	2.5	22	31.65
Mean	1.421	1.367	1.252	3.6	24	31.60
Std. Dev.	0.054	0.005	0.013	3.9	4	0.43

TABLE II-10

LONG-RANGE TESTING PLAN

A. Cycling - after heat sterilization and reconditioning

Test Termperature	30°F, 50°F, 70°F
Depth of Discharge	70%, 80%
Charge Rate	C/10, C/20
Discharge Rate	C/2
Cells Required	24 (12 prismatic, 12 cylindrical)
No. of Cycles	90 minimum, 150 planned

B. Cell Maintenance During Flight - after heat sterilization and reconditioning @70°F

Fly charged with periodic discharge and recharge - 2 cells
Fly discharged, charge at planet approach - 2 cells
Fly charged, trickle charge with constant current - 2 cells
Fly charged, float charge at constant voltage - 2 cells
Duration of wet stand shall be 7 months.

C. Cycling after Wet Stand

Cycle all cells for a minimum of 90 cycles under conditions optimized under Section A
Cell requirement for B & C is 8 cells each of prismatic and cylindrical design

TABLE II-11

IDENTIFICATION AND PHYSICAL ATTRIBUTES OF HIGH GAUGE PLAQUE

	Stack #	Gauge inches	Porosity (%)	Sinter wt g/in^2	(1) Volume Utilization (%)	(2) Electrical Resistance (mΩ)
*	170901-1	.0264	84.0	.509	88.2	10.2
*	901-2	.0301	83.6	.606	88.8	8.8
	901-3A	.0327	83.6	.673	89.7	8.9
*	901-3	.0345	83.6	.703	88.4	8.2
*	901-4	.0405	83.3	.852	89.7	7.3
	901-4A	.0447	82.4	.968	87.5	6.7
*	901-7	.0453	83.1	.952	85.3	6.9
	901-6	.0475	81.3	1.093	84.7	6.0
	901-5	.0477	81.8	1.062	85.1	6.5
*	901-4B	.0485	81.6	1.116	87.8	6.1
*	160901-1	.0266	85.3	.499	91.9	11.3
*	901-2	.0307	84.5	.602	91.1	9.1
*	902-1	.0351	84.6	.691	91.4	9.2
*	902-2	.0402	84.0	.824	92.4	8.3
	902-3	.0426	83.4	.905	91.2	7.4
*	902-4	.0490	82.4	1.108	90.8	6.5
	185902-5	.0256	81.4	.563	86.7	7.3
*	902-6	.0268	81.5	.591	87.2	7.5
*	902-7	.0299	80.7	.690	87.2	6.8
*	902-8	.0340	81.2	.784	88.5	6.5
*	902-9	.0368	80.7	.869	87.5	5.7
*	198902-10	.0250	79.6	.590	85.0	6.5
*	902-11	.0296	79.6	.730	84.5	6.1
*	902-12	.0320	79.2	.785	85.4	5.8
*	902-13	.0362	79.2	.905	86.1	5.1
*	902-14	.0398	78.9	.998	84.5	4.6
*	902-15	.0433	78.4	1.121	85.2	4.2

* Selected for impregnation

(1) Measure of the plaque shrinkage

(2) Across the length of a 3" x 1" strip

TABLE II-12

ANALYTICAL DATA HIGH CAPACITY POSITIVE IMPREGNATION EXPERIMENT I

Plate Identification		Act Mat g/in^2	Theor AH/in^2	Theor AH/in^3	Theor AH/g	% Corrosion	Initial Gauge
170	901-3	.968	.281	8.25	.171	37	.0345
		1.263	.366	11.8	.195	43	.0345
	901-4	1.124	.326	8.3	.175	37	.0405
		1.293	.376	9.9	.188	41	.0405
		1.448	.420	11.3	.197	43	.0405
	901-7	1.382	.401	8.9	.183	40	.0453
		1.593	.462	10.0	.195	44	.0453
		1.740	.505	11.5	.202	47	.0453
	901-4B	1.486	.431	9.7	.183	40	.0485
		1.664	.482	10.25	.192	44	.0485
		1.847	.535	11.4	.204	47	.0485
160	902-1	1.028	.298	9.6	.180	40	.0351
	902-2	1.227	.355	8.9	.182	38	.0402
		1.379	.400	10.25	.191	40	.0402
		1.566	.455	12.3	.203	46	.0402
	902-4	1.544	.448	9.35	.184	39	.0490
		1.730	.502	10.5	.195	41	.0490
		1.913	.556	12.0	.203	46	.0490
185	902-6	.747	.217	8.1	.159	33	.0268
		.845	.245	9.1	.168	33	.0268
		.924	.267	9.9	.178	36	.0268
	902-7	.807	.234	7.8	.154	28	.0299
		.926	.269	8.95	.160	31	.0299
		1.020	.295	10.2	.174	34	.0299
	902-8	.936	.271	7.95	.168	31	.0340
		1.053	.305	9.25	.172	34	.0340
		1.159	.333	10.0	.176	34	.0340
	902-6	1.041	.302	8.1	.162	31	.0368
		1.175	.341	9.0	.170	34	.0368
		1.301	.378	10.2	.181	34	.0368
198	902-10	.642	.186	7.5	.143	26	.0250
		.736	.213	8.6	.153	28	.0250
		.820	.238	9.2	.164	30	.0250
	902-11	.769	.223	7.7	.149	26	.0296
		.878	.255	8.8	.160	28	.0296
		.978	.284	9.8	.171	32	.0296
	902-12	.848	.247	7.7	.150	28	.0320
		.964	.279	8.8	.152	31	.0320
		1.054	.305	9.25	.167	31	.0320
	902-13	.939	.254	7.1	.139	27	.0362
		1.048	.304	8.7	.159	30	.0362
		1.164	.338	9.8	.167	31	.0362
	902-14	1.005	.292	7.6	.148	27	.0398
		1.135	.329	8.3	.158	28	.0398
		1.249	.362	9.3	.168	30	.0398
	902-15	1.102	.320	7.6	.150	28	.0433
		1.237	.360	8.4	.159	28	.0433
		1.366	.396	9.4	.168	33	.0433

TABLE II-13

ANALYTICAL DATA HIGH CAPACITY POSITIVE IMPREGNATION EXPERIMENT II

Plate Identification		Theor AH/in^2	Theor AH/in^3	Theor AH/g	% Corrosion	Initial Gauge	Flooded Cap AH/in^2	% Effic.	Flooded Cap AH/in^3
170	901-1	.206	7.9	.165	36	.0264	.195	95	7.5
		.228	8.8	.177	40		.217	95	8.4
		.243	9.3	.182	44		.229	94	8.7
	901-2	.241	8.4	.169	40	.0301	.232	96	8.1
		.273	9.4	.185	45		.260	95	8.9
		.284	9.8	.188	46		.280	98	9.6
	901-3	.285	9.2	.179	44	.0345	.269	94	8.7
		.326	10.7	.191	48		.322	99	10.6
		.353	11.6	.199	53		.316	90	10.4
	901-4	.342	9.0	.185	45	.0405	.340	99	8.9
		.385	10.1	.197	50		.370	96	9.7
		.406	10.6	.202	53		.390	96	10.2
	901-7	.398	9.1	.187	46	.0453	.399	100	9.1
		.456	10.4	.202	53		.439	96	10.0
		.472	10.7	.204	54		.468	99	10.6
	901-4B	.425	9.1	.188	42	.0485	.409	96	8.7
		.486	10.4	.200	52		.448	92	9.6
		.507	10.8	.202	53		.480	95	10.3
160	901-1	.215	8.3	.176	47	.0266	.211	98	8.1
		.241	9.4	.187	50		.233	97	9.1
		.253	9.9	.192	52		.255	100	9.9
	901-2	.272	9.7	.186	48	.0307	.252	93	9.0
		.307	11.0	.198	52		.276	90	10.9
		.320	11.4	.202	56		.285	89	10.1
	902-1	.316	9.7	.190	47	.0351	.277	88	8.5
		.358	11.0	.202	54		.322	90	10.9
		.377	11.6	.204	56		.350	93	10.8
	902-2	.359	9.6	.189	45	.0402	.284	79	7.6
		.408	10.9	.202	52		.350	86	9.4
		.431	11.5	.208	55		.358	83	9.5
	902-4	.444	8.8	.188	44	.0409	.418	94	8.3
		.500	10.2	.200	49		.434	87	8.9
		.523	10.7	.202	52		.490	94	10.1
185	902-6	.211	7.6	.159	34	.0268	.197	94	7.1
		.232	8.4	.167	36		.213	92	7.7
		.251	9.2	.176	40		.250	99	9.1
	902-7	.239	7.9	.162	38	.0299	.236	99	7.8
		.265	8.7	.172	42		.246	93	8.1
		.289	9.5	.179	43		.264	88	8.4
	902-8	.269	7.7	.163	35	.0340	.256	95	7.3
		.308	8.8	.176	40		.284	92	8.1
		.326	9.3	.183	43		.323	99	9.2
	902-9	.306	8.1	.168	38	.0368	.285	93	7.5
		.341	9.0	.180	45		.330	97	8.7
		.361	9.5	.202	46		.344	95	9.0
198	902-10	.175	6.9	.142	30	.0250	.173	99	6.8
		.198	7.6	.152	33		.192	97	7.4
		.211	8.1	.159	34		.204	97	7.9

- Cont'd. -

TABLE II-13

- Cont'd. -

Plate Identification	Theor AH/in^2	Theor AH/in^3	Theor AH/g	% Corrosion	Initial Gauge	Flooded Cap AH/in^2	% Effic.	Flooded Cap AH/in^3
198 902-11	.209	6.8	.147	33	.0296	.205	98	6.7
	.234	7.7	.156	33		.232	99	7.6
	.259	8.5	.167	36		.240	93	7.9
902-12	.249	7.5	.156	33	.0320	.240	96	7.2
	.276	8.3	.164	34		.252	91	7.6
	.301	9.2	.174	40		.289	96	8.8
902-13	.273	7.3	.152	32	.0362	.269	99	7.2
	.308	8.3	.165	37		.288	92	7.6
	.337	9.0	.176	41		.314	93	8.4
902-14	.296	7.3	.154	32	.0398	.274	92	6.7
	.332	8.3	.163	34		.320	96	8.0
	.363	8.9	.174	38		.333	92	8.2
902-15	.333	7.6	.157	34	.0433	.308	93	7.1
	.374	8.5	.168	36		.340	91	7.7
	.394	8.8	.171	37		.367	93	8.2

TABLE II-14

High Capacity Negative Theoretical and Flooded Capacity Data

	Plate Ident.	No. of Impreg Cycles	Theor Cap AH/in^2	Flooded Cap AH/in^2	% Efficiency	Init. Gauge
1700	901-1	4	.384	.235	61	.0264
		5	.407	.256	63	
		6	.443	.261	59	
	901-2	4	.430	.276	64	.0301
		5	.457	.284	62	
		6	.492	.290	59	
	901-3	4	.464	.247	53	.0340
		5	.500	.278	56	
		6	.601	.304	51	
	901-4	4	.484	.275	57	.0405
		5	.532	.291	55	
		6	.594	.318	53	
	901-7	4	.511	.287	56	.0453
		5	.567	.292	52	
		6	.604	.327	54	
	901-4B	4	.555	.287	52	.0485
		5	.606	.293	48	
1600	901-1	4	.409	.256	63	.0266
		5	.429	.274	64	
		6	.470	.282	60	
	901-2	4	.448	.281	63	.0307
		5	.484	.290	60	
		6	.531	.313	59	
	902-1	4	.458	.249	54	.0351
		5	.507	.268	53	
		6	.565	.291	52	
	902-2	4	.499	.253	51	.0402
		5	.533	.268	50	
		6	.596	.299	50	
	902-4	4	.580	.284	49	.0490
		5	.626	.300	48	
		6	.638	.326	51	
1850	902-6	4	.381	.235	62	.0268
		5	.403	.239	59	
		6	.455	.264	58	
	902-7	4	.417	.245	59	.0299
		5	.441	.248	56	
		6	.492	.278	57	
	902-8	4	.451	.258	57	.0340
		5	.480	.263	55	
		6	.528	.287	54	
	902-9	4	.484	.268	55	.0368
		5	.518	.275	53	
		6	.552	.290	53	
1980	902-10	4	.337	.211	63	.0250
		5	.371	.212	57	
		6	.396	.238	60	
	902-11	4	.396	.235	59	.0296
		5	.420	.263	63	
		6	.459	.272	59	
	902-12	4	.427	.251	59	.0320
		5	.454	.265	58	
		6	.497	.268	54	
	902-13	4	.443	.244	55	.0362
		5	.477	.302	63	
		6	.523	.310	59	
	902-14	4	.472	.287	61	.0398
		5	.504	.302	60	
		6	.545	.328	60	
	902-15	4	.485	.260	54	.0433
		5	.530	.274	52	
		6	.579	.308	53	

TABLE II-15

PLAQUE SAMPLES PREPARED TO DATE

Factor Code		Grouping No.	Plaque Lot No.	Thickness (inches)	Porosity (%)	* Ratio
Porosity	* Ratio					
High	High	I	17-901-1	.0264	84.0	2.59
			17-901-3	.0345	83.6	2.89
			17-901-4	.0405	83.3	3.40
			17-901-7	.0433	83.1	3.16
			16-902-2	.0402	84.0	3.18
			16-902-4	.0490	82.4	6.12
Low	High	II	17-901-4B	.0485	81.6	6.34
			18-902-7	.0299	80.7	2.43
			18-902-9	.0368	80.7	3.20
			19-902-15	.0433	78.4	2.40
High	Low	III	17-901-2	.0301	83.6	2.08
			16-901-1	.0266	85.3	2.06
			16-901-2	.0307	84.5	2.38
			16-902-1	.0351	84.6	2.18
Low	Low	IV	18-902-6	.0268	81.5	2.16
			18-902-8	.0340	81.2	2.17
			19-902-10	.0250	79.6	1.93
			19-902-11	.0296	79.6	1.71
			19-902-12	.0320	79.2	2.29
			19-902-13	.0362	79.2	2.19
			19-902-14	.0398	78.9	2.38
				Median	82.4	2.40

* Ratio = $\frac{\text{Pore Volume of 10}\mu\text{ to 15}\mu\text{ size pores}}{\text{Pore Volume of 15}\mu\text{ to 20}\mu\text{ size pores}}$

TABLE II-16

PLAQUE SAMPLES EVALUATED IN
THE FACTORIAL EXPERIMENT

Plaque Structure Factors						
Porosity %	Pore Ratio	Plate	Theor Cap AH/in^2	Flooded Capacity AH/in^2	Flooded Capacity AH/in^3	Gauge in
High	High					
83.1	3.16	Pos	.399	.399	8.8	.045
83.1	3.16	Neg	.604	.327	7.2	.045
Low	High					
80.7	3.20	Pos	.361	.344	9.4	.037
80.7	3.20	Neg	.552	.290	7.9	.037
High	Low					
84.6	2.18	Pos	.358	.322	9.2	.035
84.6	2.18	Neg	.565	.291	8.3	.035
Low	Low					
79.2	2.19	Pos	.337	.314	8.7	.036
78.9	2.38	Neg	.545	.328	8.2	.040

LIST OF FIGURES IN APPENDIX II-A

- Cont'd. -

LIST OF FIGURES IN APPENDIX II-A

- CONT'D. -

FIGURE II-A

Crimped Polymeric Seal

Section thru Heat Sterilized Unit

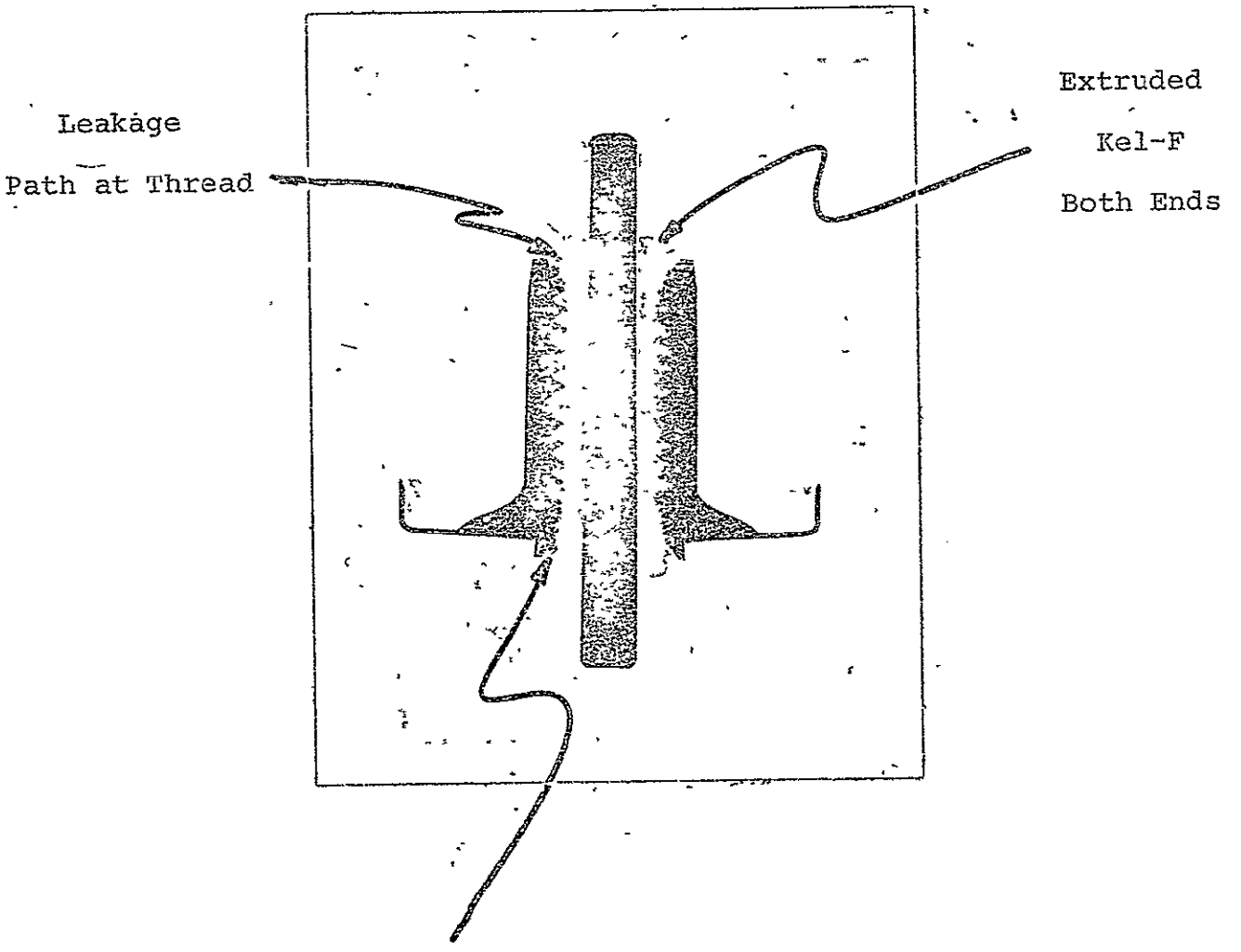

FIGURE II-B

Modification 1

CRIMPED POLYMERIC SEAL

Section thru heat sterilized unit

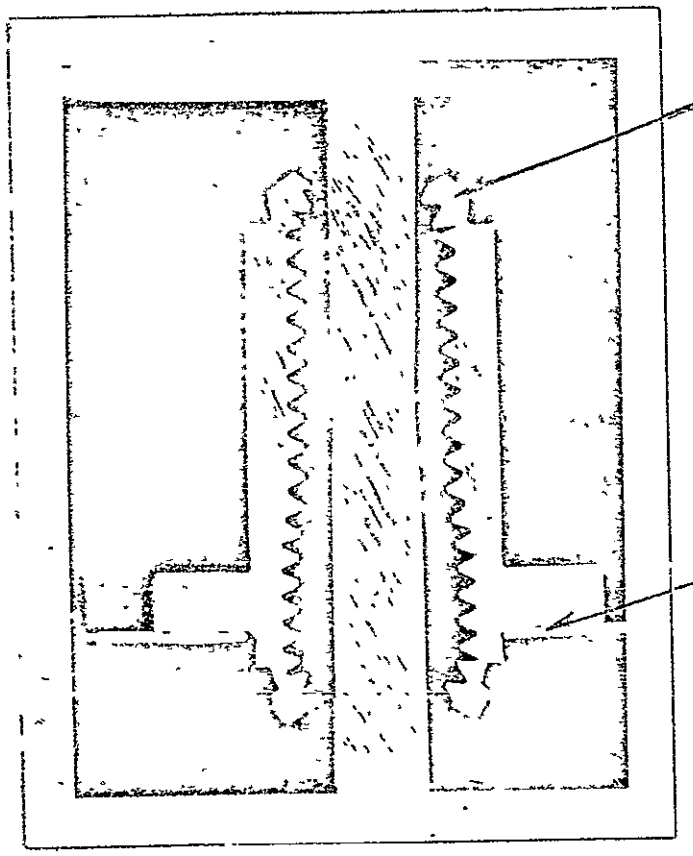

2 X

100 X

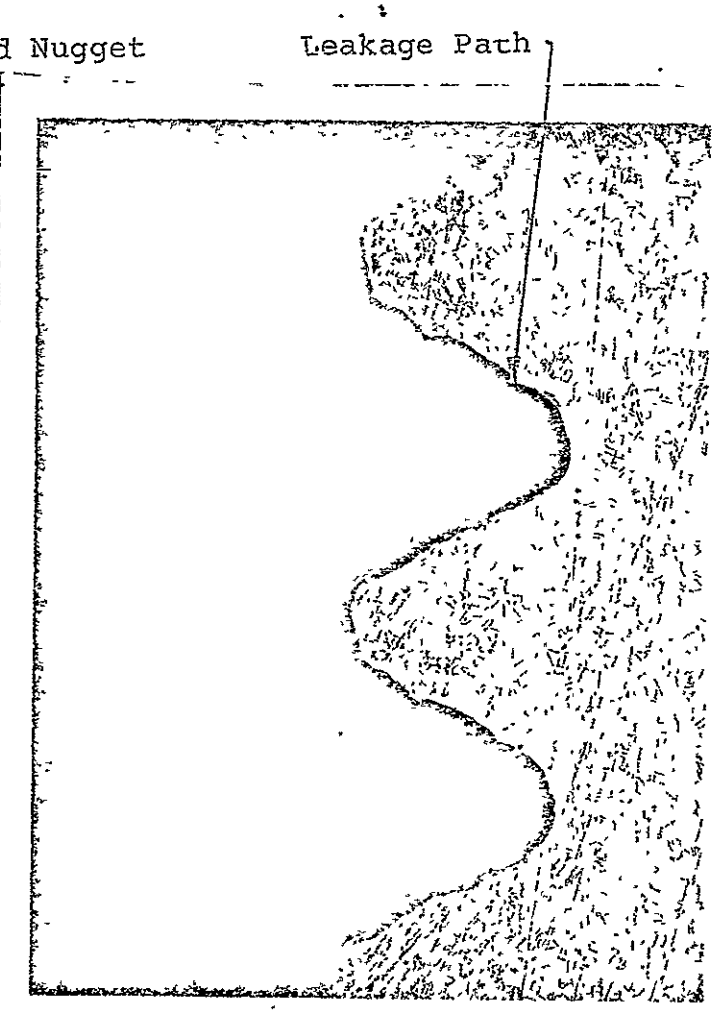

metallurgical
materials division

FIGURE II-C

CRIMPED POLYMERIC SEAL -- Modification 2

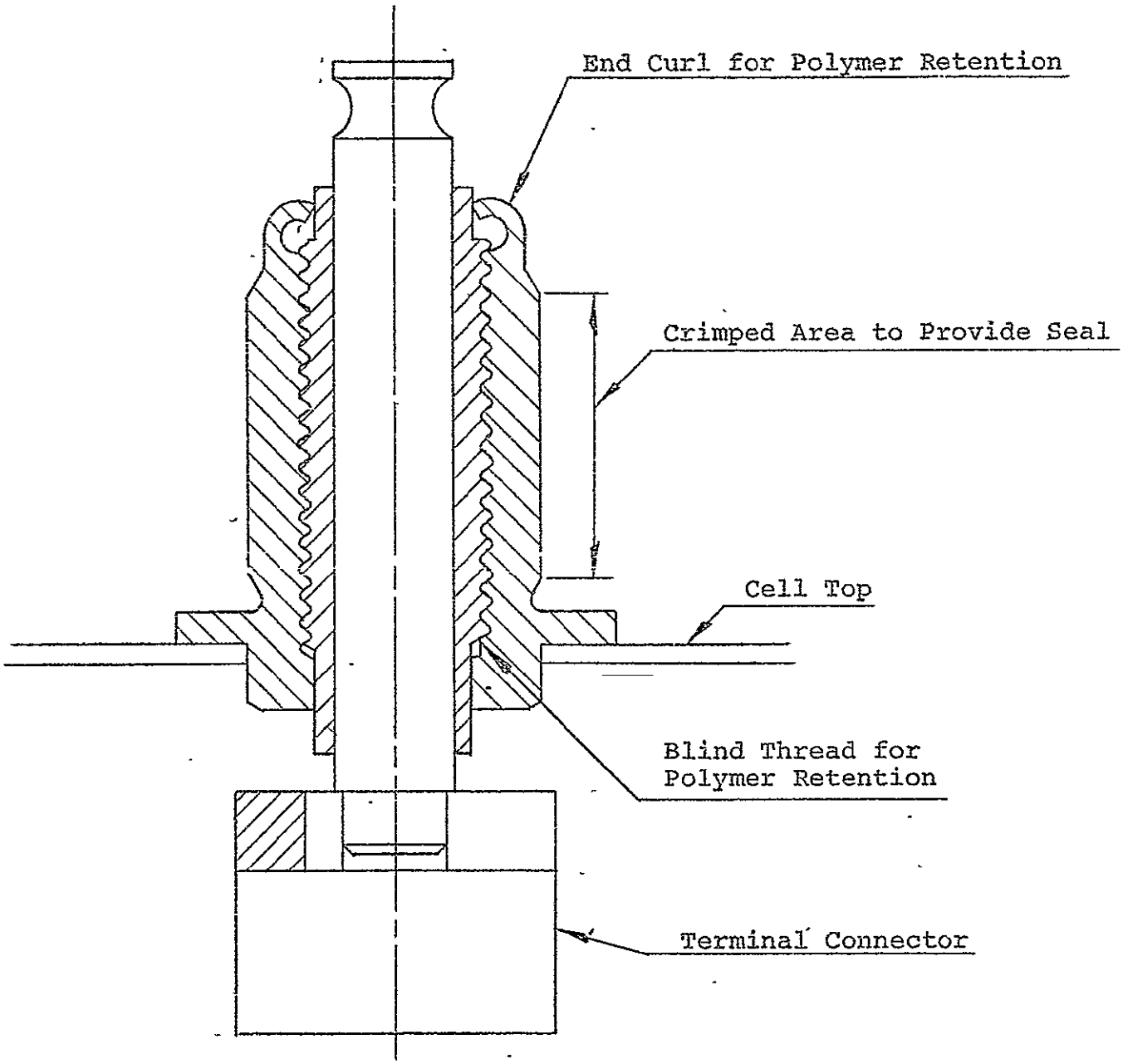

TEXAS INSTRUMENTS INCORPORATED ATTLEBORO, MASS., U.S.A.	SCHEMATIC REPRESENTATION HEAT-STERILIZEABLE CRIMPED POLYMERIC SEAL

Figure II-D

MICRO SECTION OF WELD JOINT

Typical of Joints Made on Taylor-Winfield
30 KVA Resistance Welding Machine

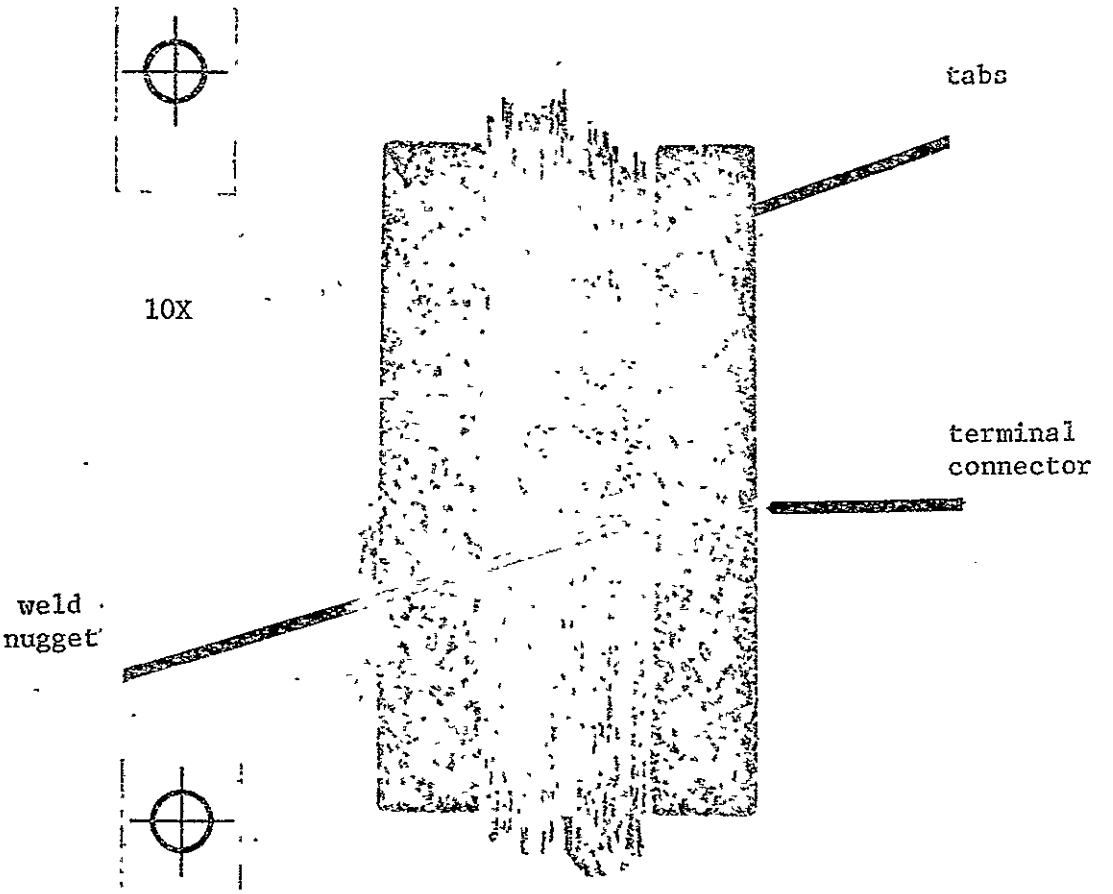

FIGURE II-E

PERFORMANCE DATA

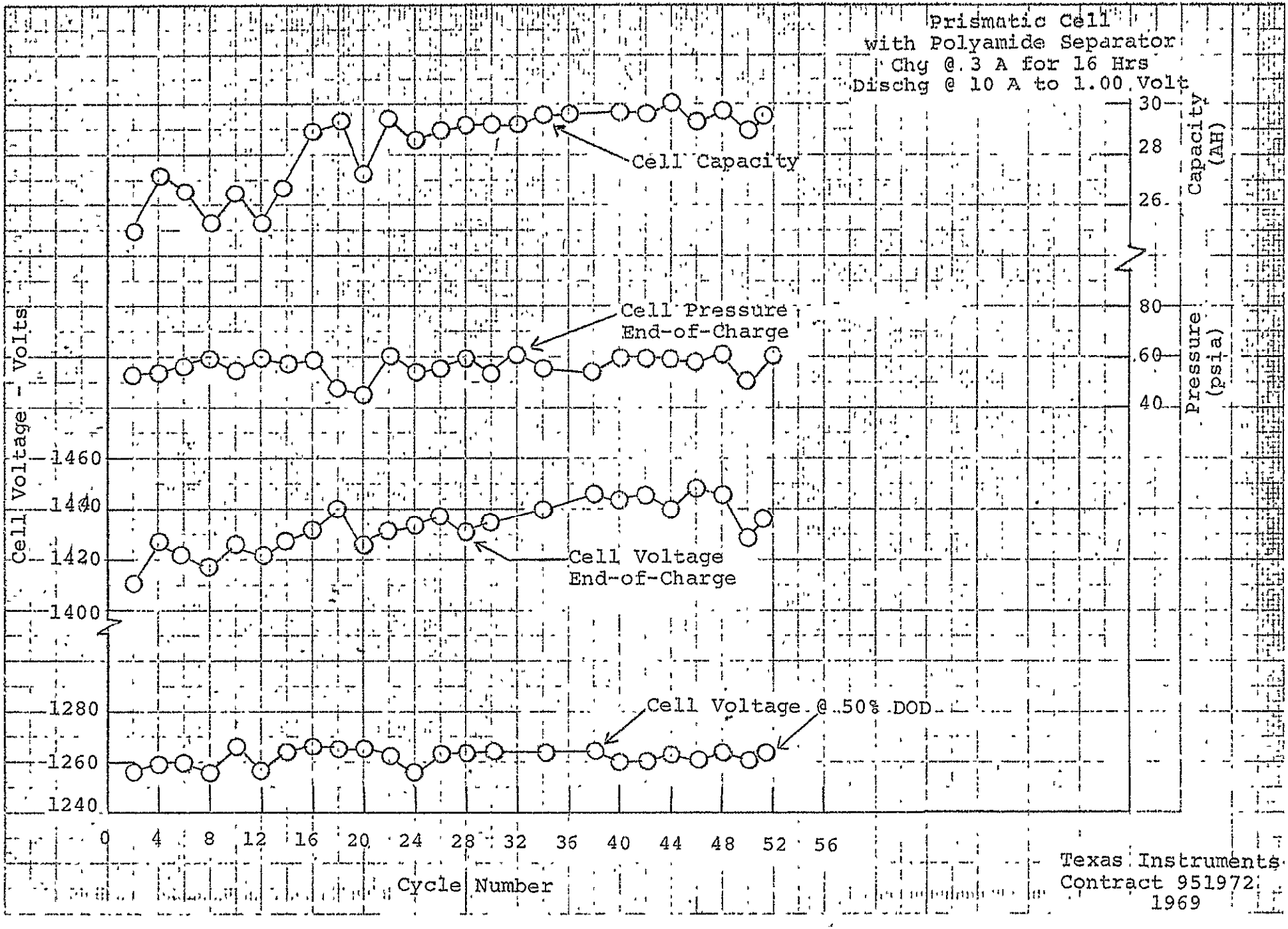

Texas Instruments
Contract 951972
1969

FIGURE II-F
PERFORMANCE DATA

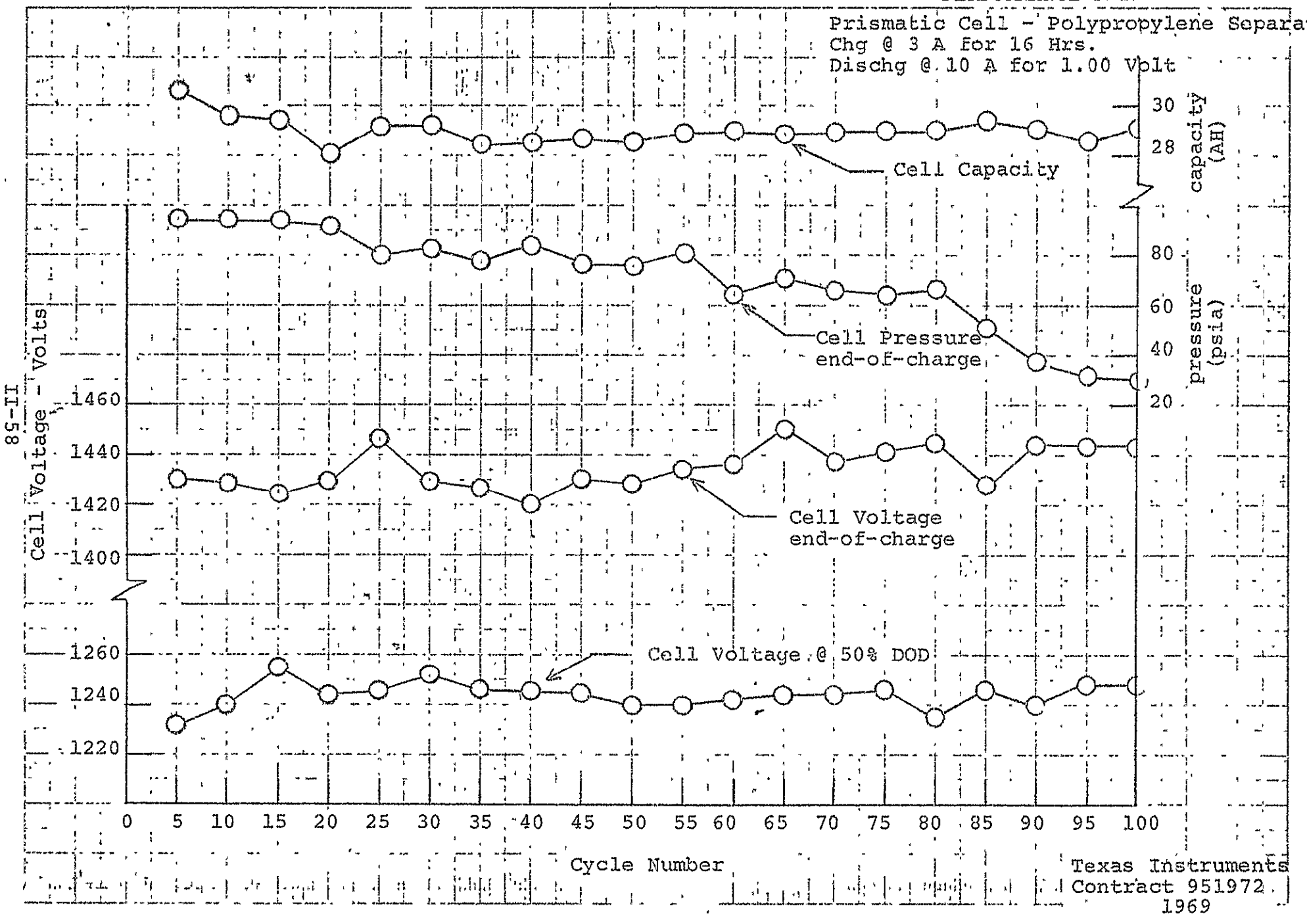

FIGURE II-G
PERFORMANCE DATA
Prismatic Cell
Polypropylene Separator
(heat sterilized)
Chg @ 3 A for 16 hrs
Dischg @ 10 A 1.0 Volt

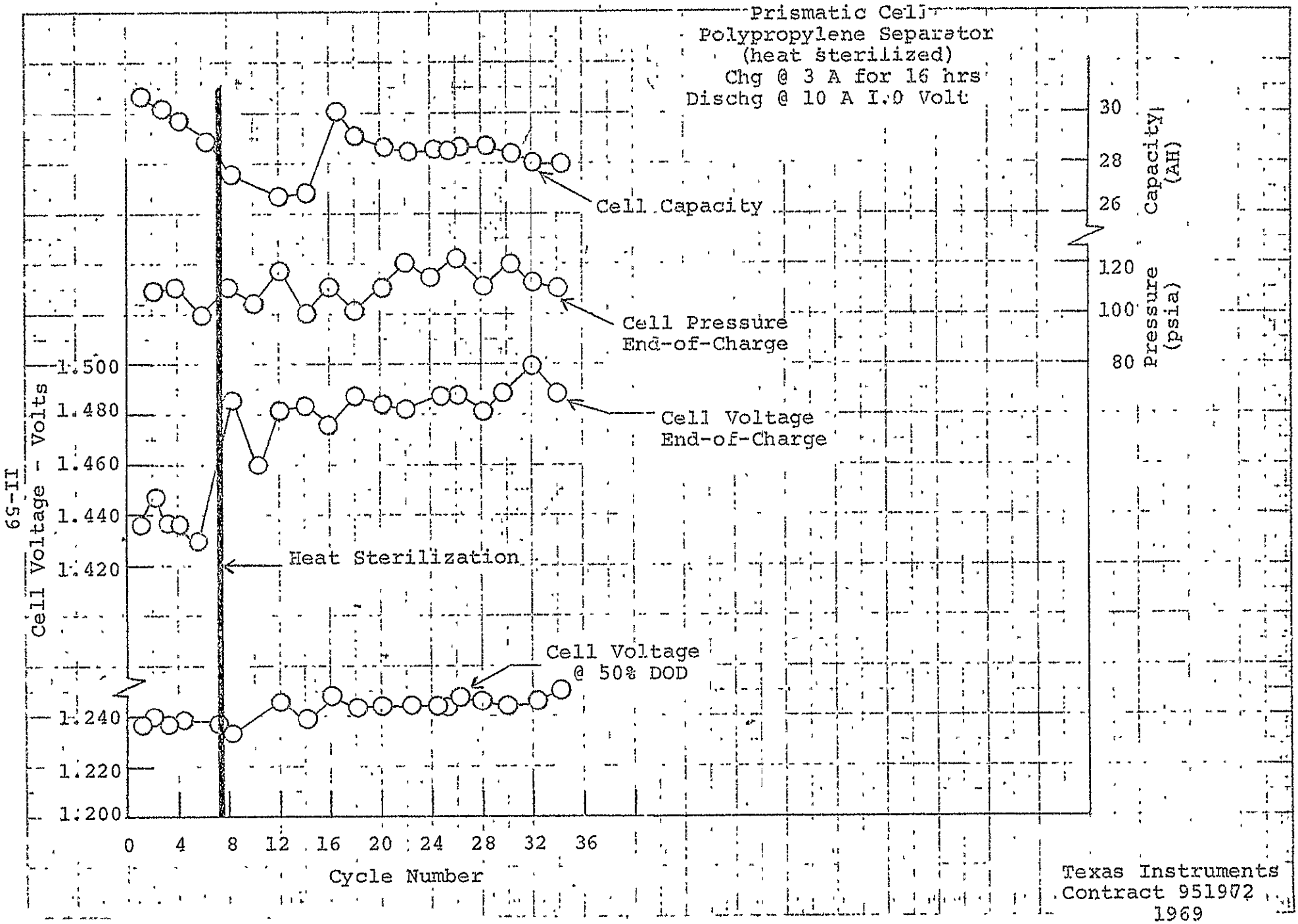

Texas Instruments
Contract 951972
1969

FIGURE II-H
Performance Data
10 Prismatic Cells
Polypropylene Separator
Chg @ 3 A for 16 Hrs
Dischg @ 3 A to 1.00 Volt

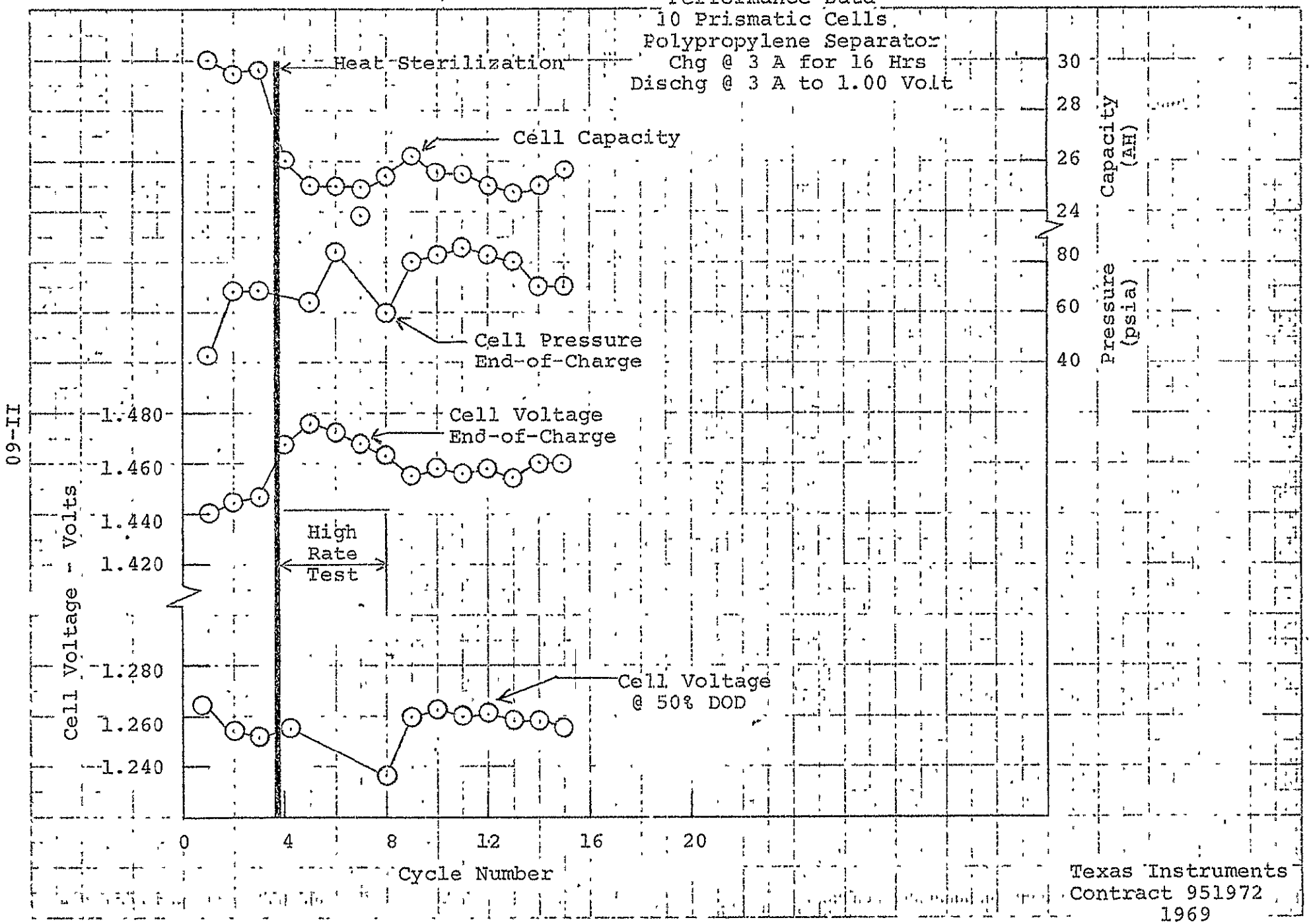

II-60

Texas Instruments
Contract 951972
1969

FIGURE II-I
Performance Data
Initial Cylindrical Cell - Polyamide Separator
Chg @ 3 A for 16 hrs
Dischg @ 10 A to 1.00 V

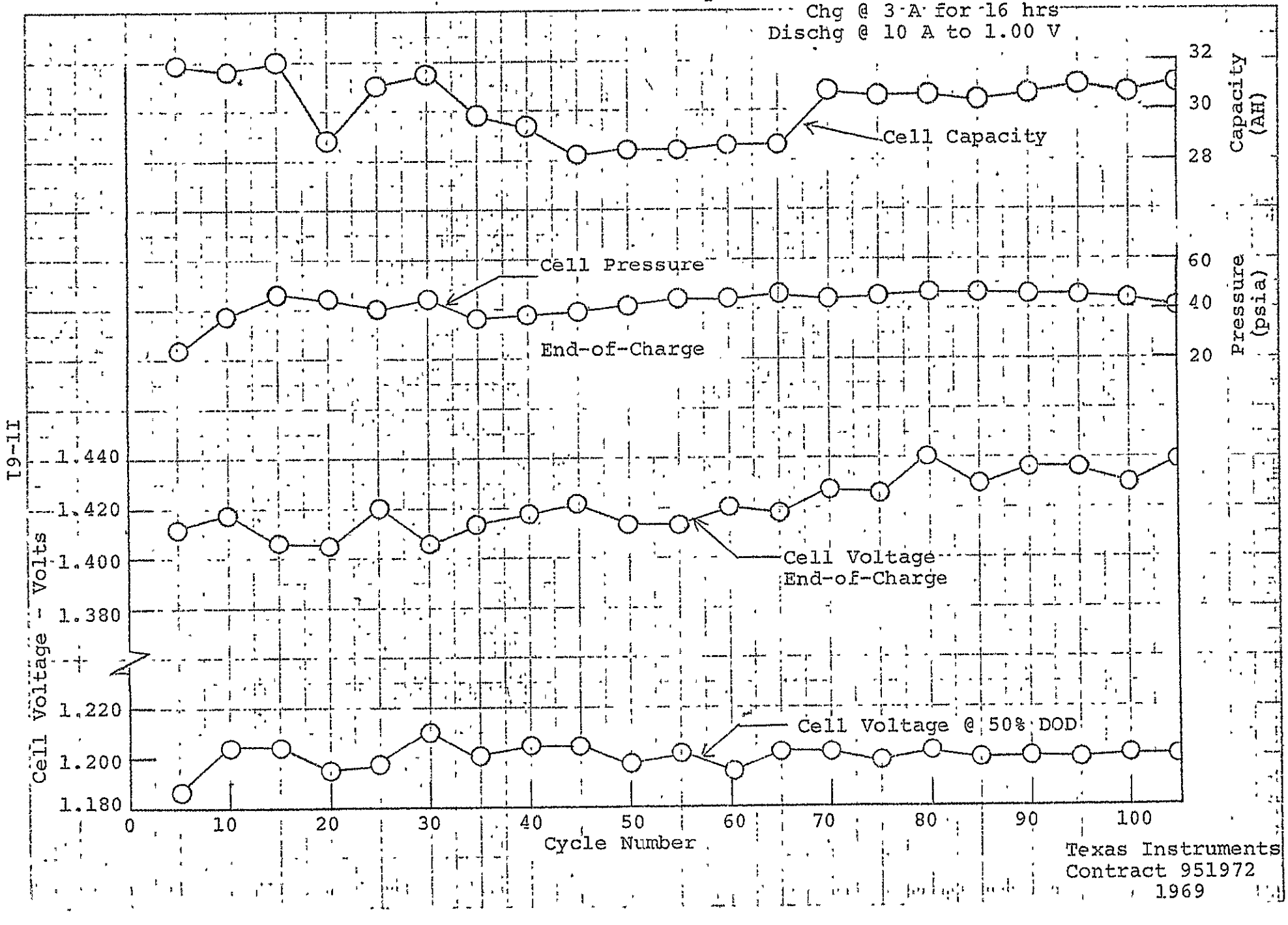

Texas Instruments
Contract 951972
1969

I9-1I

FIGURE II-J

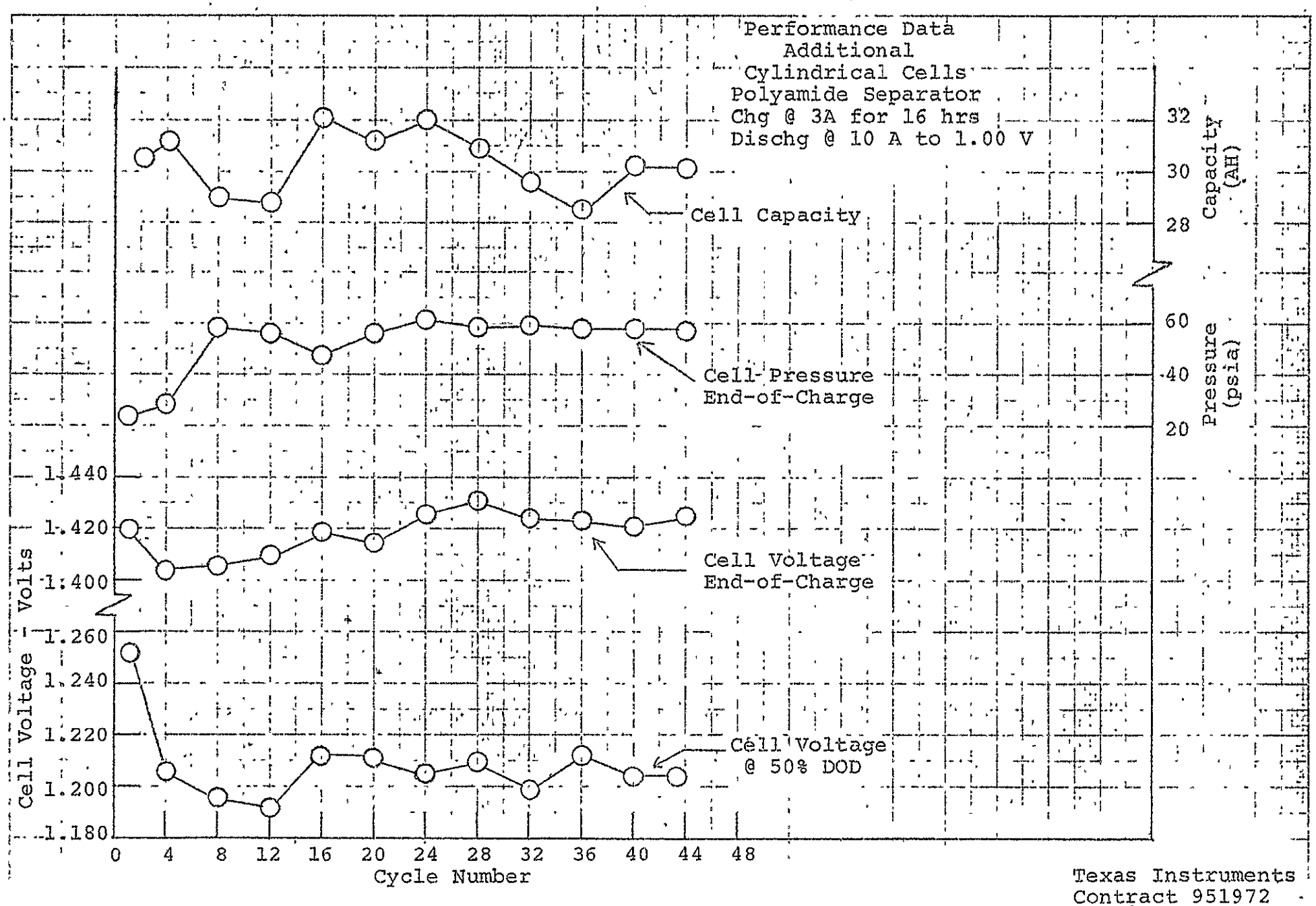

Texas Instruments
Contract 951972
196

FIGURE II-K
Performance Data
Cylindrical Cell
Polypropylene Separator
Chg. @ 3 A for 16 Hrs
Dischg @ 10 A to 1.00 V

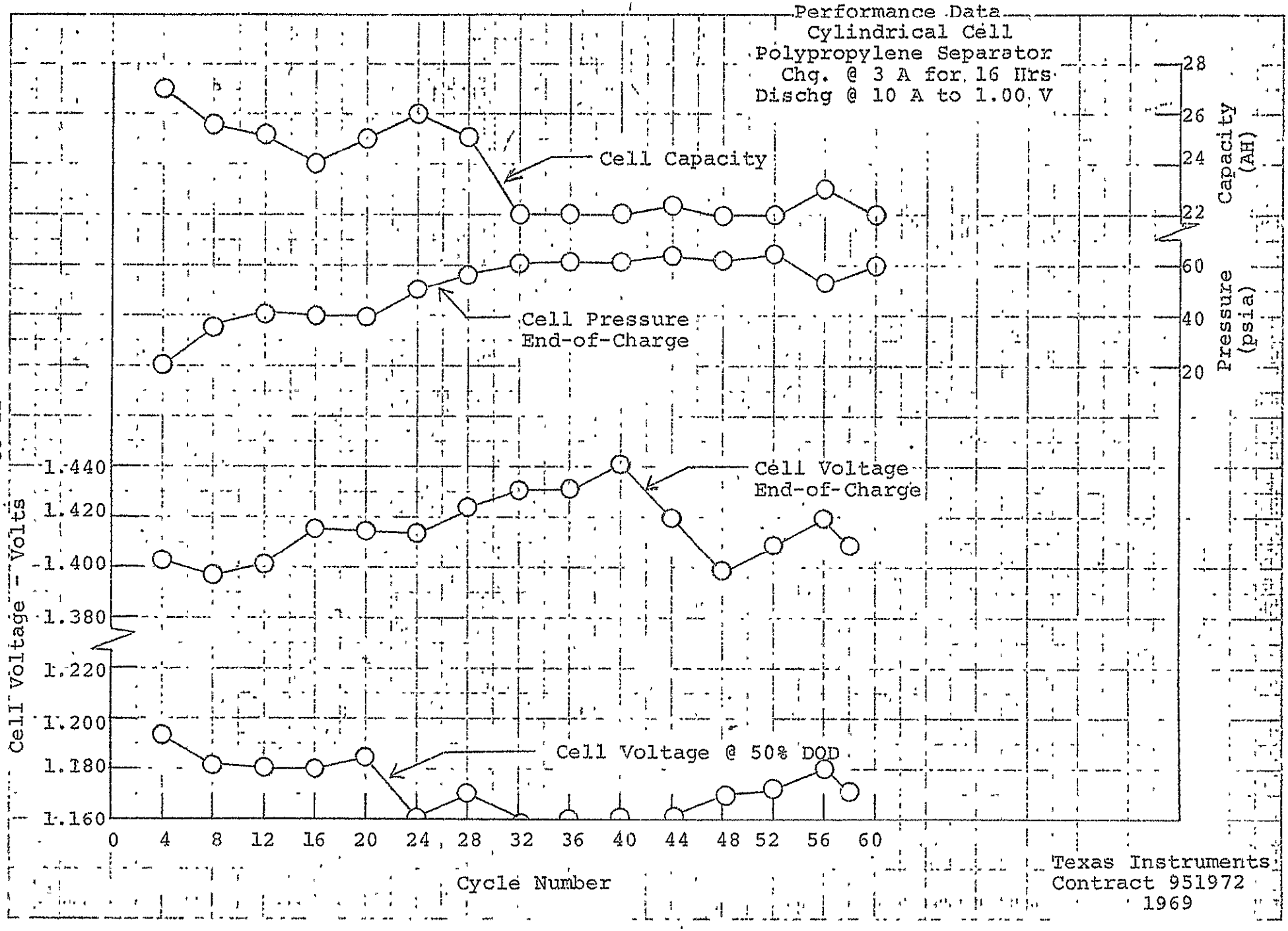

Texas Instruments
Contract 951972
1969

FIGURE II-L
Performance Data
Improved Cylindrical Cell
Polyamide Separator
Chg. @ 3 A for 16 Hrs
Dischg @ 10 A to 1.00 V

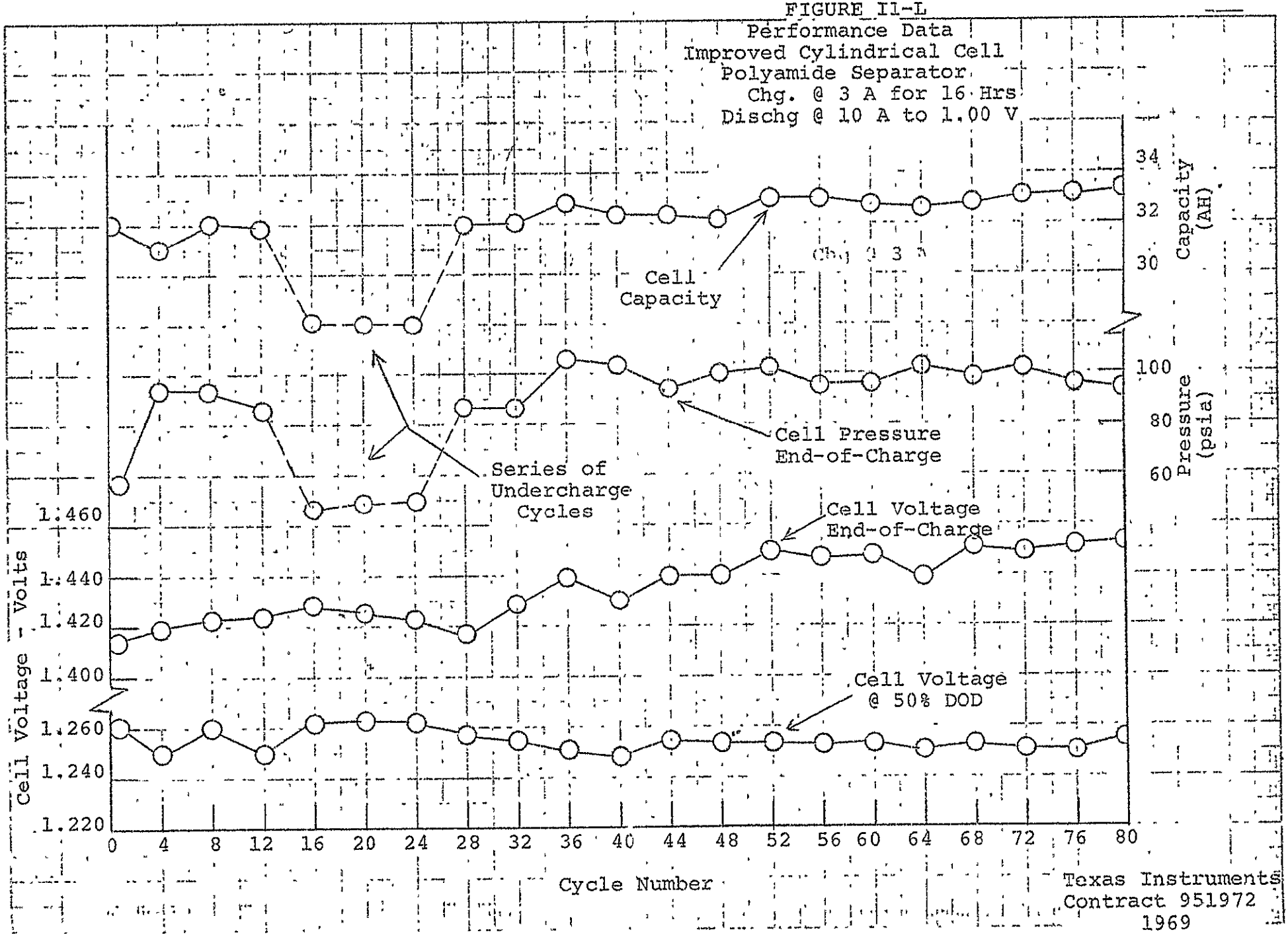

Texas Instruments
Contract 951972
1969

FIGURE II-M
Performance Data
Improved Cylindrical Cell
Polypropylene Separator (Heat Sterilized)
Chg @ 3 A for 16 Hrs
Dischg @ 10 A to 1.00 V

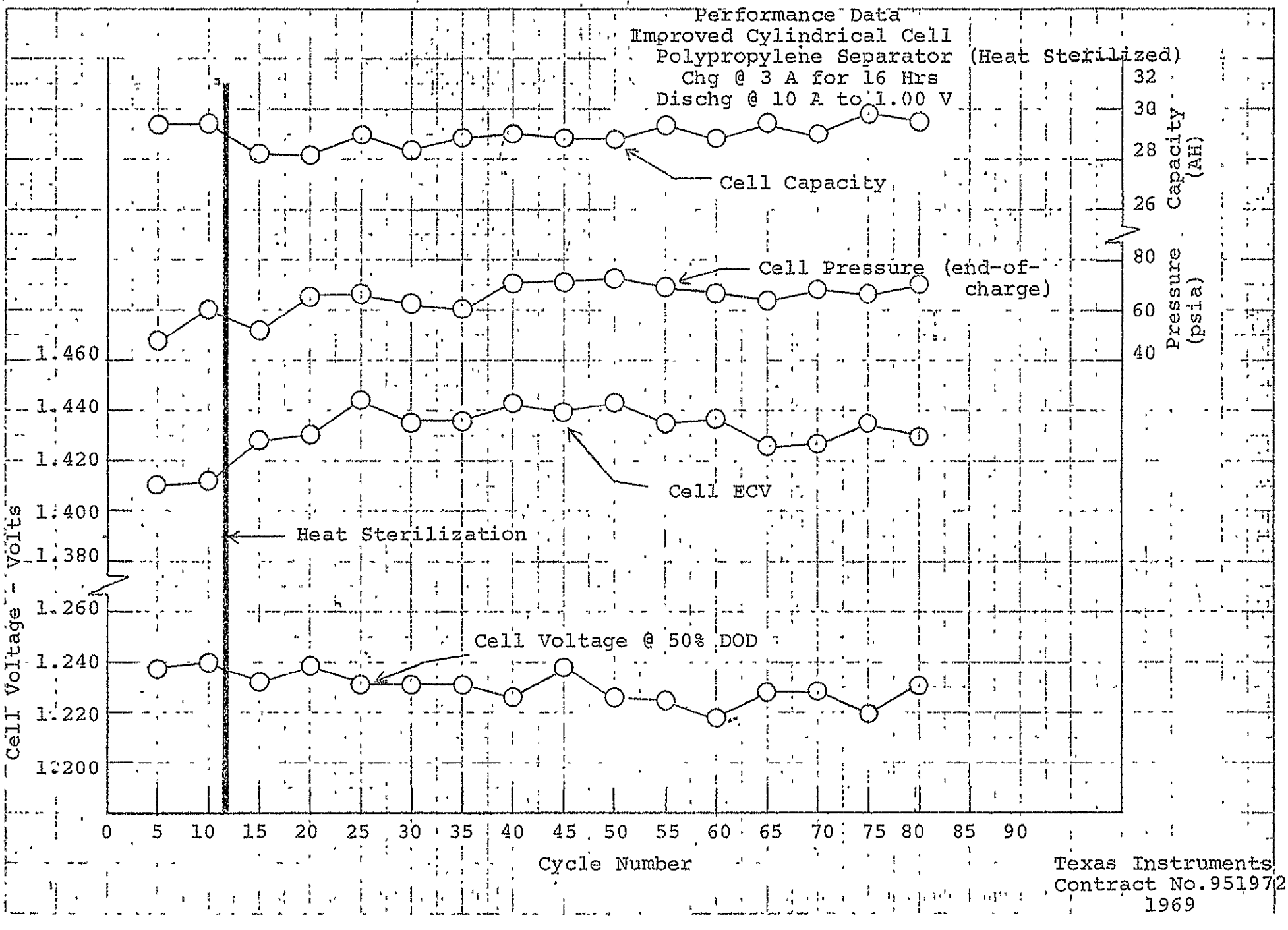

Texas Instruments
Contract No. 951972
1969

FIGURE II-N
Performance Data
Preliminary Design
10 Cylindrical Cells
Polypropylene Separator
Chg @ 3 A for 16 Hrs
Dischg @ 3 A for 1.00 V

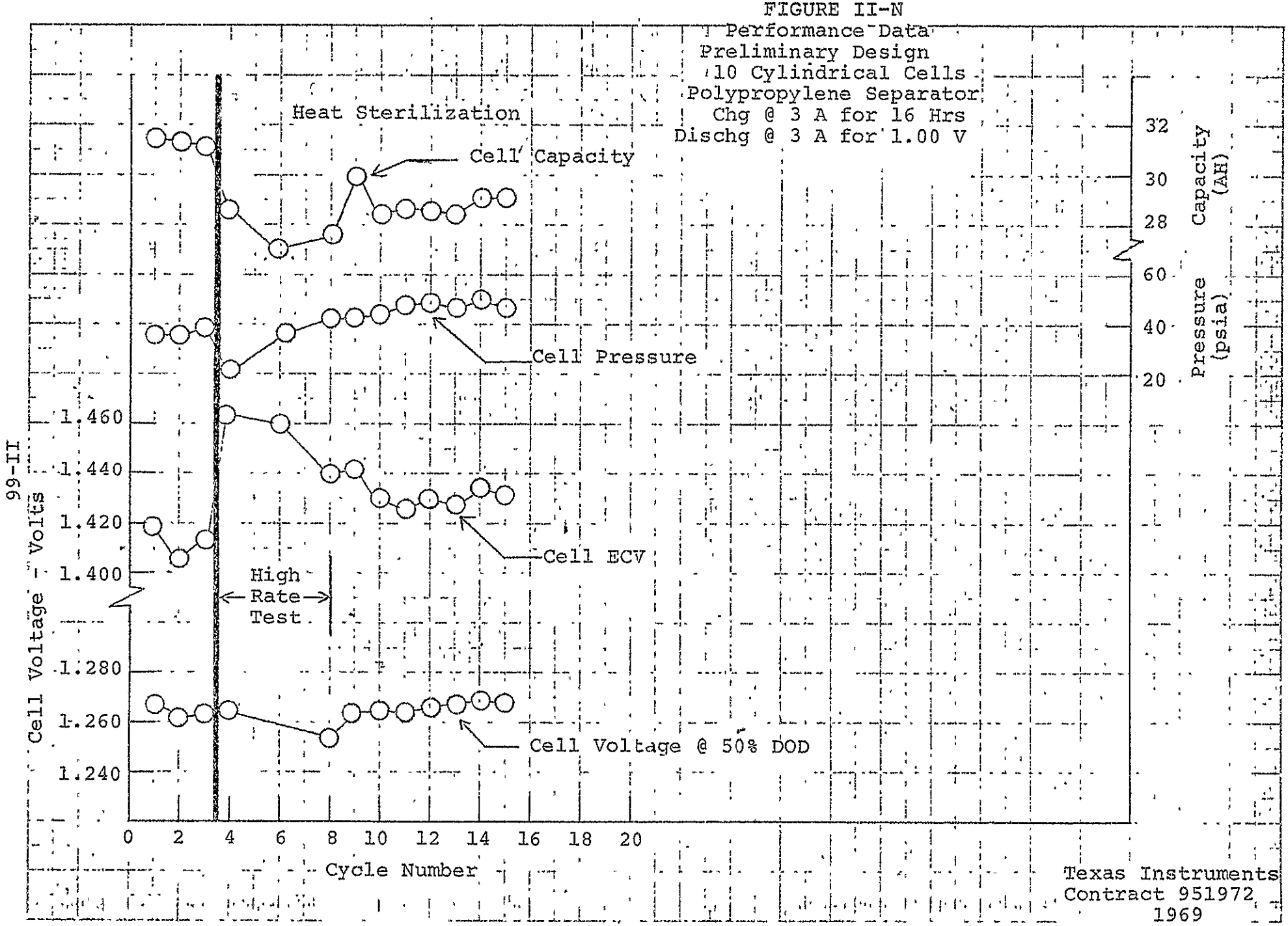

99-II

Texas Instruments
Contract 951972
1969

FIGURE II-O

RELATIONSHIP OF SINTER WEIGHT TO
GAUGE FOR A GIVEN POROSITY

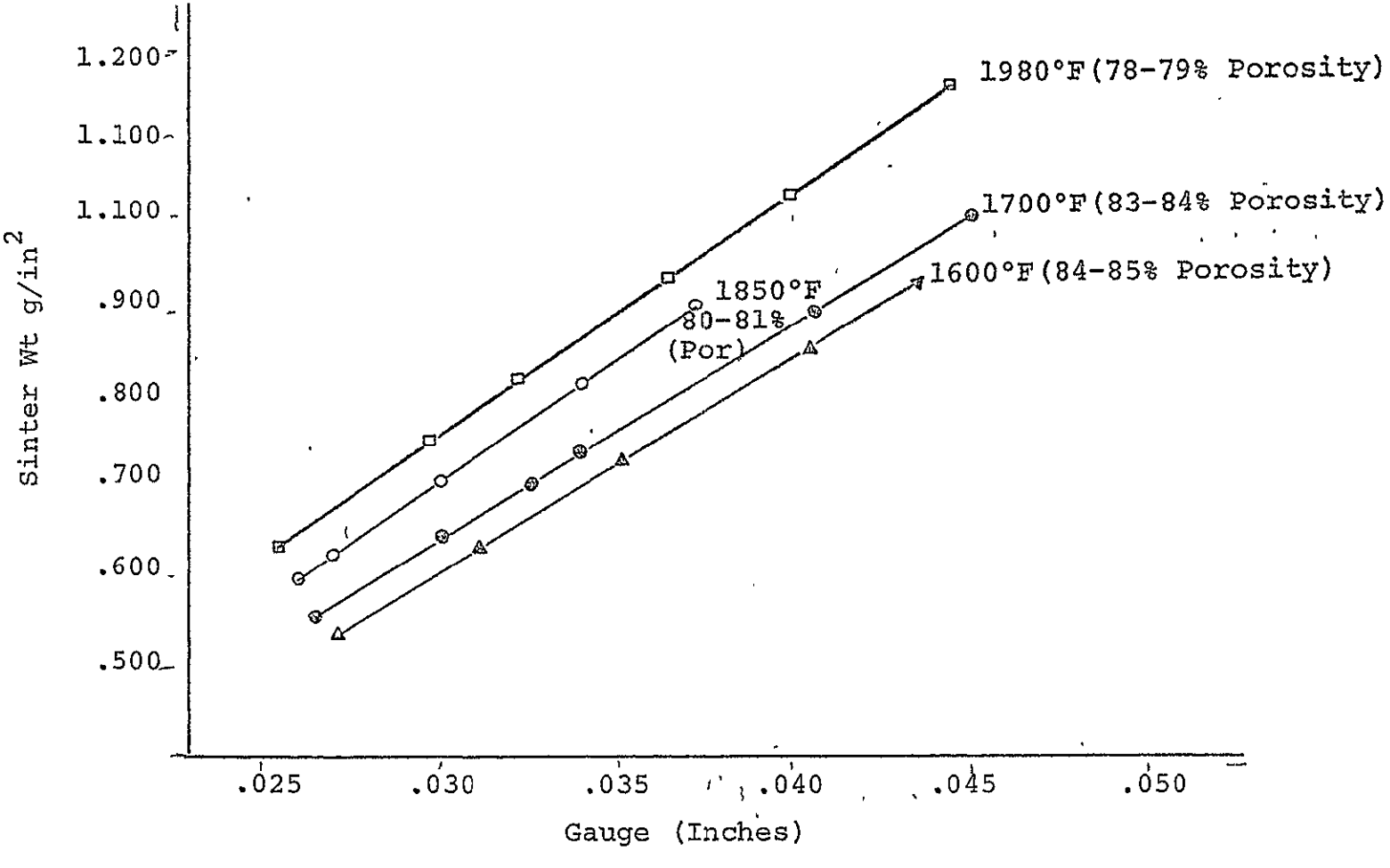

FIGURE II-P

LOADING CHARACTERISTICS

Positive Plate Impregnation

1980°F Sinter (78-79% Porosity)

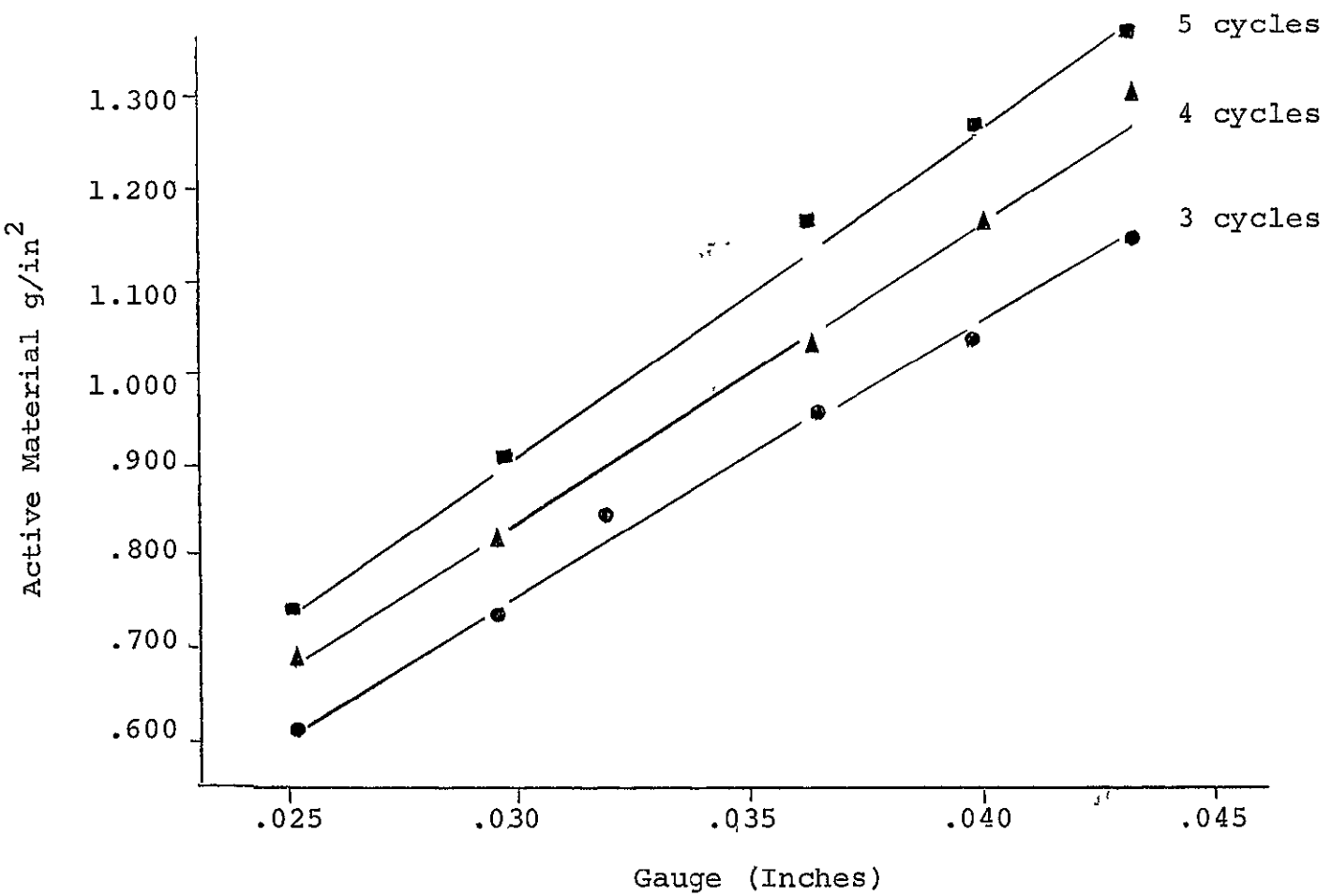

FIGURE II-Q

LOADING CHARACTERISTICS

Positive Plate Impregnation

1850°F Sinter (80-81% Porosity)

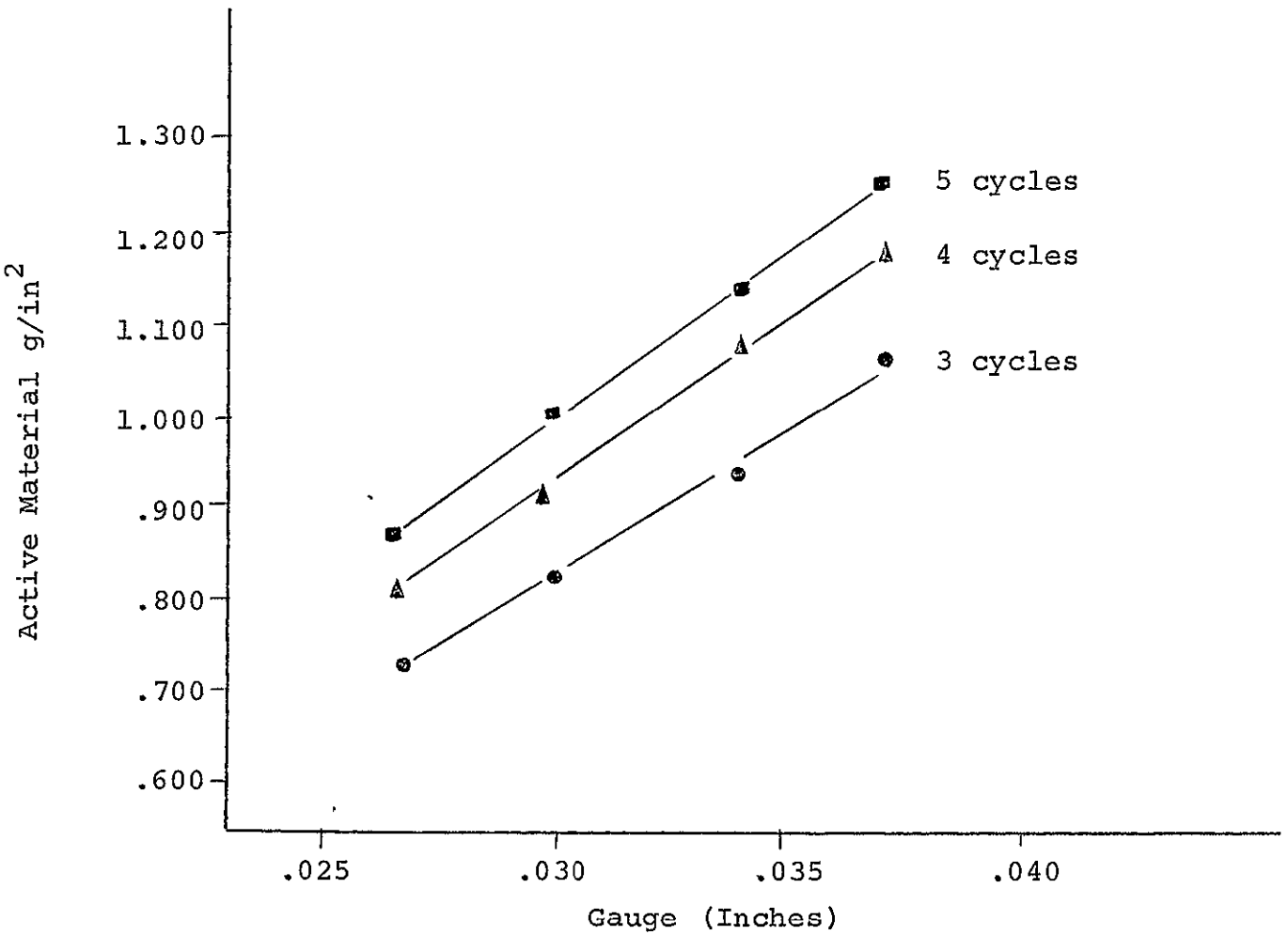

FIGURE II-R

LOADING CHARACTERISTICS

Positive Plate Impregnation

1700°F Sinter (83-84% Porosity)

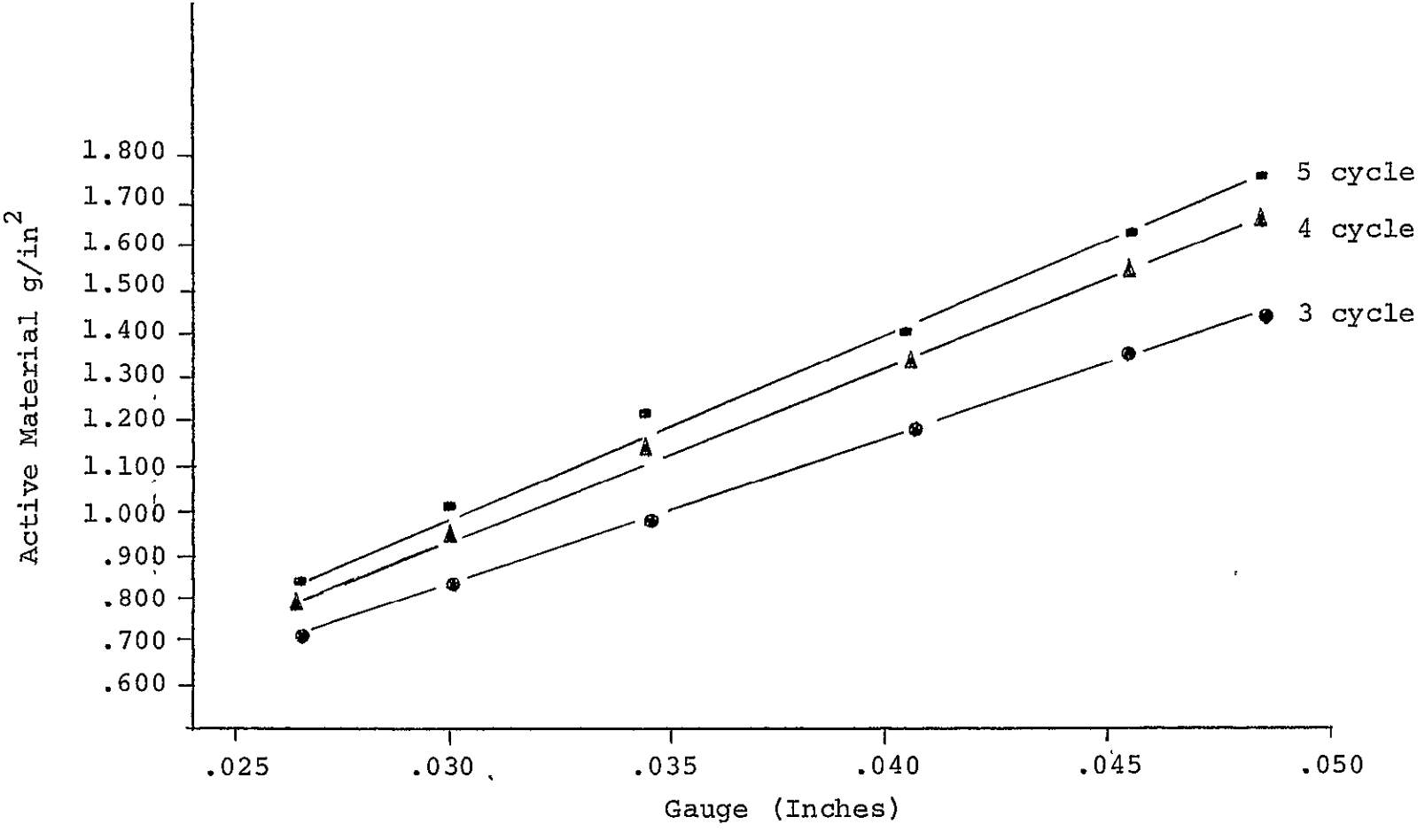

FIGURE II-S

LOADING CHARACTERISTICS

Positive Plate Impregnation

1600°F Sinter (84-85% Porosity)

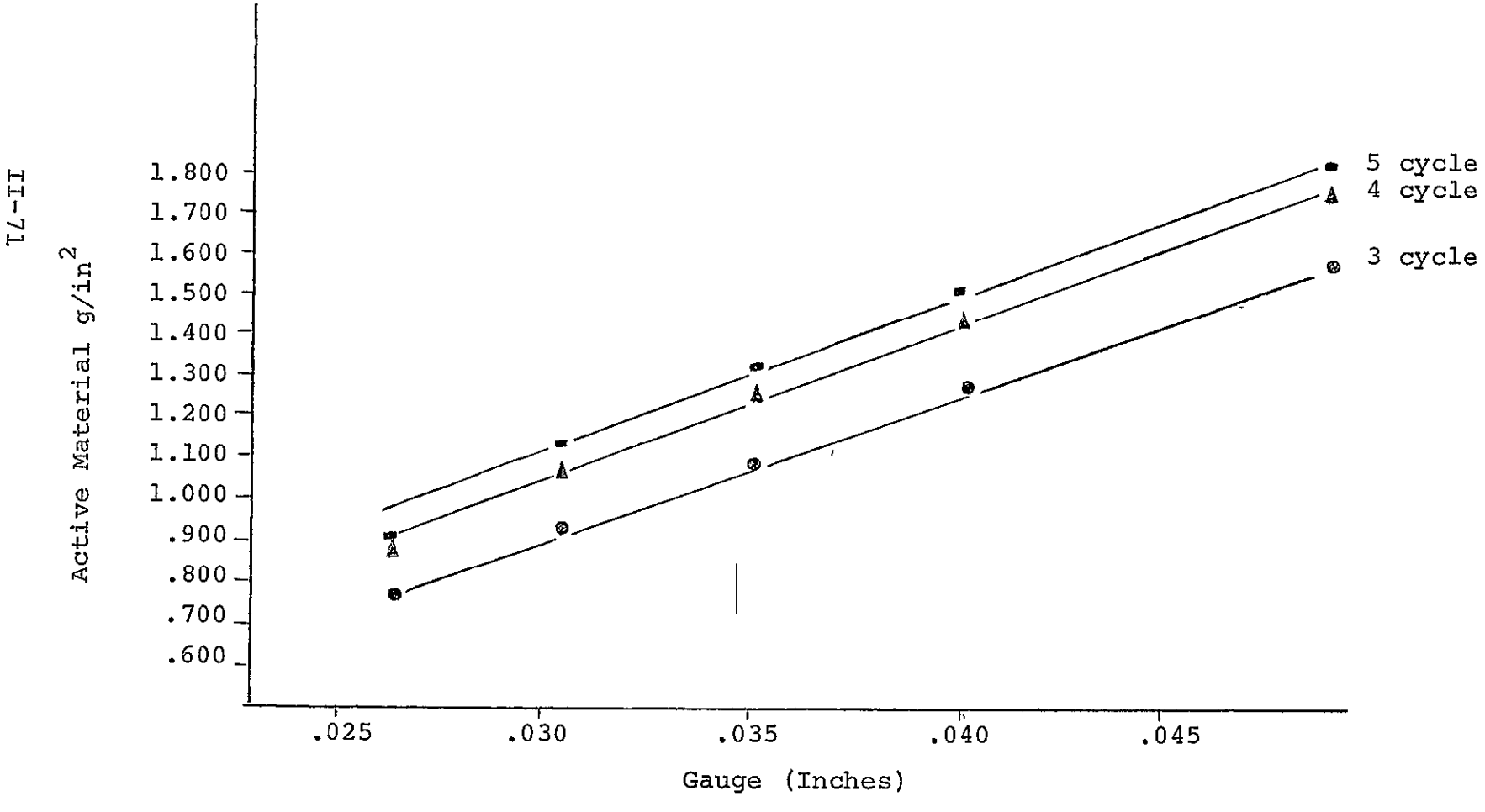

FIGURE II-T

TYPICAL CORROSION OF POSITIVE IMPREGNATED PLAQUE
PRODUCED AT VARIOUS SINTERING TEMPERATURES

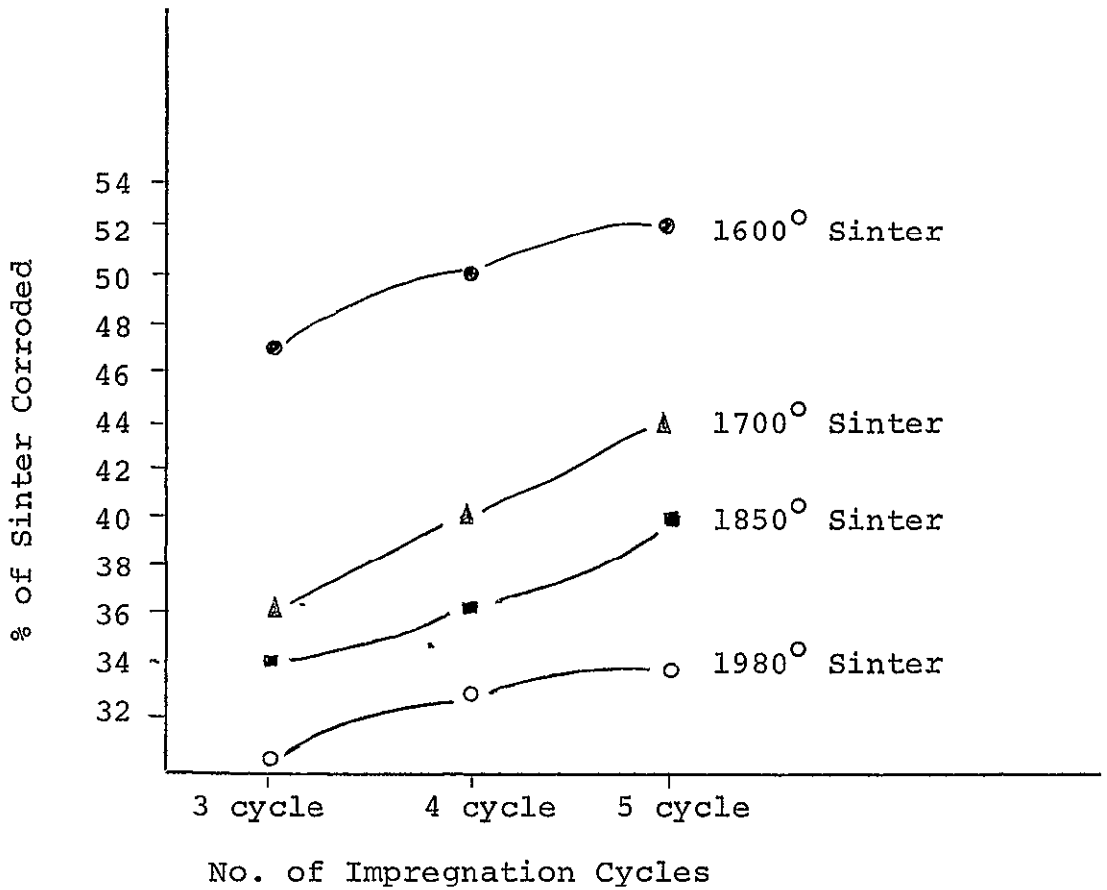

FIGURE II-U

PROJECTED HIGHER ENERGY DENSITY Ni-Cd CELL (HEAT STERILIZED)

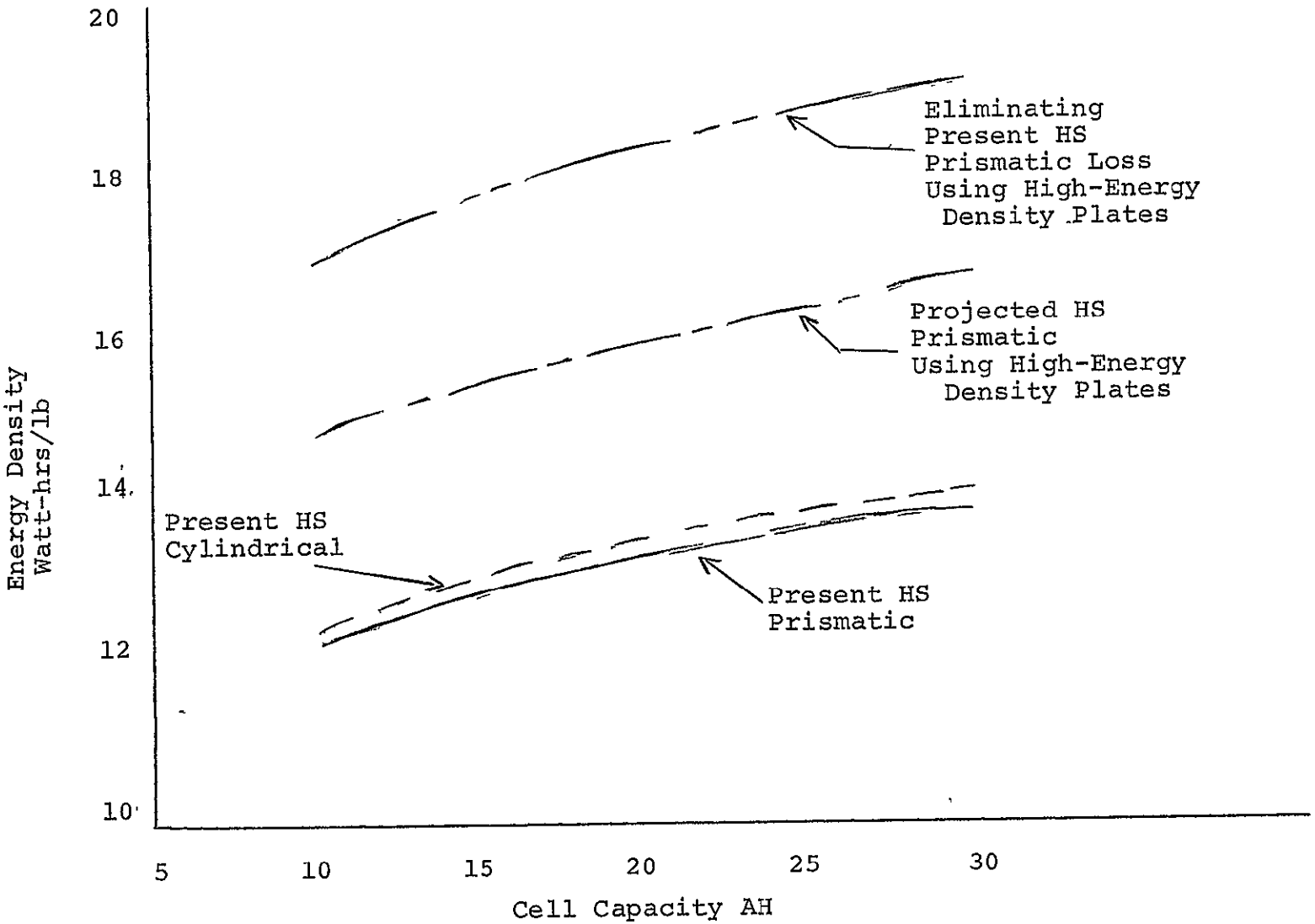

FIGURE II-V

HIGH ENERGY DENSITY PLATE
FACTORIAL EXPERIMENT OUTLINE

INDEPENDENT VARIABLES

TEST SEQUENCE I

Factor Ident.	Independent Variables	Levels 0	1
A	Porosity	78.9 - 80.7%	83.1 - 84.6%
B	Ratio	2.19 - 2.38	3.16 - 3.20
C	Electrolyte Fill Level	60%	70%

TEST SEQUENCE II

A & B	As above		
C	Electrolyte Fill Level	60%	80%

TEST SEQUENCE III

A & B	As above		
C	Electrolyte Fill Level	70%	80%

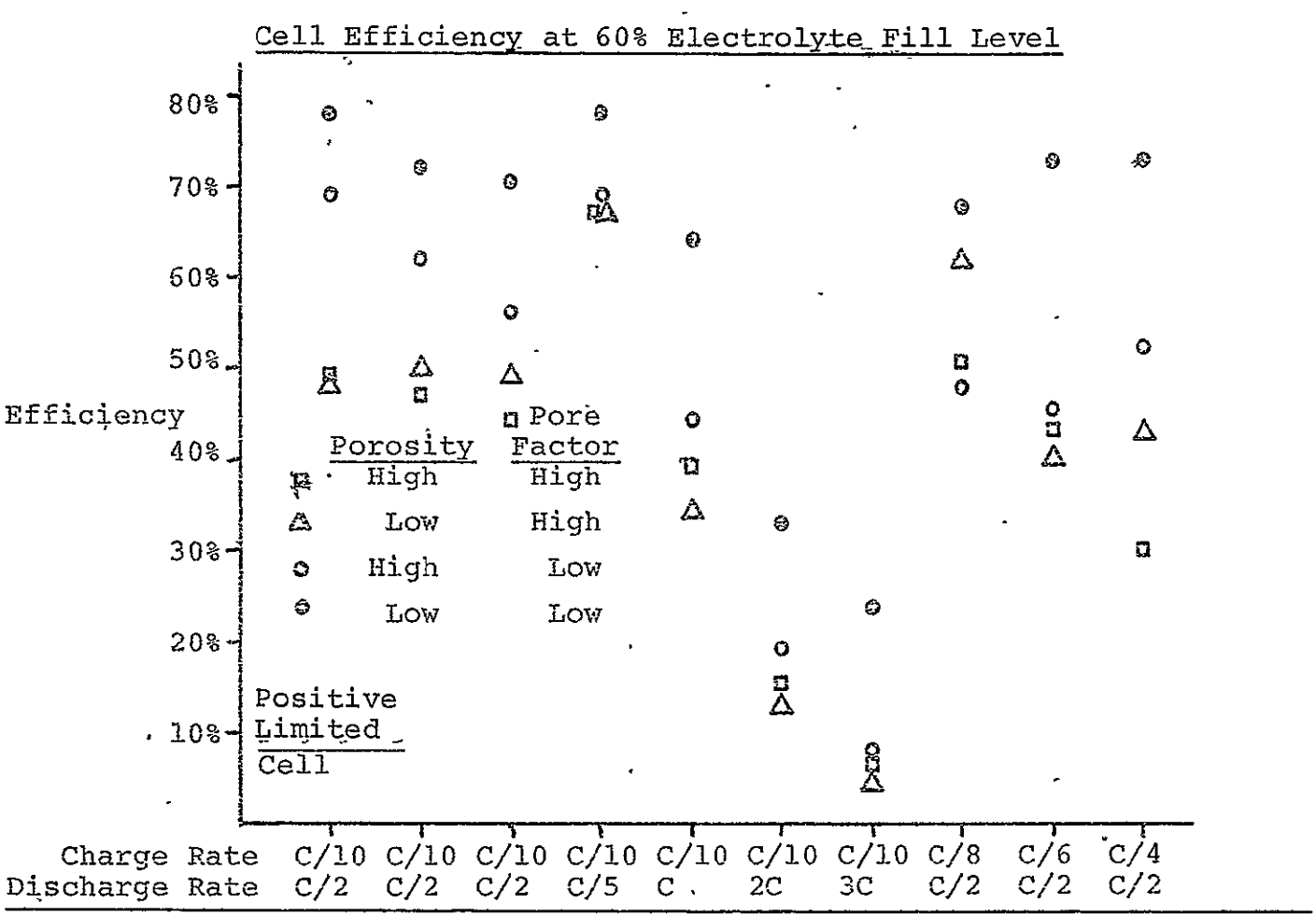
Cell Efficiency at 60% Electrolyte Fill Level
80%
70%
60%
50%
40%
30%
20%
10%
Efficiency
Porosity
Pore Factor
High High
Low High
High Low
Low Low
Positive Limited Cell
Charge Rate C/10 C/10 C/10 C/10 C/10 C/10 C/10 C/8 C/6 C/4
Discharge Rate C/2 C/2 C/2 C/5 C 2C 3C C/2 C/2 C/2

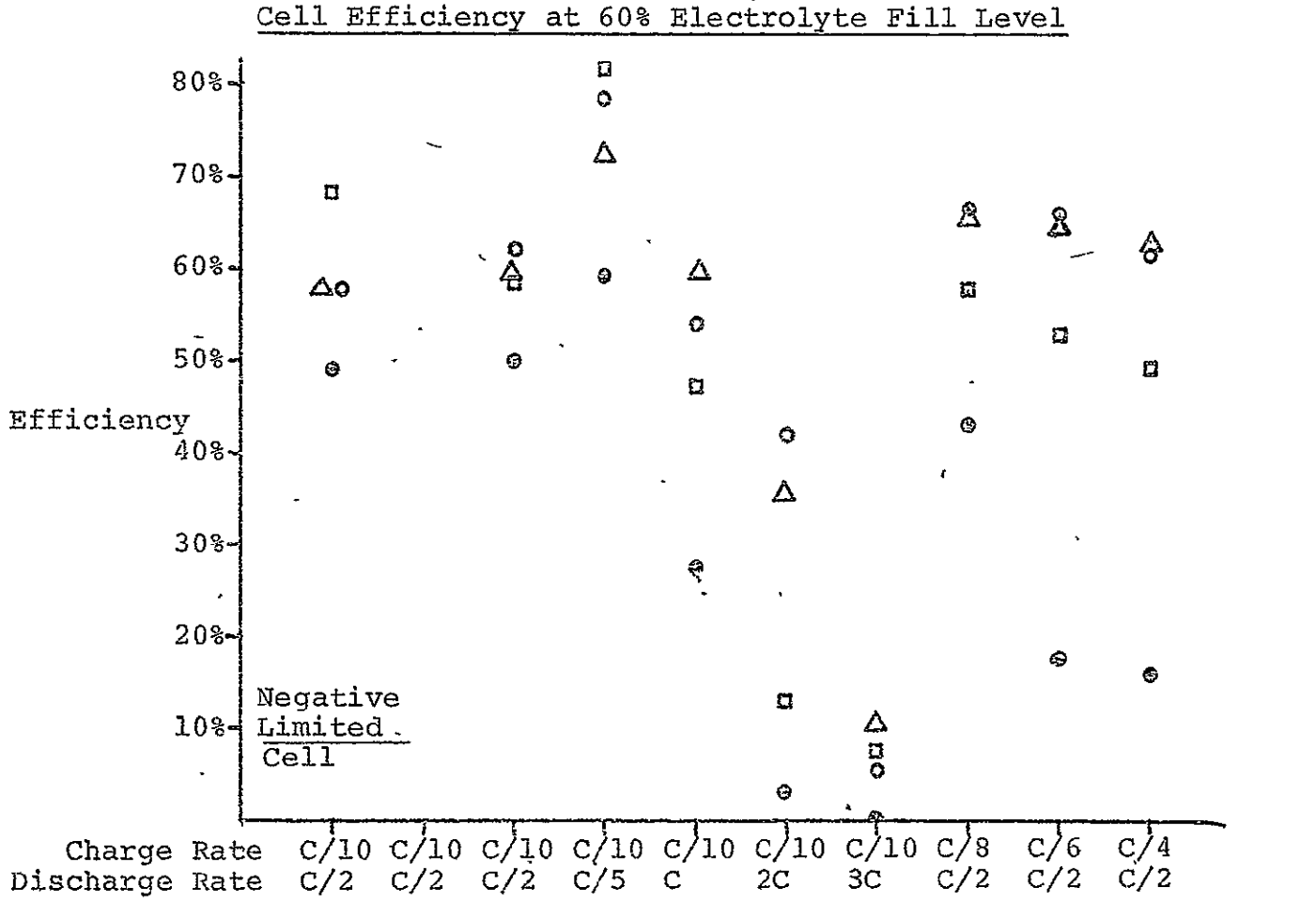
Cell Efficiency at 60% Electrolyte Fill Level
80%
70%
60%
50%
40%
30%
20%
10%
Efficiency
Negative Limited Cell
Charge Rate C/10 C/10 C/10 C/10 C/10 C/10 C/10 C/8 C/6 C/4
Discharge Rate C/2 C/2 C/2 C/5 C 2C 3C C/2 C/2 C/2

FIGURE II-W

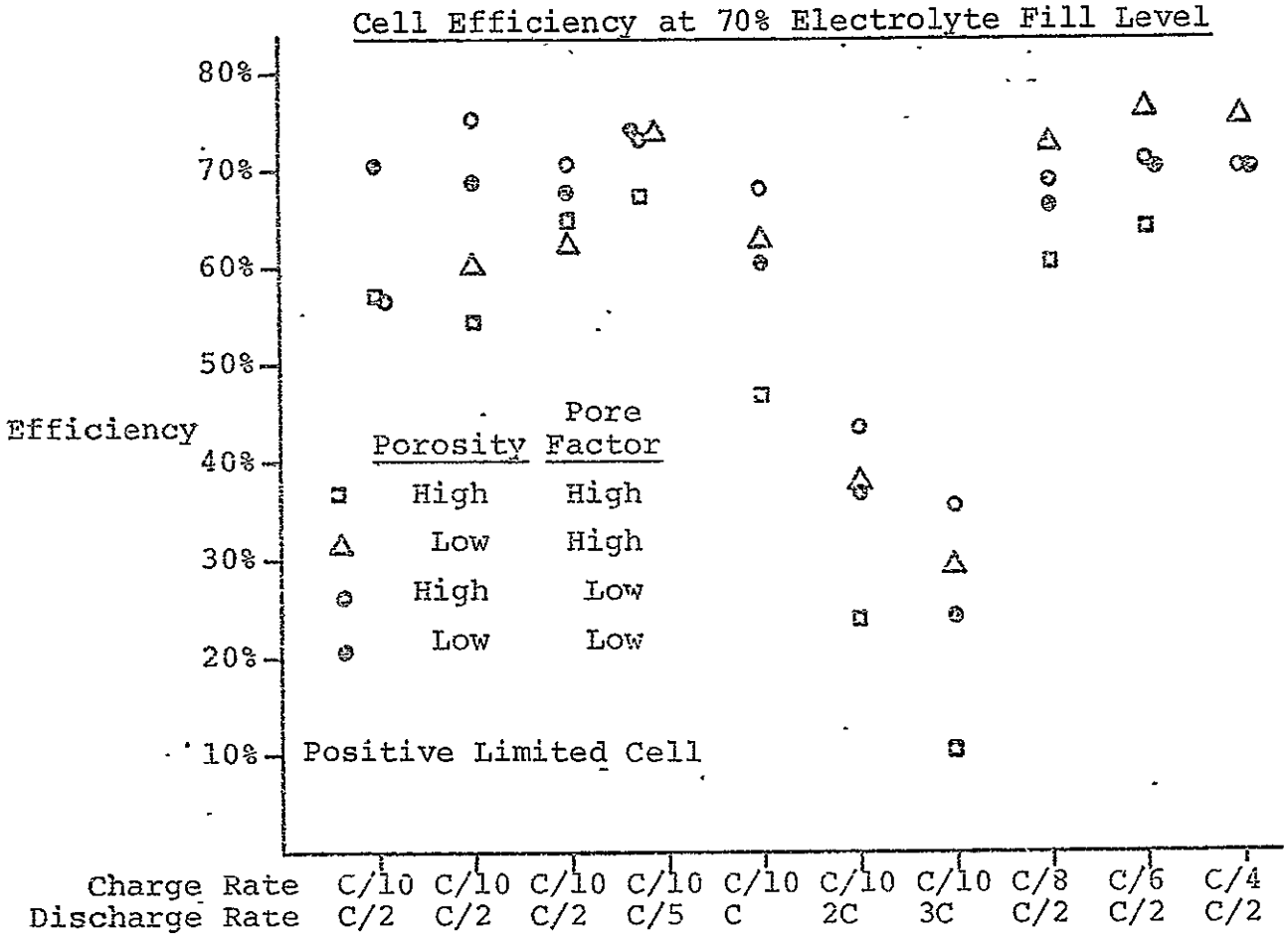
Cell Efficiency at 70% Electrolyte Fill Level
80%
70%
60%
50%
40%
30%
20%
10%
Efficiency
Porosity
Pore Factor
High High
Low High
High Low
Low Low
Positive Limited Cell
Charge Rate C/10 C/10 C/10 C/10 C/10 C/10 C/10 C/8 C/6 C/4
Discharge Rate C/2 C/2 C/2 C/5 C 2C 3C C/2 C/2 C/2

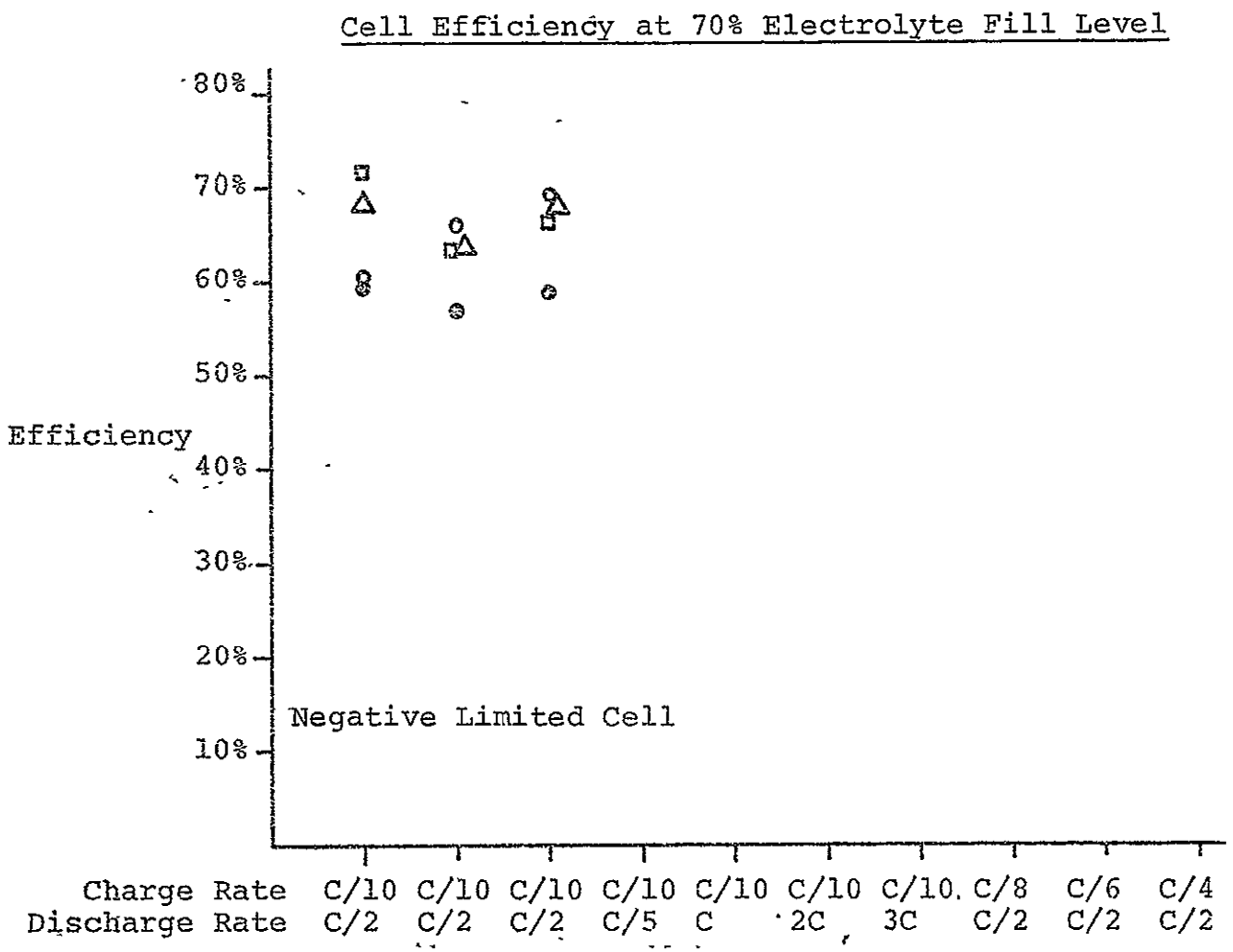
Cell Efficiency at 70% Electrolyte Fill Level
80%
70%
60%
50%
40%
30%
20%
10%
Efficiency
Negative Limited Cell
Charge Rate C/10 C/10 C/10 C/10 C/10 C/10 C/10 C/8 C/6 C/4
Discharge Rate C/2 C/2 C/2 C/5 C 2C 3C C/2 C/2 C/2

FIGURE II-X

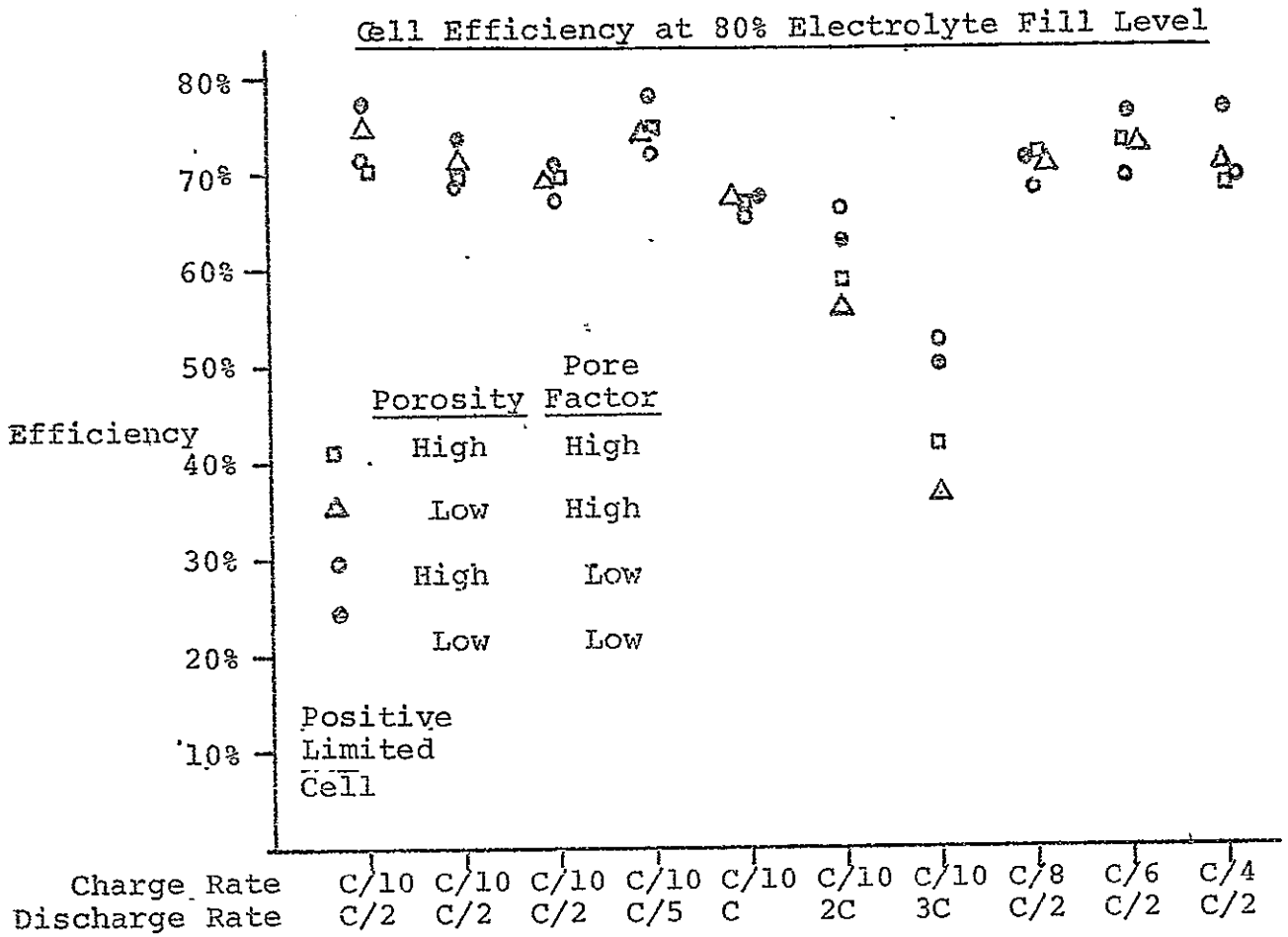
Cell Efficiency at 80% Electrolyte Fill Level
80%
70%
60%
50%
40%
30%
20%
10%
Efficiency
Porosity
Pore Factor
High High
Low High
High Low
Low Low
Positive Limited Cell
Charge Rate C/10 C/10 C/10 C/10 C/10 C/10 C/10 C/8 C/6 C/4
Discharge Rate C/2 C/2 C/2 C/5 C 2C 3C C/2 C/2 C/2

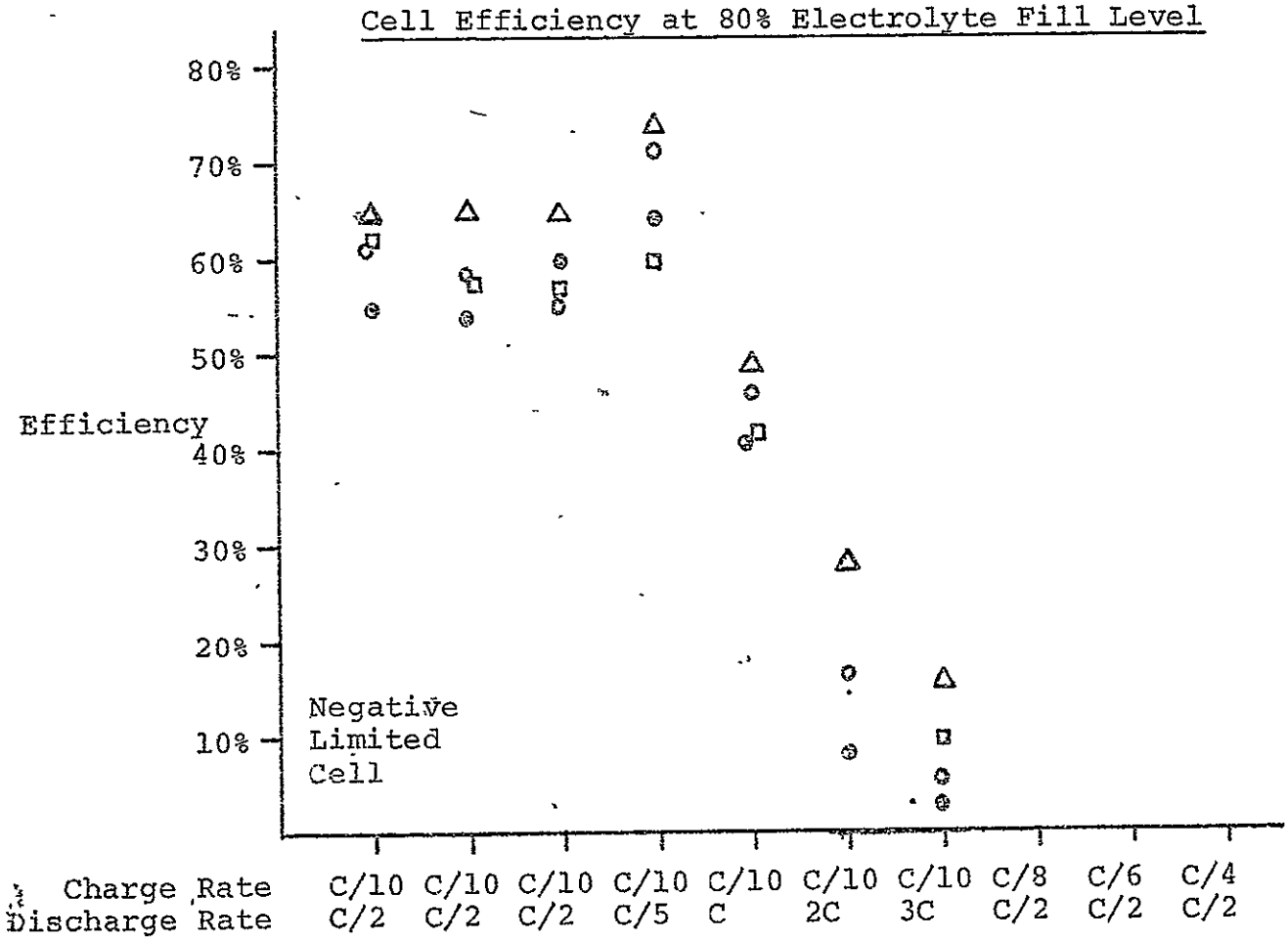
Cell Efficiency at 80% Electrolyte Fill Level
80%
70%
60%
50%
40%
30%
20%
10%
Efficiency
Negative Limited Cell
Charge Rate C/10 C/10 C/10 C/10 C/10 C/10 C/10 C/8 C/6 C/4
Discharge Rate C/2 C/2 C/2 C/5 C 2C 3C C/2 C/2 C/2

FIGURE II-Y

ENGINEERING DESIGN AND EVALUATION

CONTRACT NUMBER 951972

PERFORMED BY TEXAS INSTRUMENTS INCORPORATED

APPENDIX II-B

(LONG-RANGE TEST PROGRAM)

LIST OF FIGURES IN APPENDIX II-B

FIGURE II-AA

LONG RANGE CYCLE TESTING OUTLINE

Charge Rate	Cell Type	Temperature					
		30°F		50°F		70°F	
		Depth of Discharge		Depth of Discharge		Depth of Discharge	
		70%	80%	70%	80%	70%	80%
C/10	Cyl Prism	C-24 P-24	C-23 P-23	C-25 P-20	C-15 P-19	C-12 P-12	C-21 P-13
C/20	Cyl Prism	C-27 P-27	C-28 P-25	C-26 P-21	C-13 P-22	C-10 P-10	C-11 P-11

FIGURE II-BB

LONG-RANGE CYCLE TEST -- CELL LISTING (Numberical Order)

Cell No.	Cell Type	Test Conditions			Figure Number
		Temp. (°F)	Depth of Discharge (%)	Charge Rate	
C-10	Cyl.	70	70	C/20	II-OO
C-11	Cyl.	70	80	C/20	II-PP
C-12	Cyl.	70	70	C/10	II-QQ
C-13	Cyl.	50	80	C/20	II-RR
C-15	Cyl.	50	80	C/10	II-SS
C-21	Cyl.	70	80	C/10	II-TT
C-23	Cyl.	30	80	C/10	II-UU
C-24	Cyl.	30	70	C/10	II-VV
C-25	Cyl.	50	70	C/10	II-WW
C-26	Cyl.	50	70	C/20	II-XX
C-27	Cyl.	30	70	C/20	II-YY
C-28	Cyl.	30	80	C/20	II-ZZ
P-10	Prism.	70	70	C/20	II-CC
P-11	Prism.	70	80	C/20	II-DD
P-12	Prism.	70	70	C/10	II-EE
P-13	Prism.	70	80	C/10	II-FF
P-19	Prism.	50	80	C/10	II-GG
P-20	Prism.	50	70	C/10	II-HH
P-21	Prism.	50	70	C/20	II-II
P-22	Prism.	50	80	C/20	II-JJ
P-23	Prism.	30	80	C/10	II-KK
P-24	Prism.	30	70	C/10	II-LL
P-25	Prism.	30	80	C/20	II-MM
P-27	Prism.	30	70	C/20	II-NN

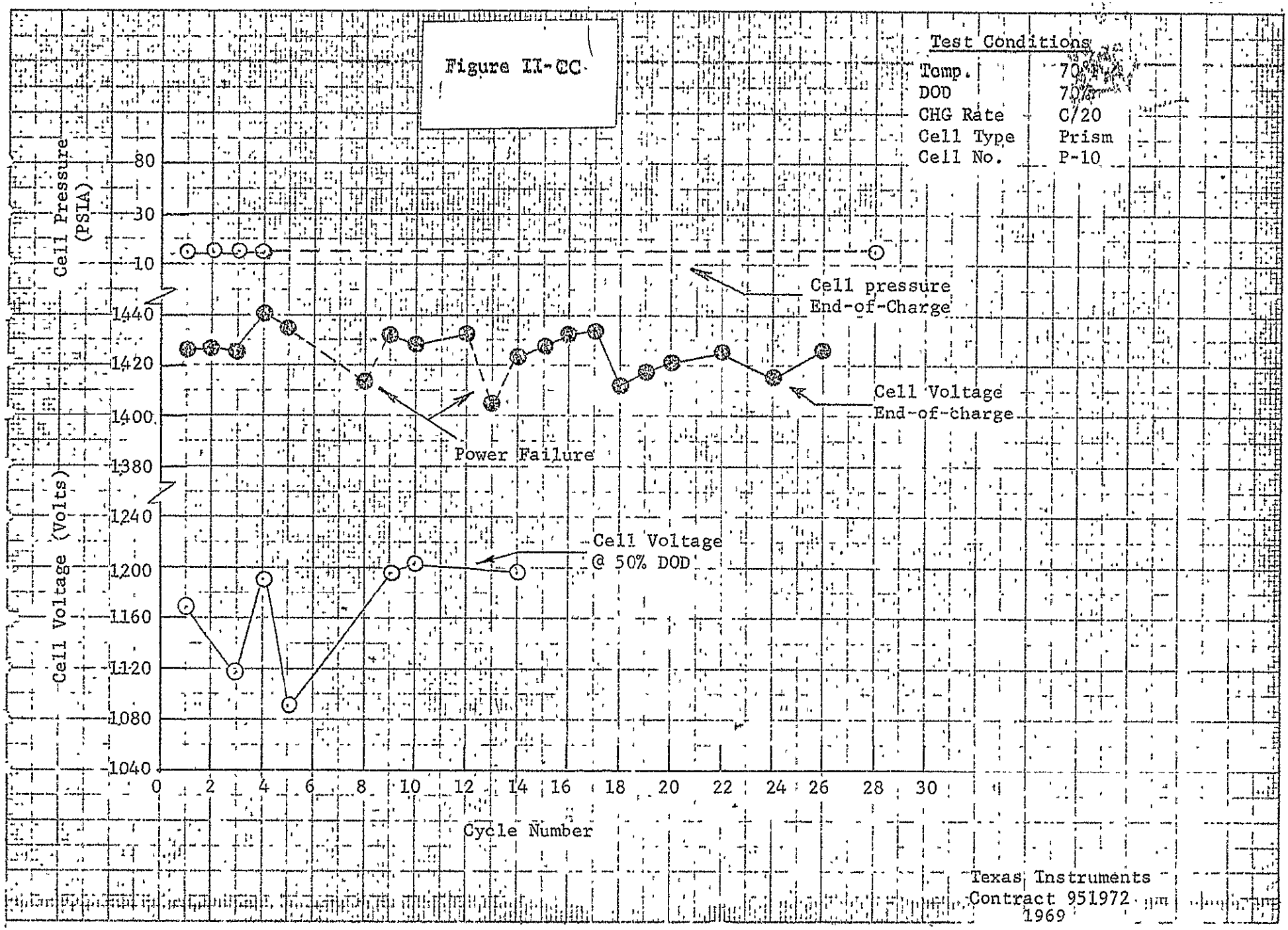
Figure II-CC
Test Conditions
Temp. 70°F
DOD 70%
CHG Rate C/20
Cell Type Prism
Cell No. P-10
Cell Pressure (PSIA)
80
30
10
Cell pressure End-of-Charge
1440
1420
1400
1380
Cell Voltage End-of-charge
Power Failure
1240
1200
1160
1120
1080
1040
Cell Voltage (Volts)
Cell Voltage @ 50% DOD
0 2 4 6 8 10 12 14 16 18 20 22 24 26 28 30
Cycle Number
Texas Instruments
Contract 951972
1969

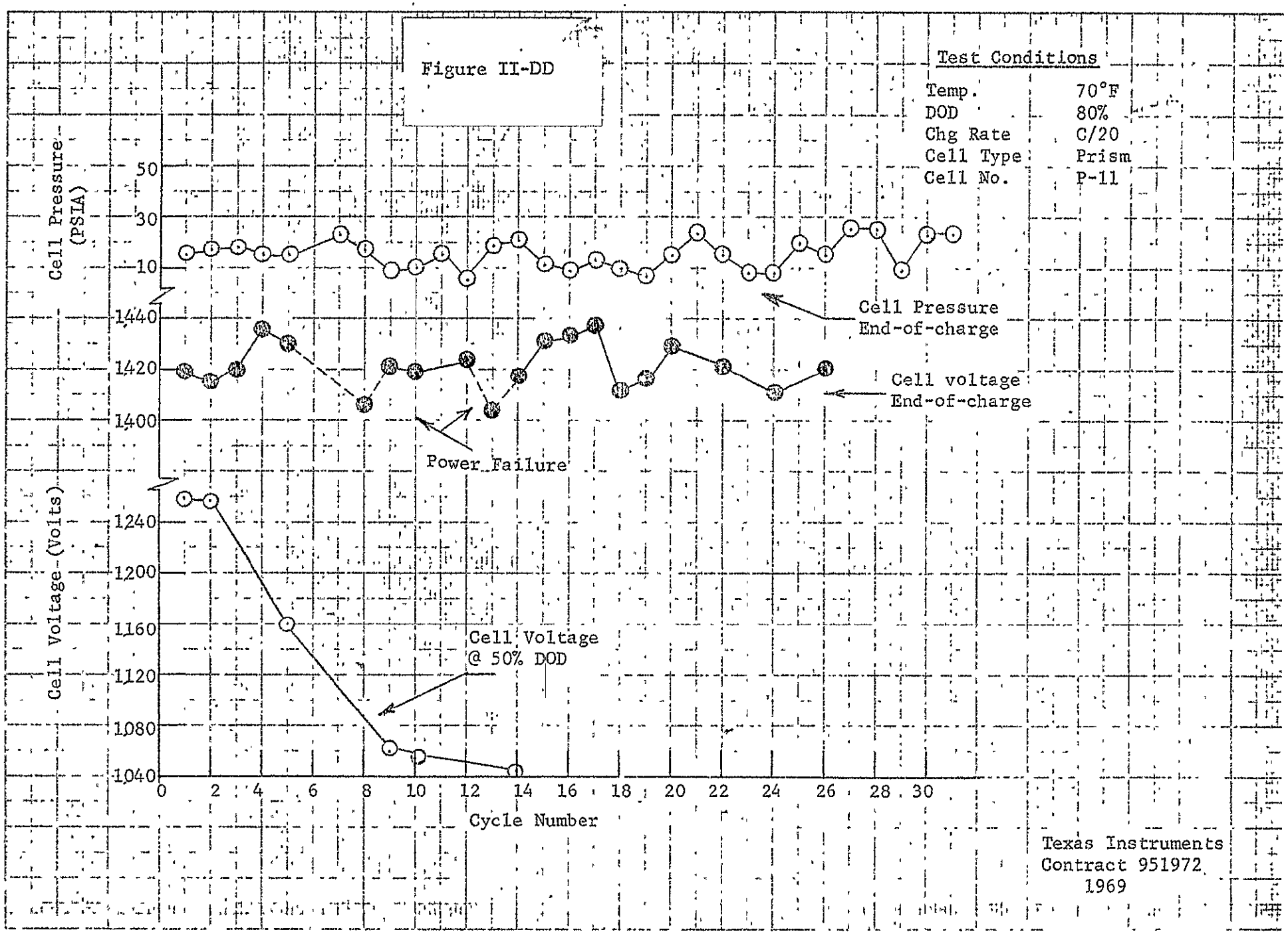
Figure II-DD
Test Conditions
Temp. 70°F
DOD 80%
Chg Rate C/20
Cell Type Prism
Cell No. P-11
Cell Pressure (PSIA)
Cell Voltage (Volts)
50
30
10
1440
1420
1400
1240
1200
1160
1120
1080
1040
0 2 4 6 8 10 12 14 16 18 20 22 24 26 28 30
Cycle Number
Cell Pressure End-of-charge
Cell voltage End-of-charge
Power Failure
Cell Voltage @ 50% DOD
Texas Instruments
Contract 951972
1969

Figure II-EE

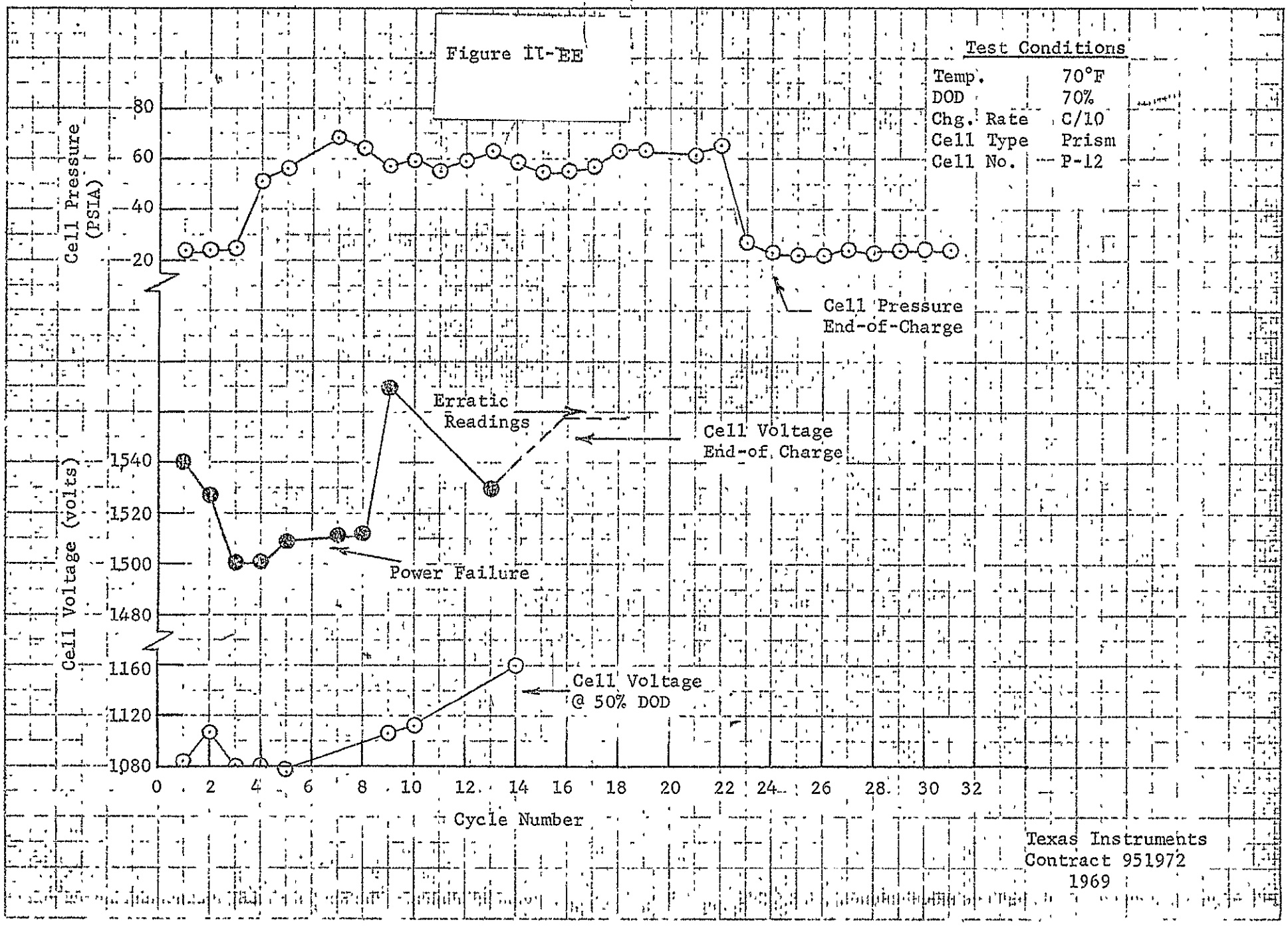
Test Conditions
Temp. 70°F
DOD 70%
Chg. Rate C/10
Cell Type Prism
Cell No. P-12
Cell Pressure (PSIA)
80
60
40
20
Cell Pressure End-of-Charge
Erratic Readings
Cell Voltage End-of-Charge
Cell Voltage (volts)
1540
1520
1500
1480
1160
1120
1080
Power Failure
Cell Voltage @ 50% DOD
0 2 4 6 8 10 12 14 16 18 20 22 24 26 28 30 32
Cycle Number
Texas Instruments
Contract 951972
1969

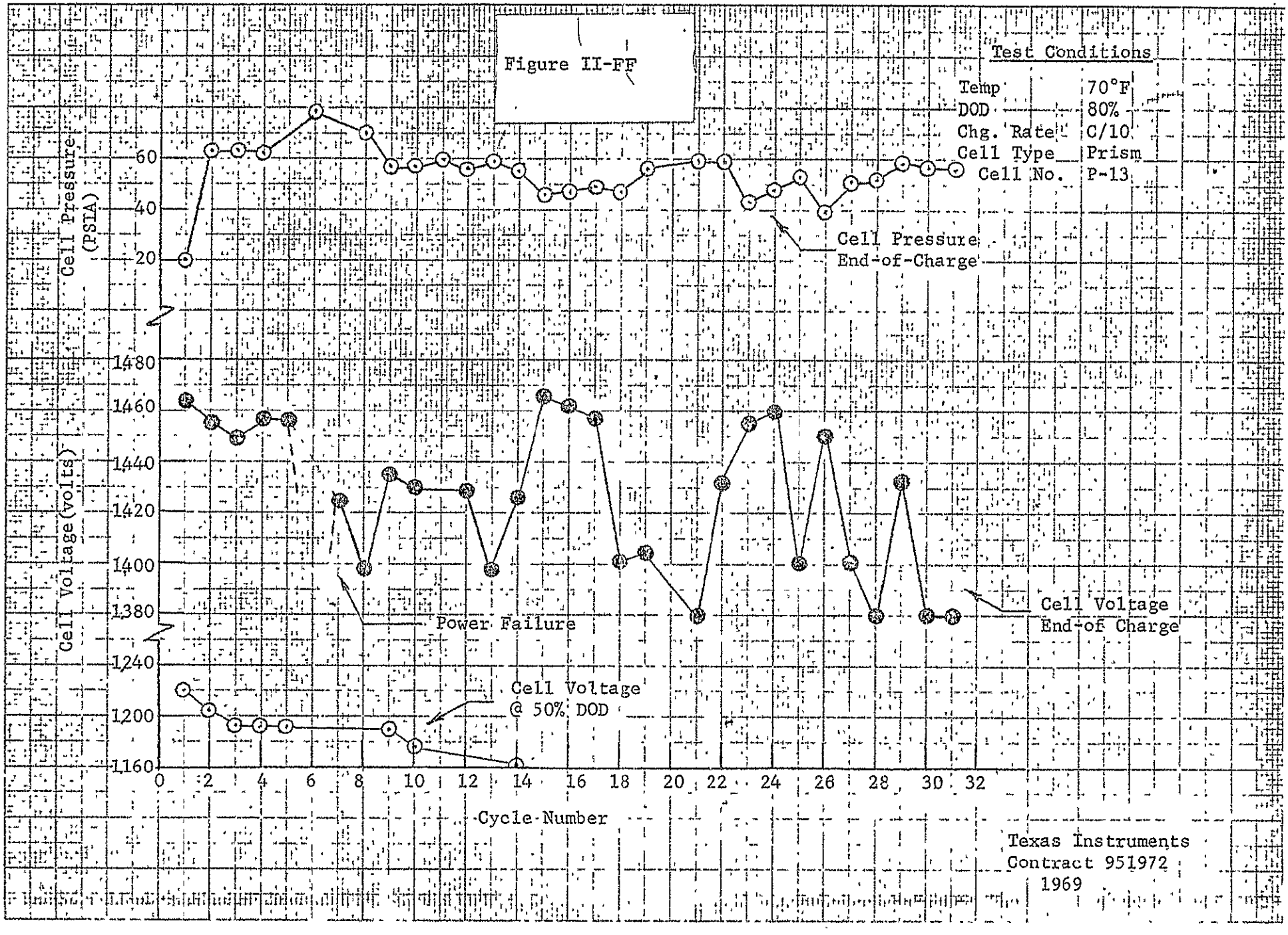
Figure II-FF
Test Conditions
Temp 70°F
DOD 80%
Chg. Rate C/10
Cell Type Prism
Cell No. P-13
Cell Pressure End-of-Charge
Cell Voltage End-of-Charge
Power Failure
Cell Voltage @ 50% DOD
Cell Pressure (PSIA)
Cell Voltage (volts)
Cycle Number
60
40
20
1480
1460
1440
1420
1400
1380
1240
1200
1160
0 2 4 6 8 10 12 14 16 18 20 22 24 26 28 30 32
Texas Instruments
Contract 951972
1969

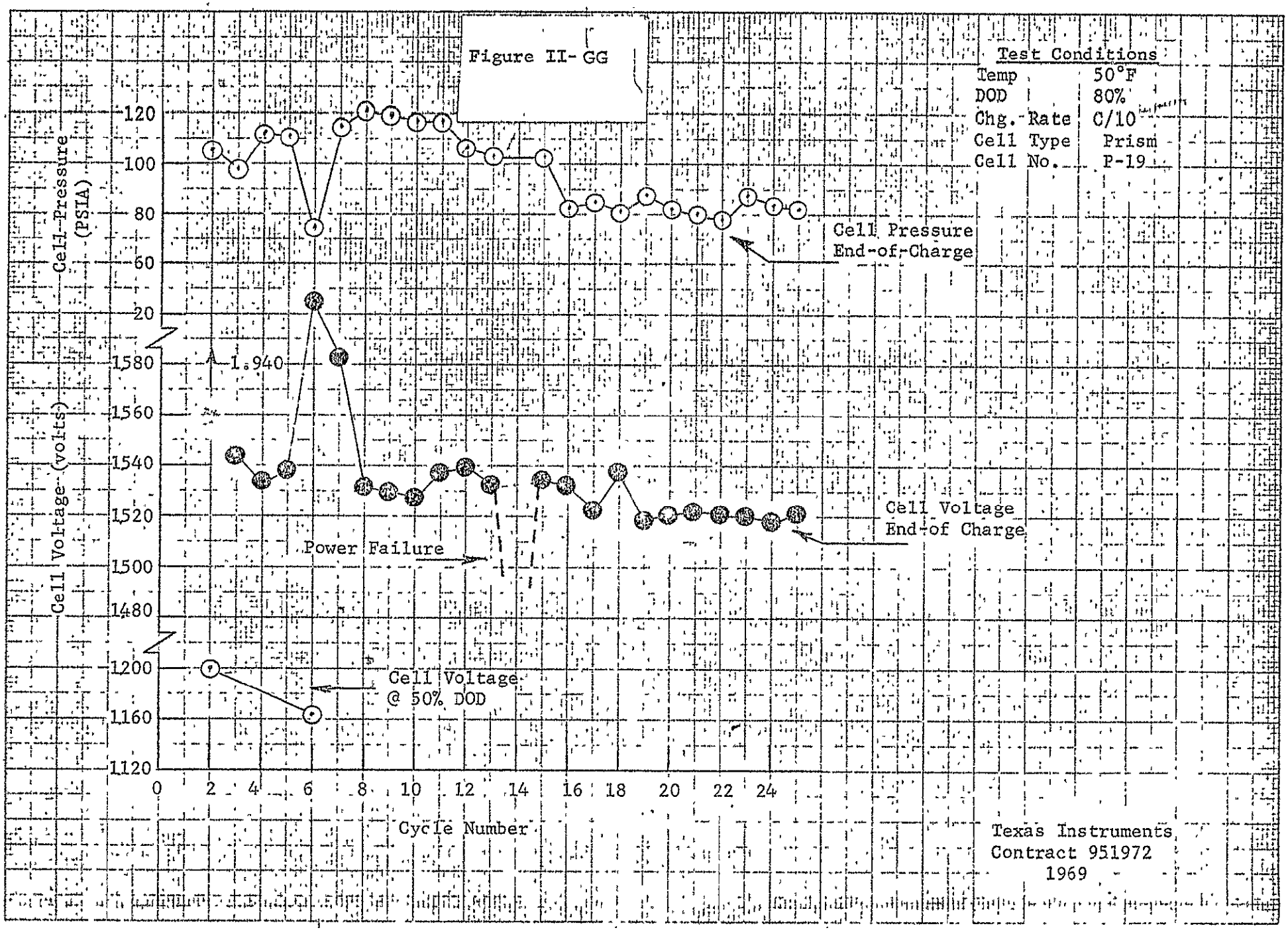
Figure II-GG
Test Conditions
Temp 50°F
DOD 80%
Chg. Rate C/10
Cell Type Prism
Cell No. P-19
Cell Pressure (PSIA)
Cell Voltage (volts)
120
100
80
60
20
1580
1560
1540
1520
1500
1480
1200
1160
1120
1.940
Cell Pressure End-of-Charge
Cell Voltage End-of Charge
Power Failure
Cell Voltage @ 50% DOD
0 2 4 6 8 10 12 14 16 18 20 22 24
Cycle Number
Texas Instruments
Contract 951972
1969

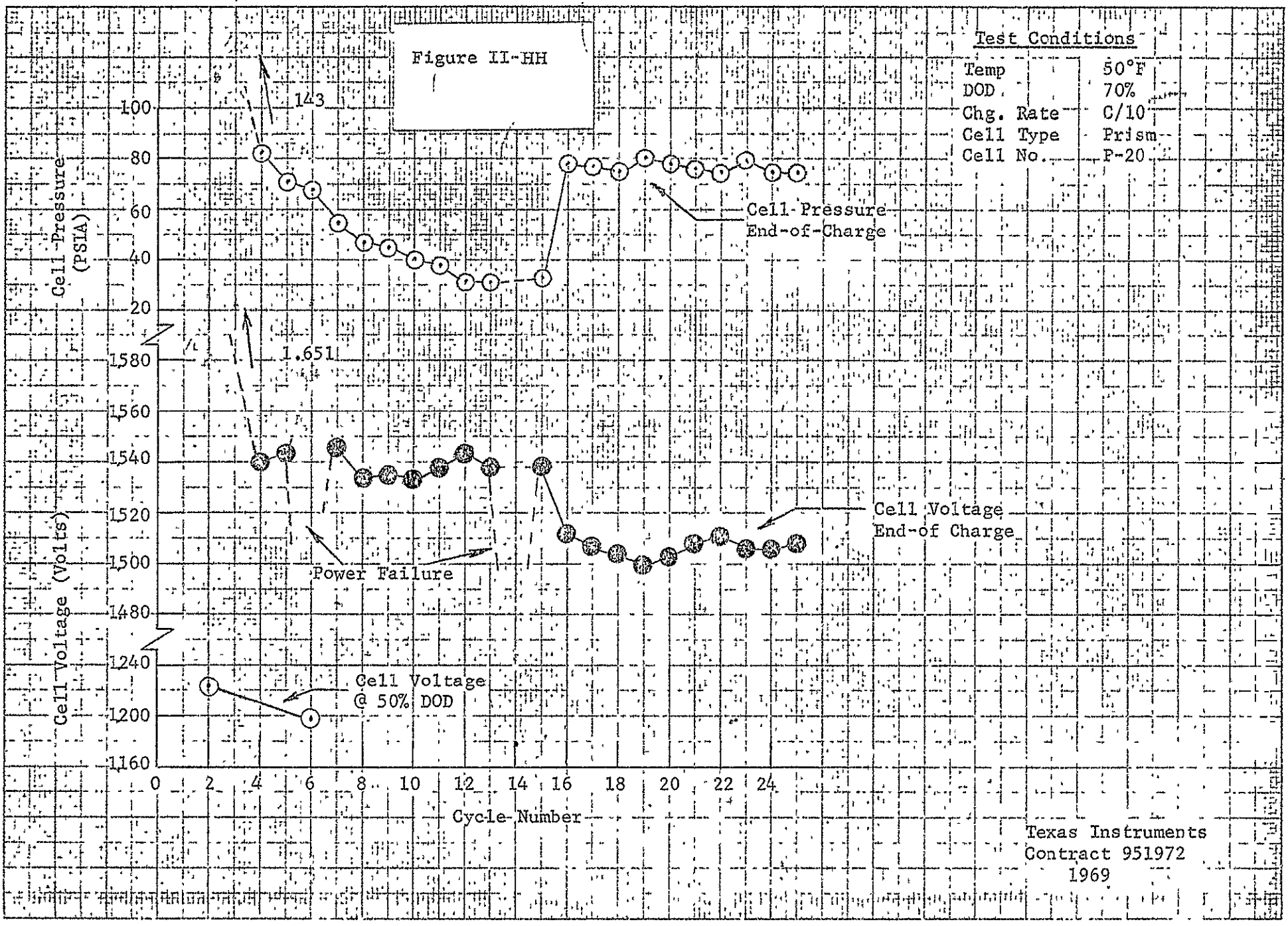
Figure II-HH
Test Conditions
Temp 50°F
DOD 70%
Chg. Rate C/10
Cell Type Prism
Cell No. P-20
143
1.651
Cell Pressure End-of-Charge
Cell Voltage End-of Charge
Power Failure
Cell Voltage @ 50% DOD
Cell Pressure (PSIA)
Cell Voltage (Volts)
Cycle Number
100
80
60
40
20
1580
1560
1540
1520
1500
1480
1240
1200
1160
0
2
4
6
8
10
12
14
16
18
20
22
24
Texas Instruments
Contract 951972
1969

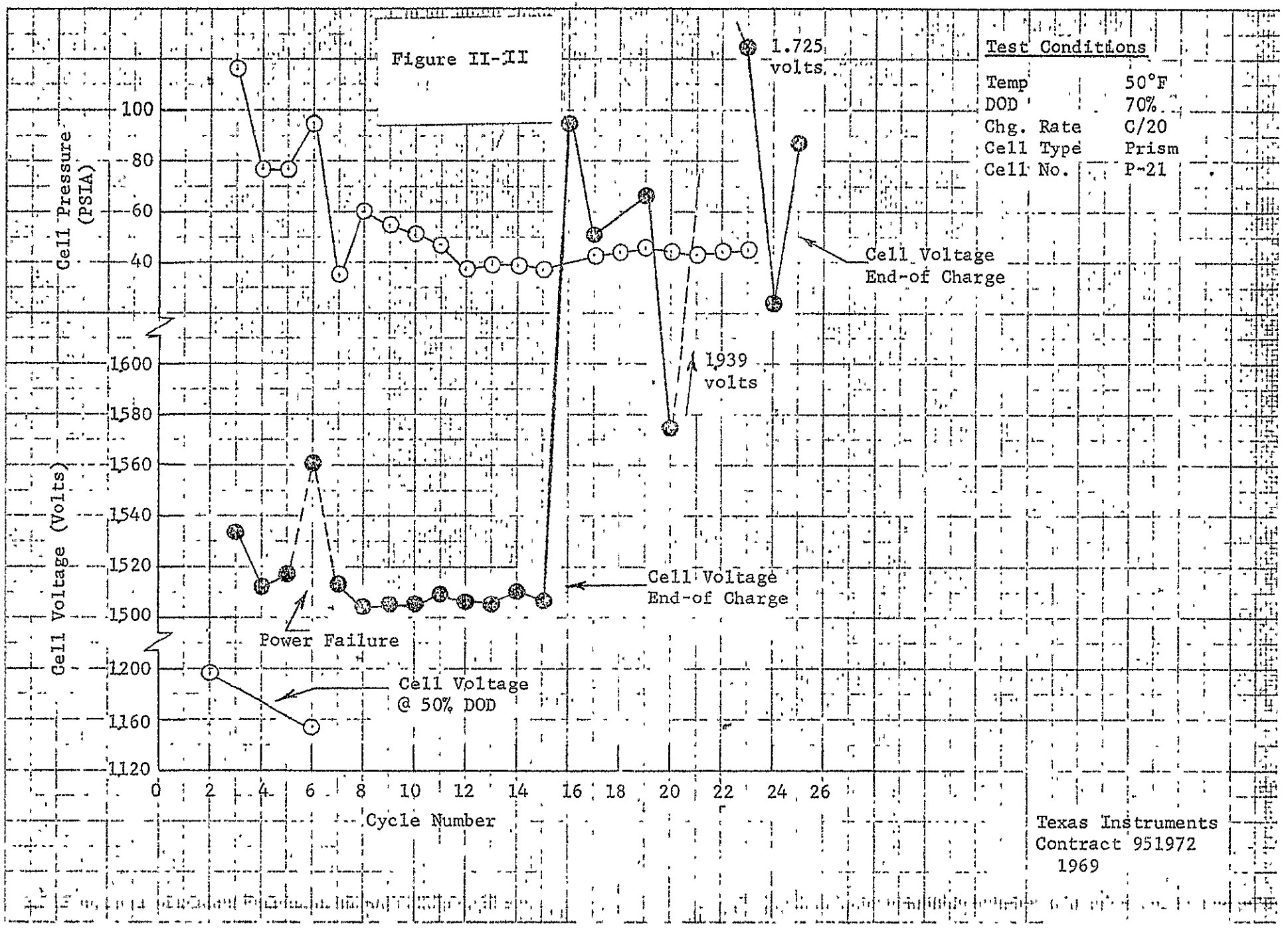
Figure II-II
Cell Pressure (PSIA)
Cell Voltage (Volts)
100
80
60
40
1600
1580
1560
1540
1520
1500
1200
1160
1120
0
2
4
6
8
10
12
14
16
18
20
22
24
26
Cycle Number
1.725 volts
1939 volts
Cell Voltage End-of Charge
Cell Voltage End-of Charge
Power Failure
Cell Voltage @ 50% DOD
Test Conditions
Temp 50°F
DOD 70%
Chg. Rate C/20
Cell Type Prism
Cell No. P-21
Texas Instruments
Contract 951972
1969

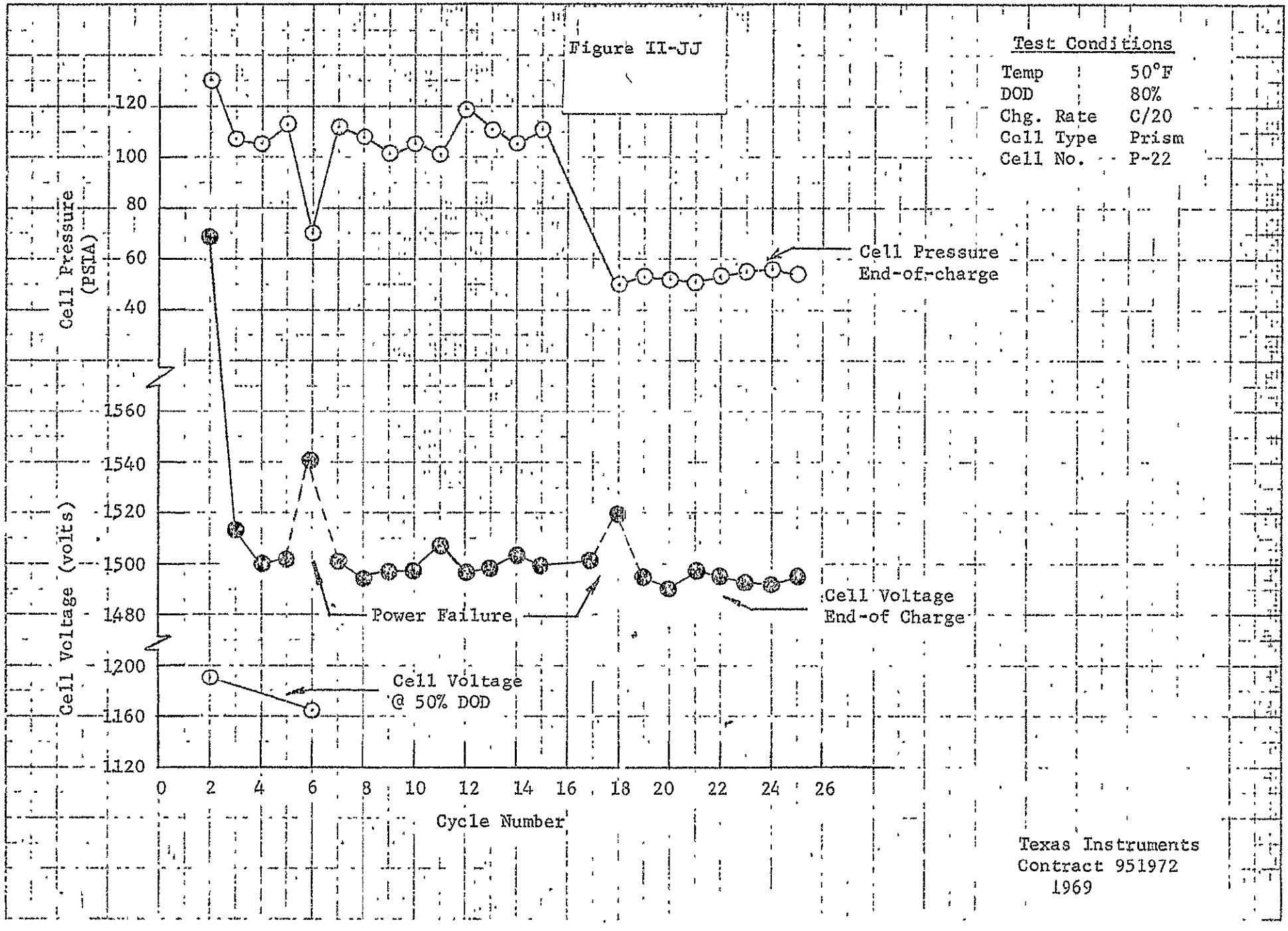
Figure II-JJ
Test Conditions
Temp 50°F
DOD 80%
Chg. Rate C/20
Cell Type Prism
Cell No. P-22
Cell Pressure (PSIA)
120
100
80
60
40
Cell Pressure End-of-charge
Cell Voltage (volts)
1560
1540
1520
1500
1480
1200
1160
1120
Power Failure
Cell Voltage End-of Charge
Cell Voltage @ 50% DOD
0 2 4 6 8 10 12 14 16 18 20 22 24 26
Cycle Number
Texas Instruments
Contract 951972
1969

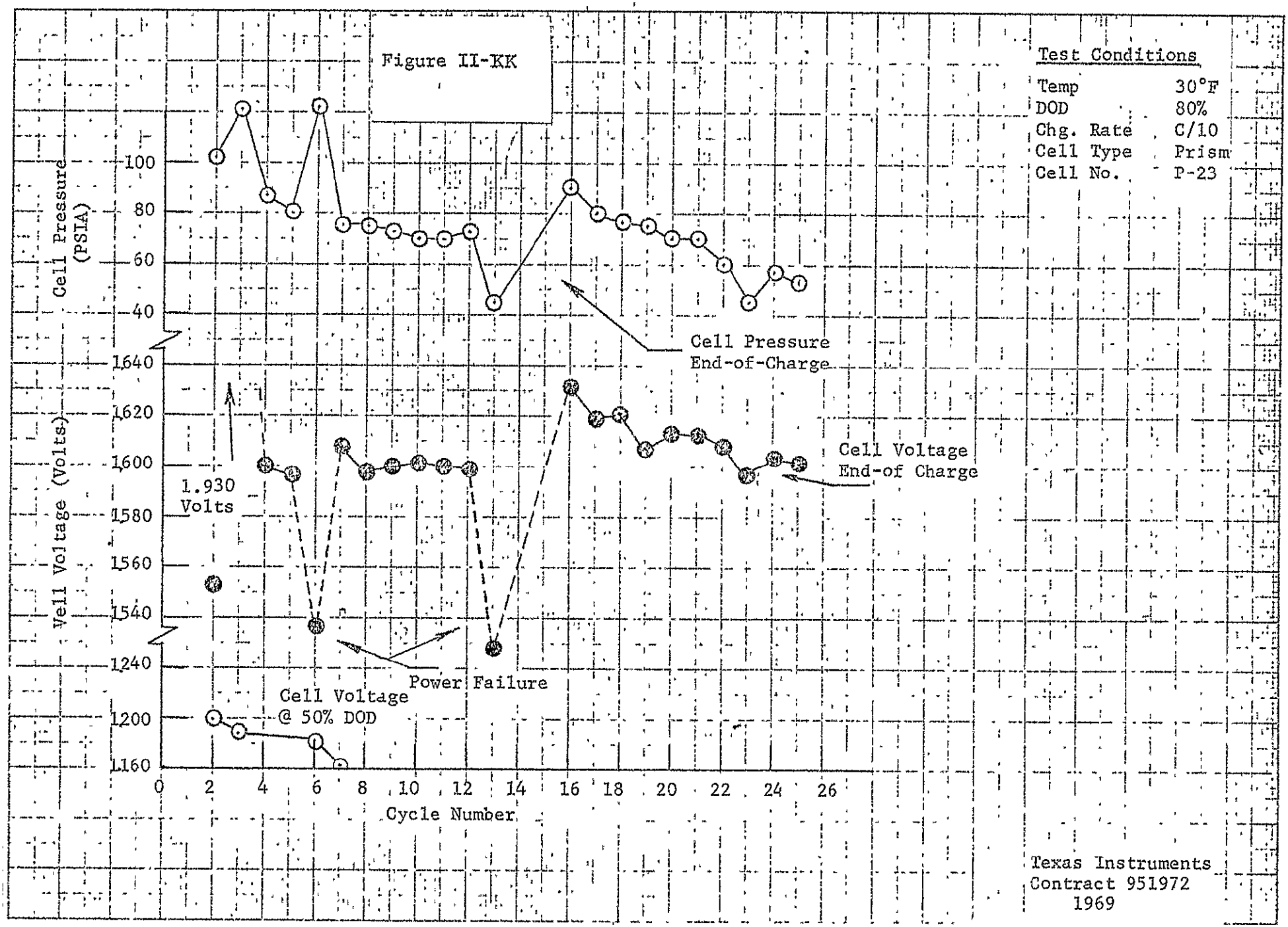
Figure II-KK
Test Conditions
Temp 30°F
DOD 80%
Chg. Rate C/10
Cell Type Prism
Cell No. P-23
Cell Pressure (PSIA)
Cell Voltage (Volts)
100
80
60
40
1640
1620
1600
1580
1560
1540
1240
1200
1160
0 2 4 6 8 10 12 14 16 18 20 22 24 26
Cycle Number
Cell Pressure End-of-Charge
Cell Voltage End-of Charge
1.930 Volts
Power Failure
Cell Voltage @ 50% DOD
Texas Instruments
Contract 951972
1969

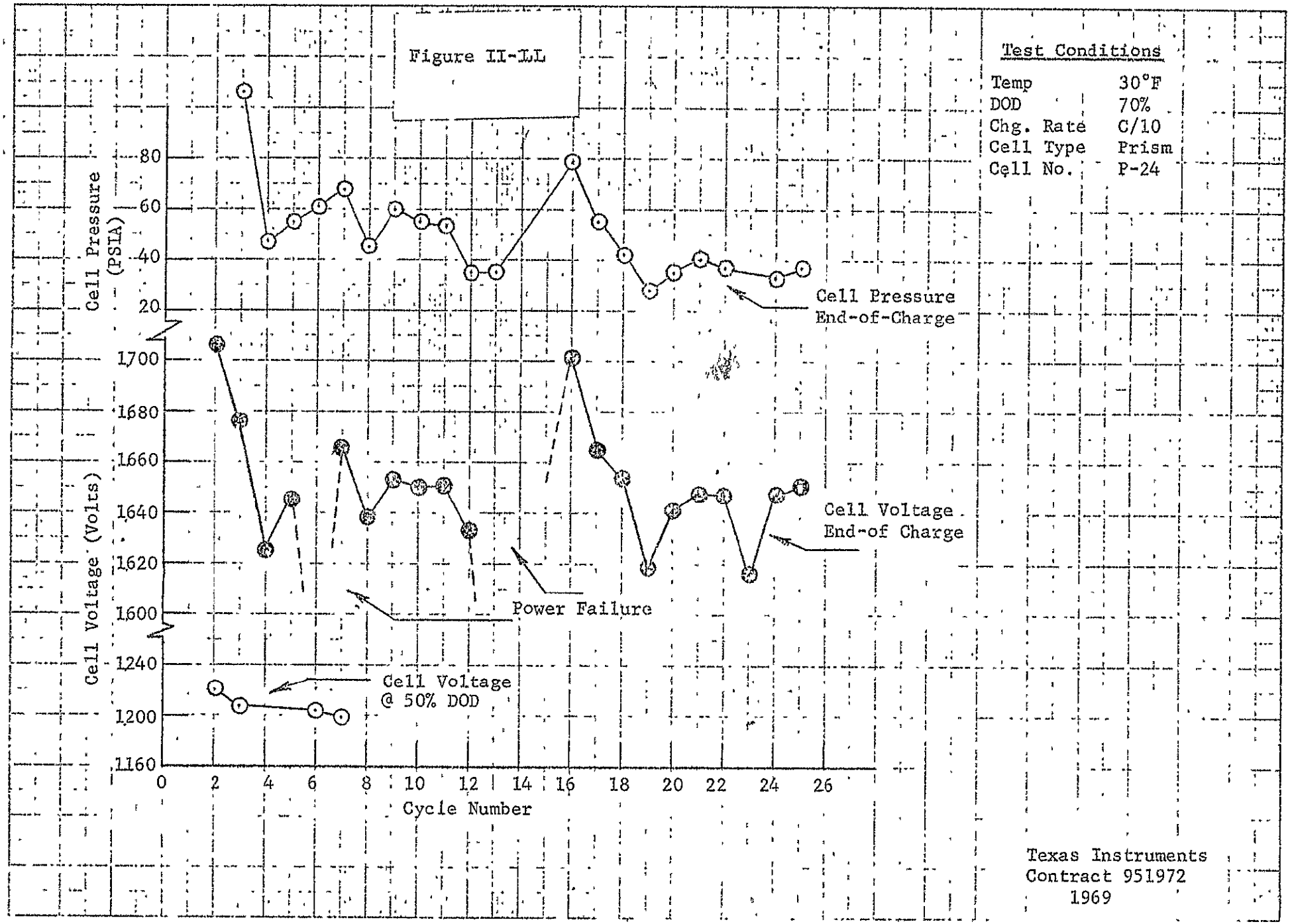
Figure II-LL
Test Conditions
Temp 30°F
DOD 70%
Chg. Rate C/10
Cell Type Prism
Cell No. P-24
Cell Pressure (PSIA)
80
60
40
20
Cell Voltage (Volts)
1700
1680
1660
1640
1620
1600
1240
1200
1160
0 2 4 6 8 10 12 14 16 18 20 22 24 26
Cycle Number
Cell Pressure End-of-Charge
Cell Voltage End-of Charge
Power Failure
Cell Voltage @ 50% DOD
Texas Instruments
Contract 951972
1969

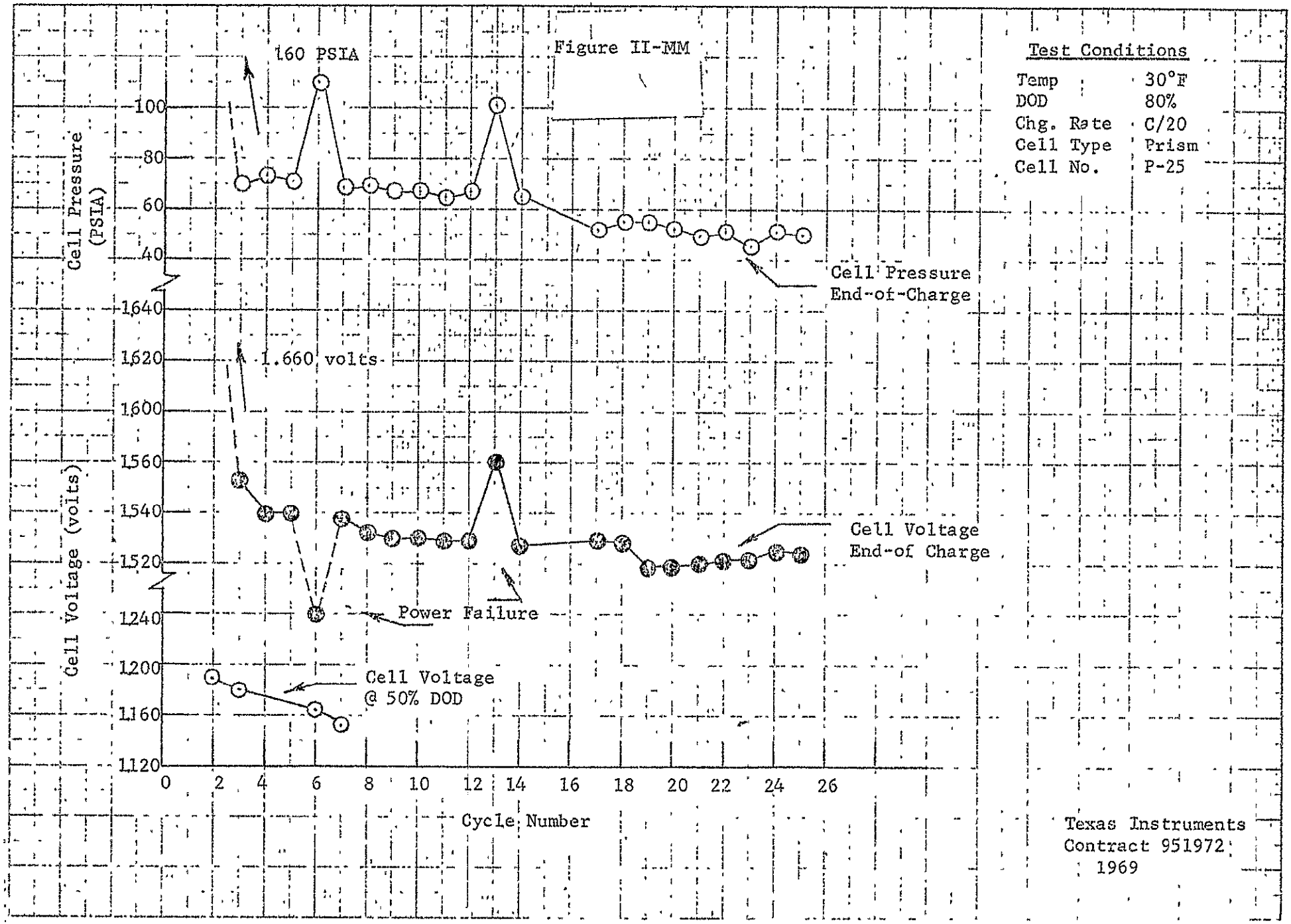

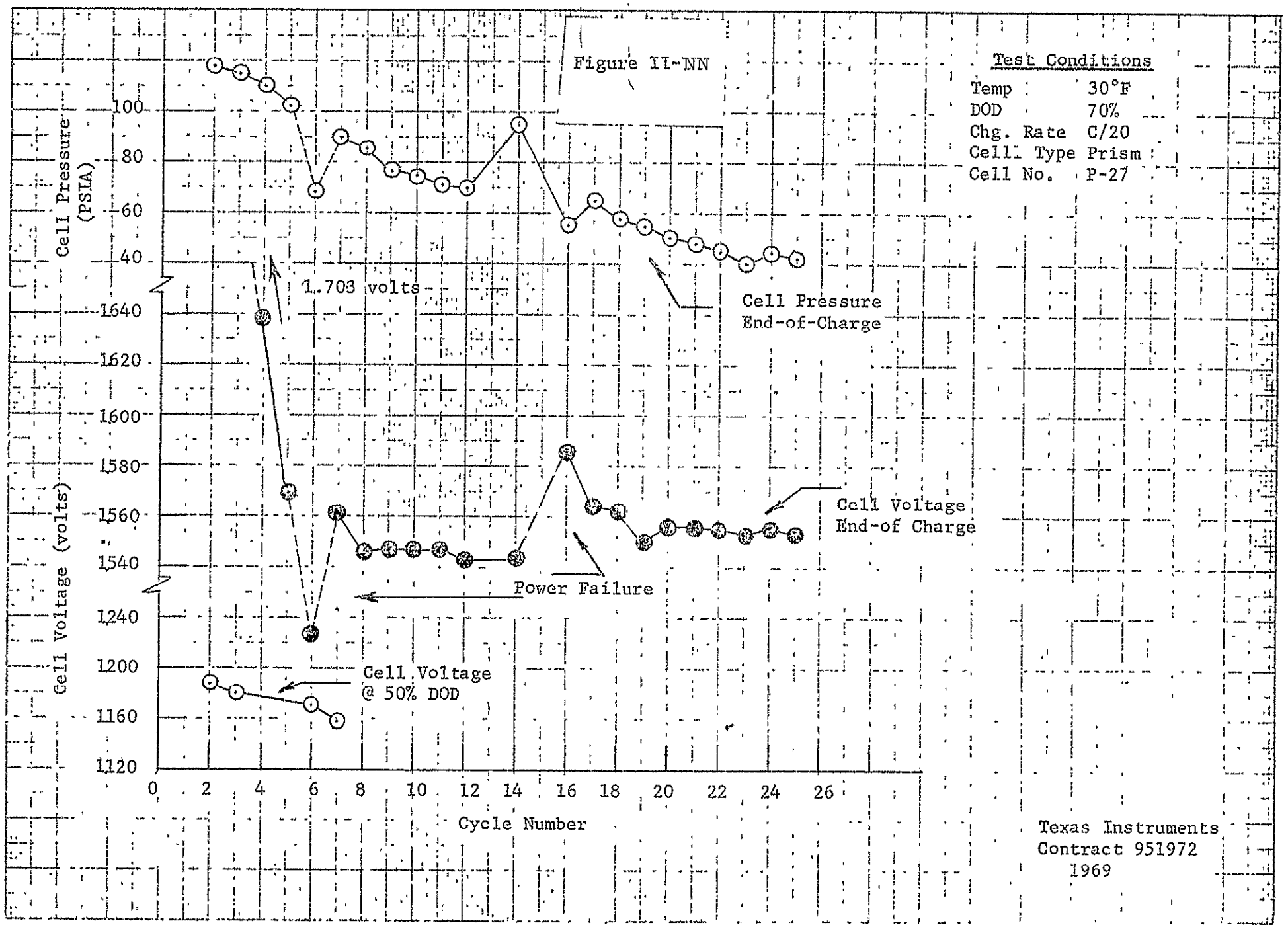
Figure II-NN
Test Conditions
Temp 30°F
DOD 70%
Chg. Rate C/20
Cell Type Prism
Cell No. P-27
Cell Pressure (PSIA)
Cell Voltage (volts)
1.703 volts
Cell Pressure End-of-Charge
Cell Voltage End-of Charge
Power Failure
Cell Voltage @ 50% DOD
Cycle Number
Texas Instruments
Contract 951972
1969

Figure II-00

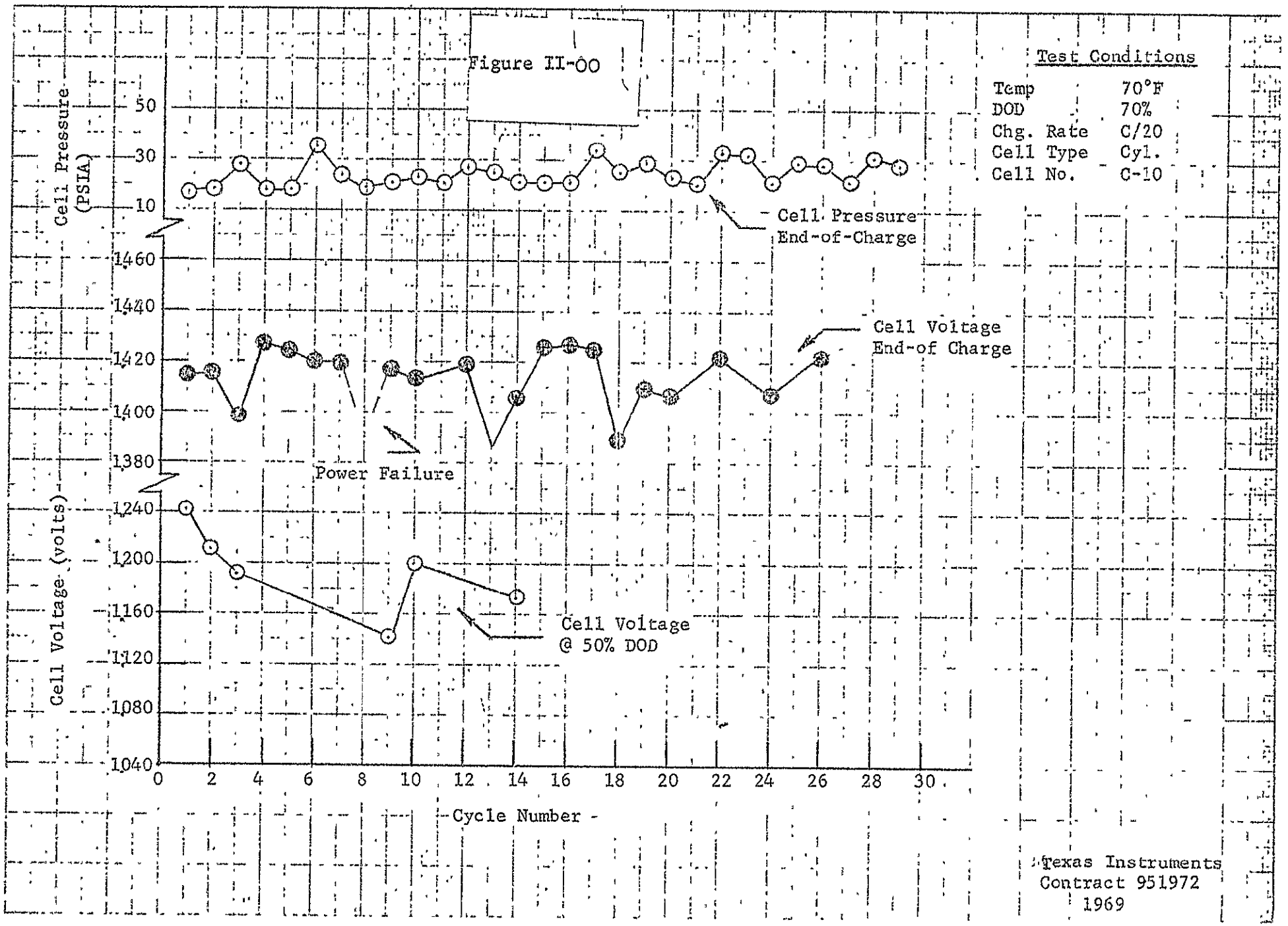
Test Conditions
Temp 70°F
DOD 70%
Chg. Rate C/20
Cell Type Cyl.
Cell No. C-10
Cell Pressure (PSIA)
50
30
10
Cell Pressure End-of-Charge
1460
1440
1420
1400
1380
Cell Voltage End-of Charge
Power Failure
Cell Voltage (volts)
1240
1200
1160
1120
1080
1040
Cell Voltage @ 50% DOD
0 2 4 6 8 10 12 14 16 18 20 22 24 26 28 30
Cycle Number
Texas Instruments
Contract 951972
1969

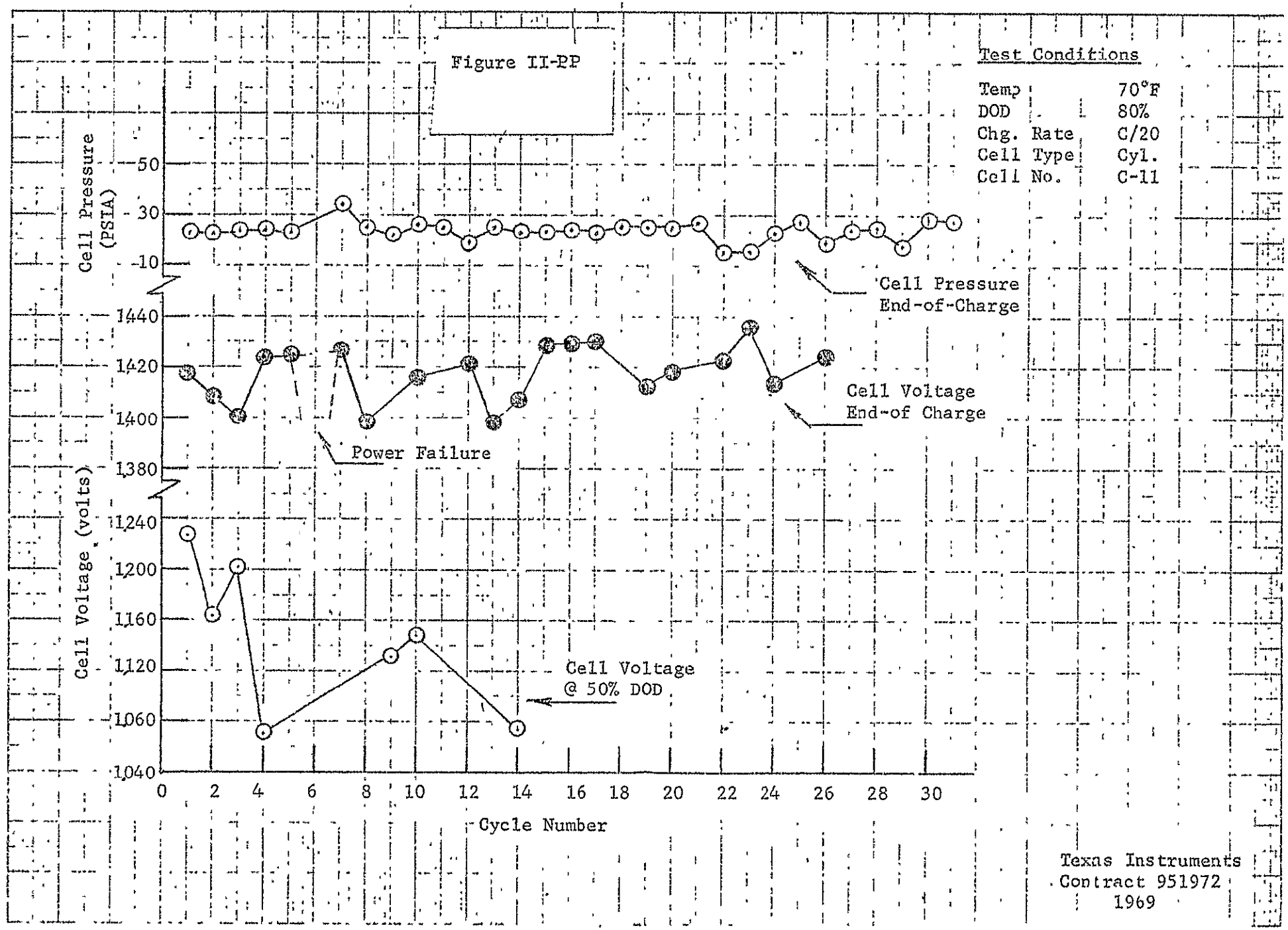
Figure II-PP
Test Conditions
Temp 70°F
DOD 80%
Chg. Rate C/20
Cell Type Cyl.
Cell No. C-11
Cell Pressure (PSIA)
50
30
-10
Cell Pressure End-of-Charge
Cell Voltage (volts)
1440
1420
1400
1380
1240
1200
1160
1120
1060
1040
Cell Voltage End-of Charge
Power Failure
Cell Voltage @ 50% DOD
0 2 4 6 8 10 12 14 16 18 20 22 24 26 28 30
Cycle Number
Texas Instruments Contract 951972 1969

Figure II-QQ

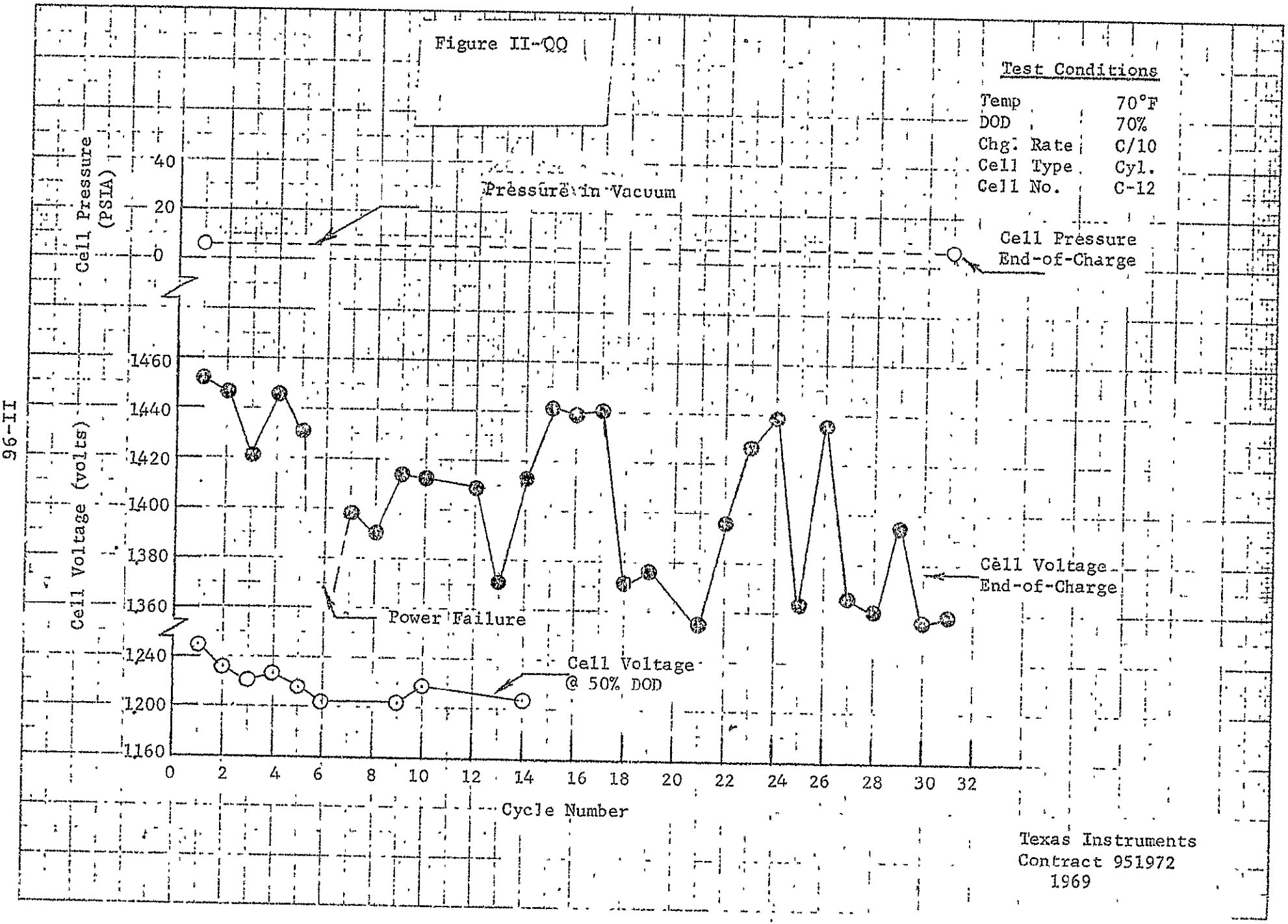
Test Conditions
Temp 70°F
DOD 70%
Chg. Rate C/10
Cell Type Cyl.
Cell No. C-12
Cell Pressure (PSIA)
40
20
0
Pressure in Vacuum
Cell Pressure End-of-Charge
Cell Voltage (volts)
1460
1440
1420
1400
1380
1360
1240
1200
1160
Power Failure
Cell Voltage @ 50% DOD
Cell Voltage End-of-Charge
0 2 4 6 8 10 12 14 16 18 20 22 24 26 28 30 32
Cycle Number
Texas Instruments
Contract 951972
1969

Figure II-1RR

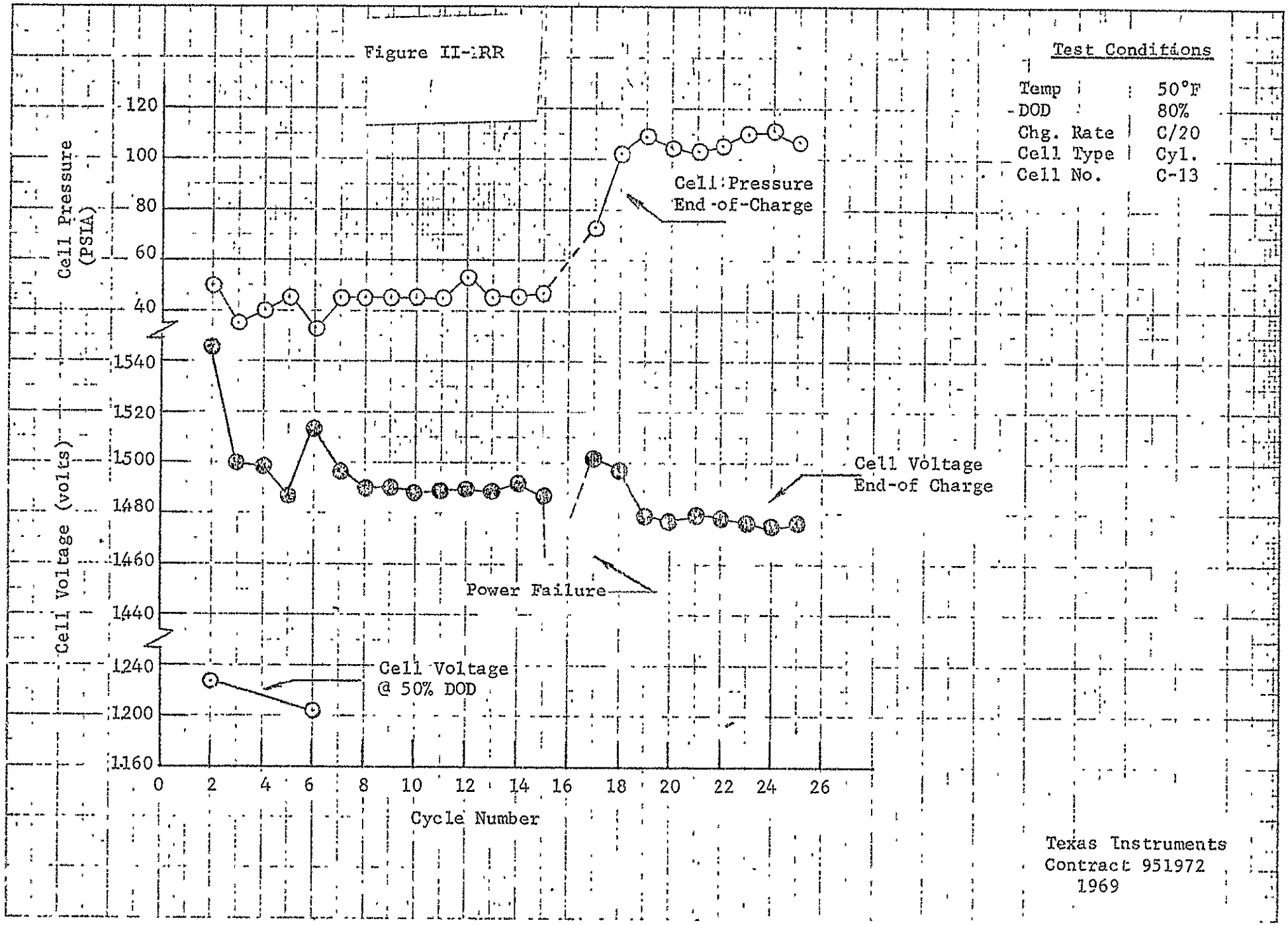

Figure II-SS

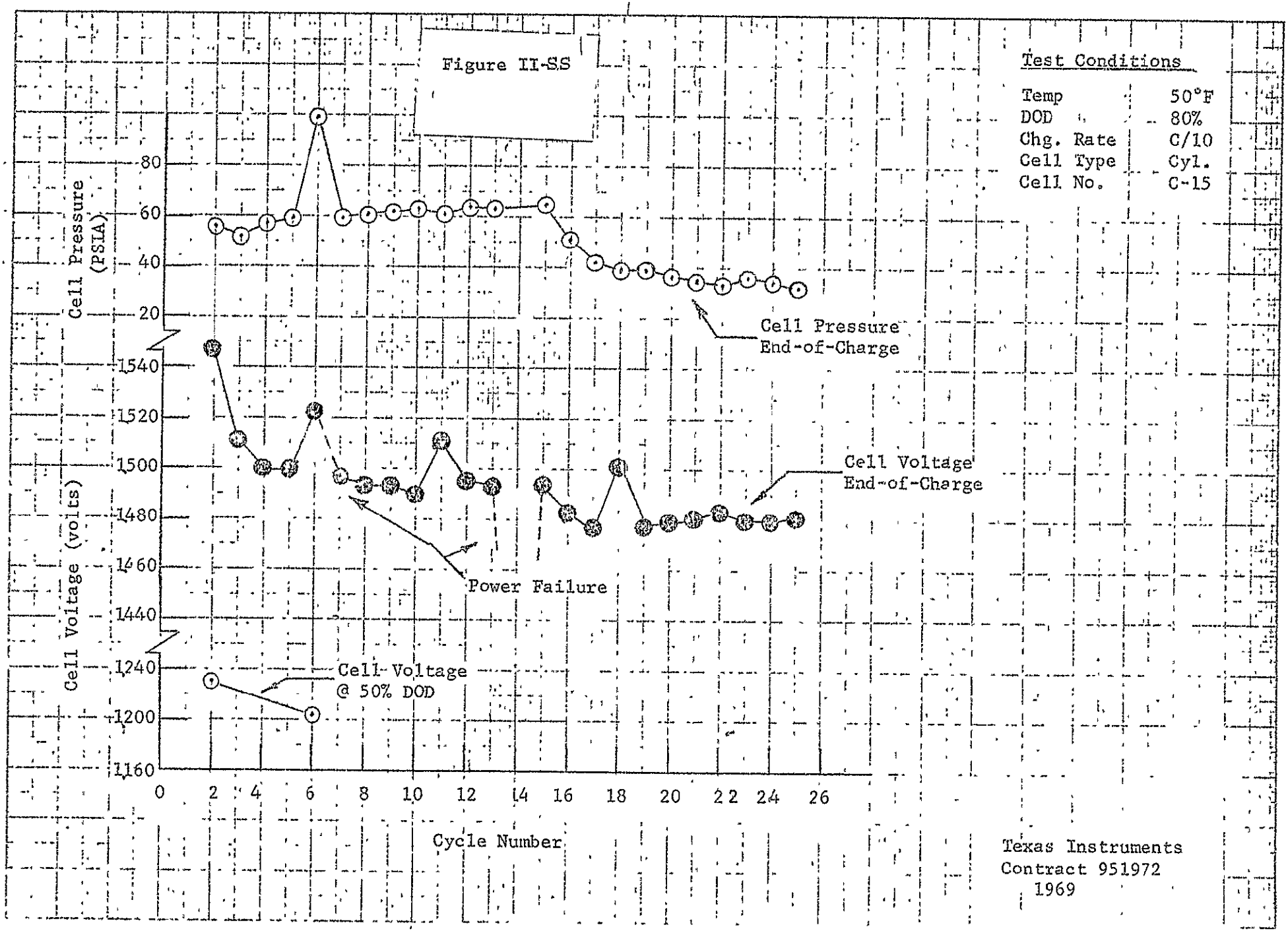
Test Conditions
Temp 50°F
DOD 80%
Chg. Rate C/10
Cell Type Cyl.
Cell No. C-15
Cell Pressure (PSIA)
80
60
40
20
Cell Pressure End-of-Charge
Cell Voltage (volts)
1540
1520
1500
1480
1460
1440
1240
1200
1160
Cell Voltage End-of-Charge
Power Failure
Cell Voltage @ 50% DOD
0 2 4 6 8 10 12 14 16 18 20 22 24 26
Cycle Number
Texas Instruments
Contract 951972
1969

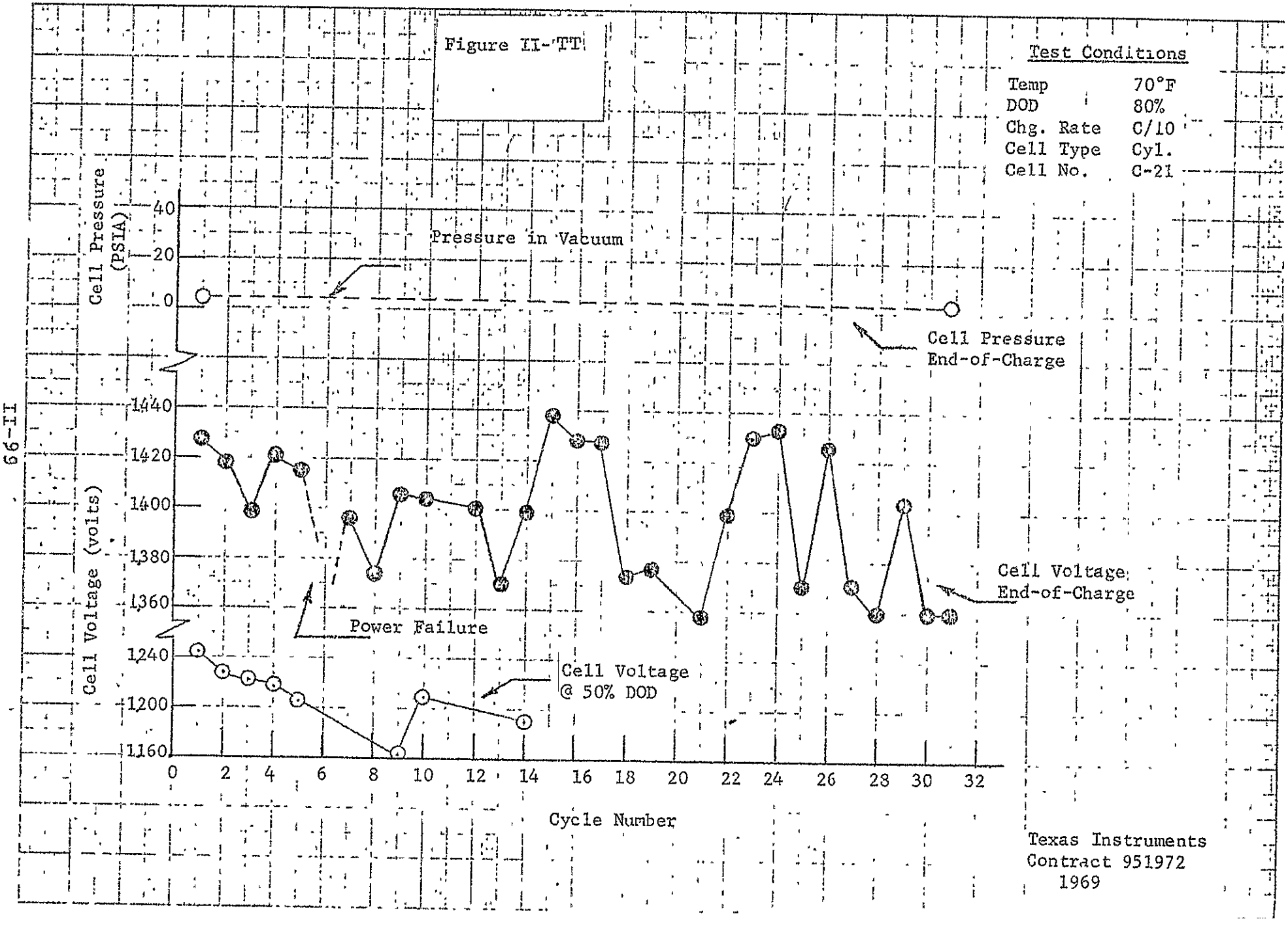
Figure II-TT
Test Conditions
Temp 70°F
DOD 80%
Chg. Rate C/10
Cell Type Cyl.
Cell No. C-21
Cell Pressure (PSIA)
40
20
0
Pressure in Vacuum
Cell Pressure End-of-Charge
1440
1420
1400
1380
1360
Cell Voltage (volts)
Cell Voltage End-of-Charge
Power Failure
1240
1200
1160
Cell Voltage @ 50% DOD
0 2 4 6 8 10 12 14 16 18 20 22 24 26 28 30 32
Cycle Number
Texas Instruments
Contract 951972
1969

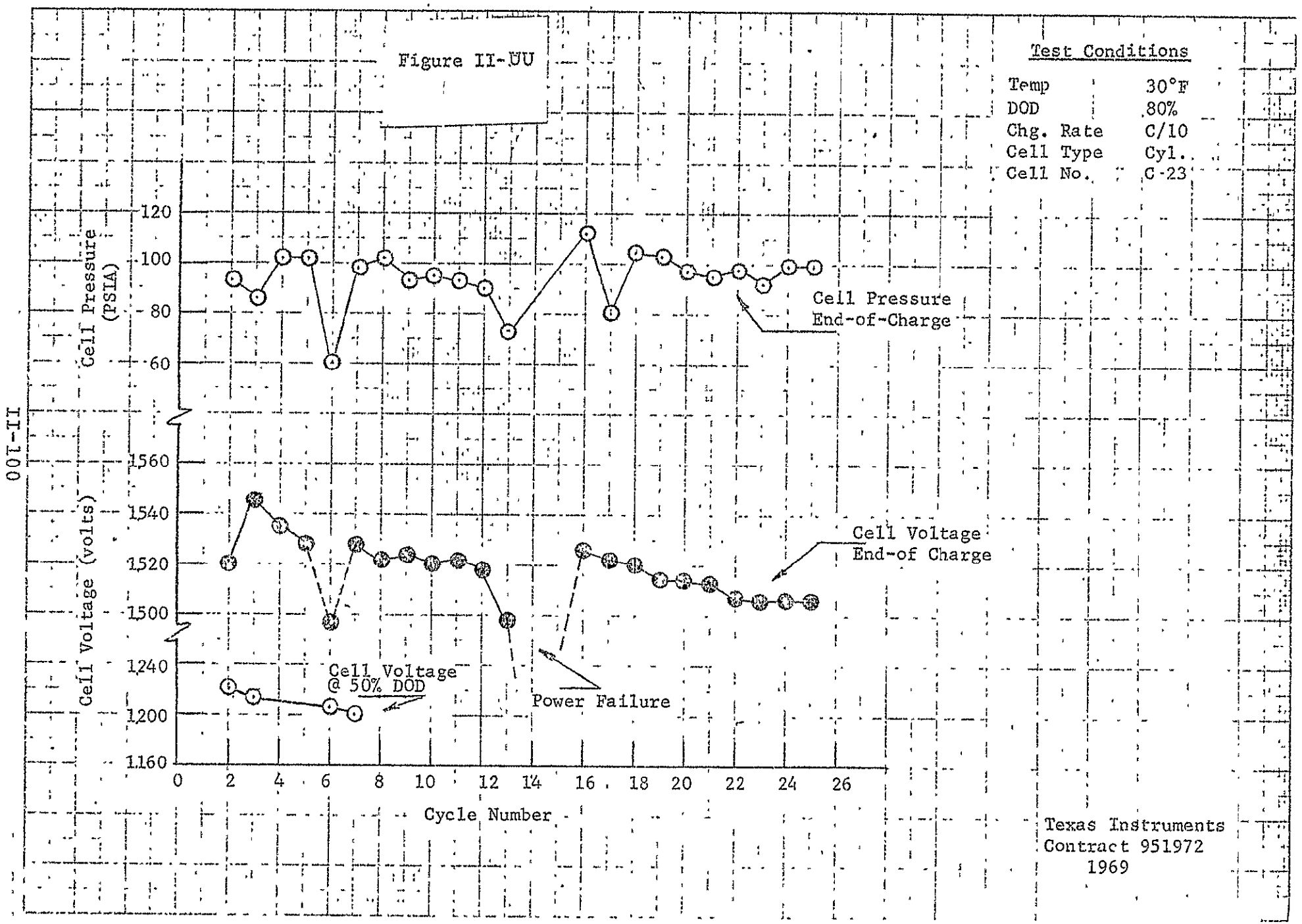
Figure II-UU
Test Conditions
Temp 30°F
DOD 80%
Chg. Rate C/10
Cell Type Cyl.
Cell No. C-23
Cell Pressure (PSIA)
120
100
80
60
Cell Pressure End-of-Charge
Cell Voltage (volts)
1560
1540
1520
1500
1240
1200
1160
Cell Voltage End-of Charge
Cell Voltage @ 50% DOD
Power Failure
0 2 4 6 8 10 12 14 16 18 20 22 24 26
Cycle Number
Texas Instruments
Contract 951972
1969

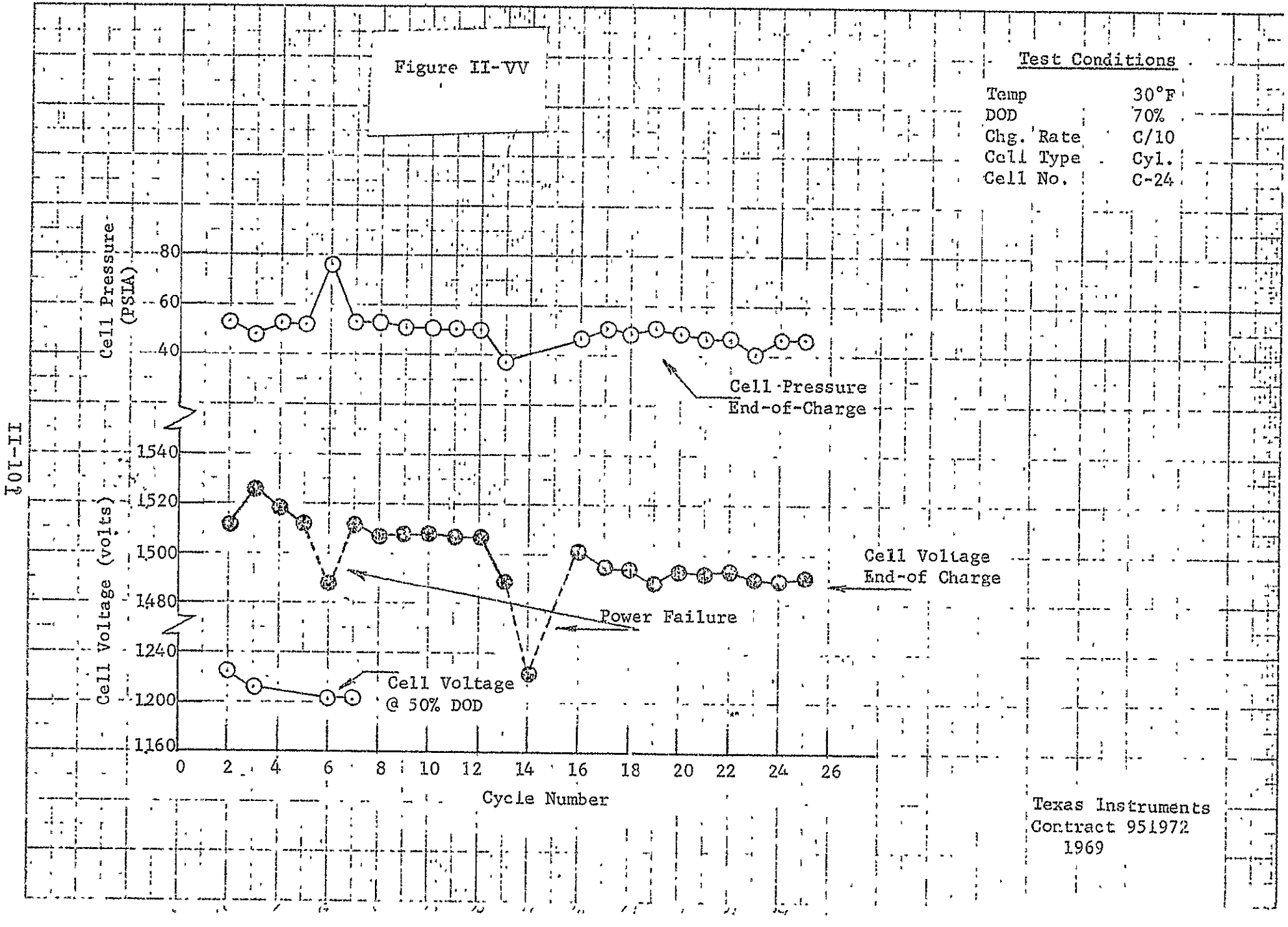
Figure II-VV
Test Conditions
Temp 30°F
DOD 70%
Chg. Rate C/10
Cell Type Cyl.
Cell No. C-24
Cell Pressure (PSIA)
80
60
40
Cell Pressure End-of-Charge
Cell Voltage (volts)
1540
1520
1500
1480
1240
1200
1160
Cell Voltage End-of Charge
Power Failure
Cell Voltage @ 50% DOD
0 2 4 6 8 10 12 14 16 18 20 22 24 26
Cycle Number
Texas Instruments
Contract 951972
1969

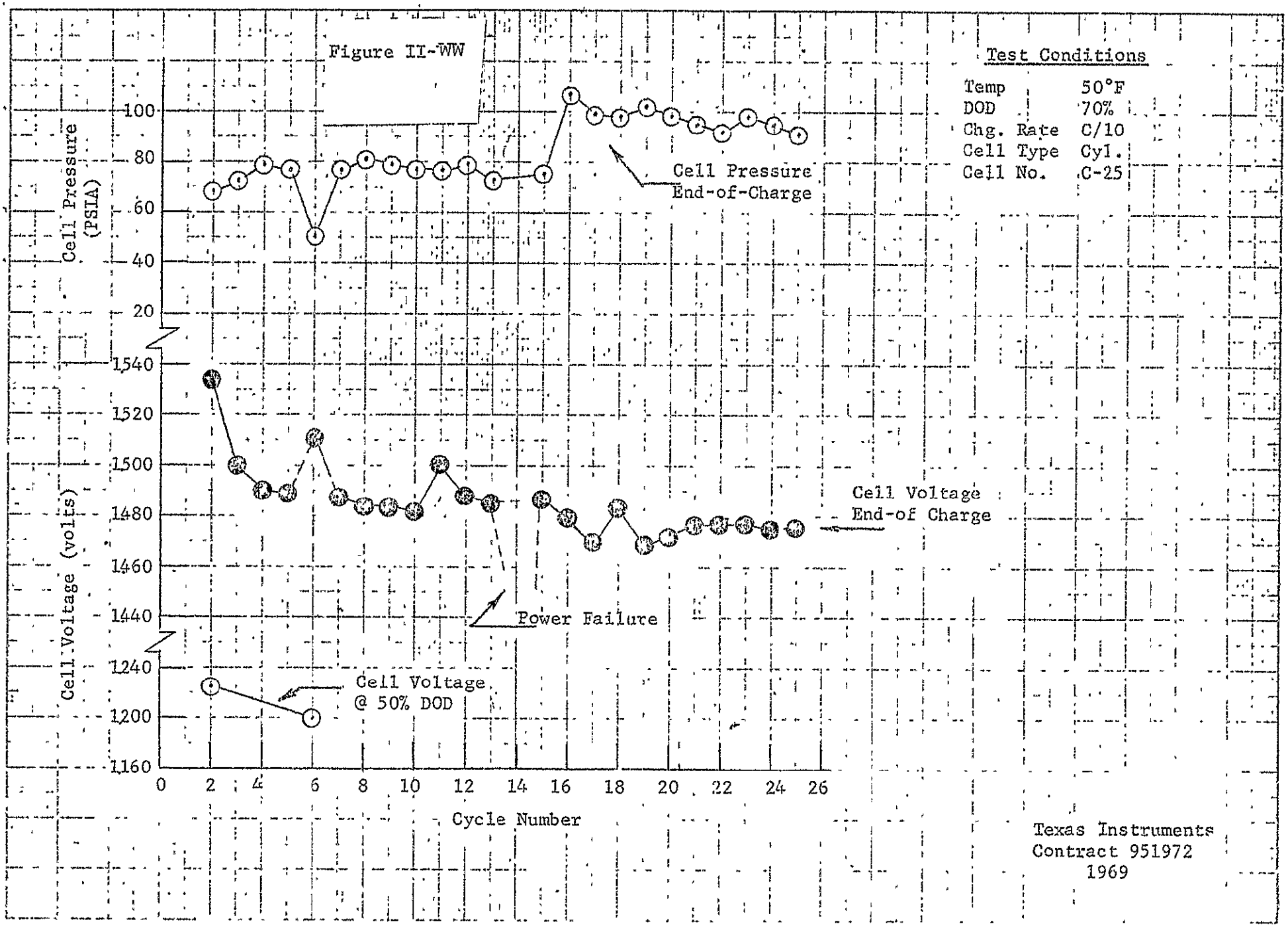
Figure II-WW
Test Conditions
Temp 50°F
DOD 70%
Chg. Rate C/10
Cell Type Cyl.
Cell No. C-25
Cell Pressure (PSIA)
100
80
60
40
20
Cell Pressure End-of-Charge
Cell Voltage (volts)
1540
1520
1500
1480
1460
1440
1240
1200
1160
Cell Voltage End-of Charge
Power Failure
Cell Voltage @ 50% DOD
0 2 4 6 8 10 12 14 16 18 20 22 24 26
Cycle Number
Texas Instruments
Contract 951972
1969

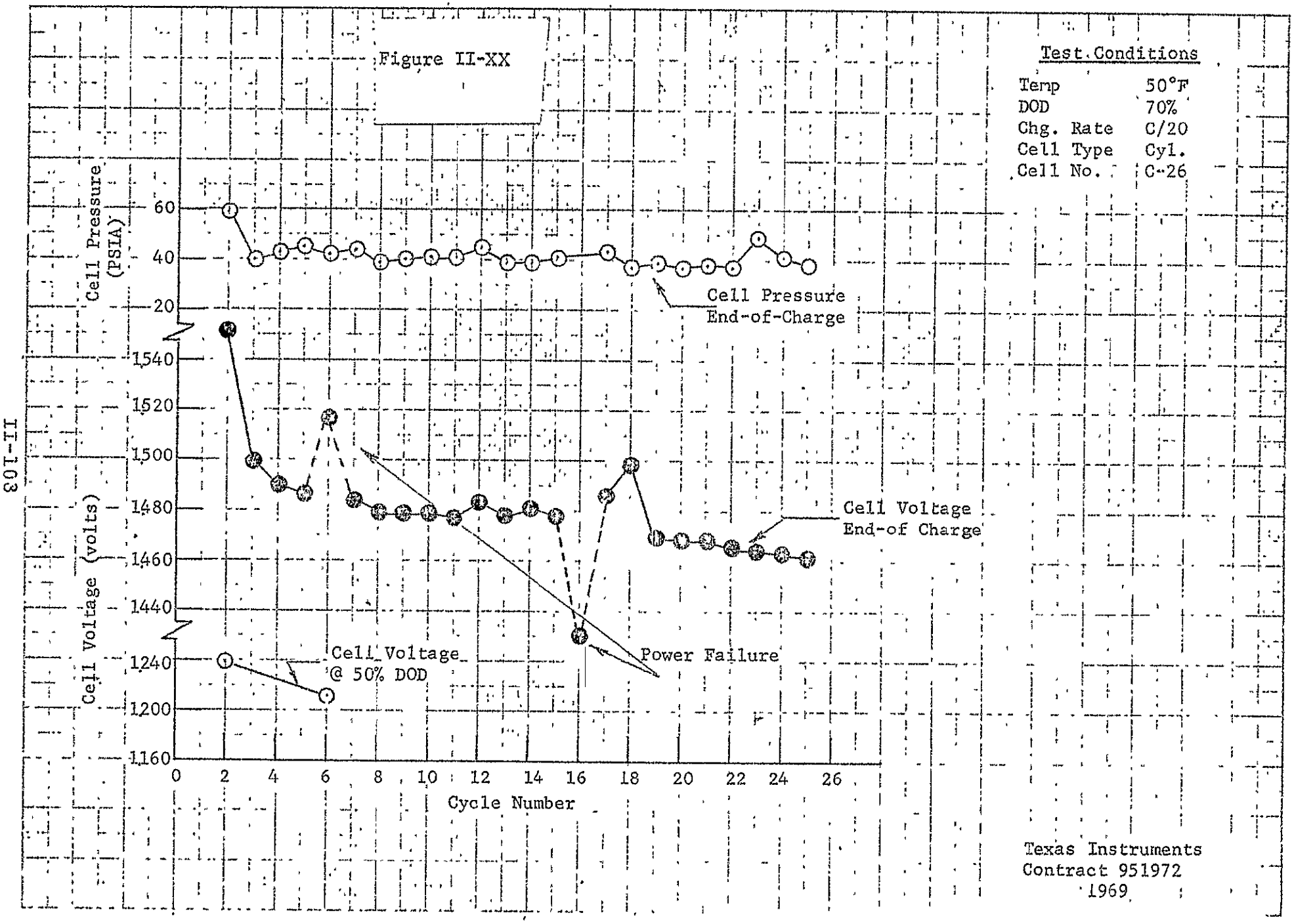
Figure II-XX
Test Conditions
Temp 50°F
DOD 70%
Chg. Rate C/20
Cell Type Cyl.
Cell No. C-26
Cell Pressure (PSIA)
60
40
20
Cell Pressure End-of-Charge
Cell Voltage (volts)
1540
1520
1500
1480
1460
1440
1240
1200
1160
Cell Voltage End-of Charge
Cell Voltage @ 50% DOD
Power Failure
0 2 4 6 8 10 12 14 16 18 20 22 24 26
Cycle Number
Texas Instruments
Contract 951972
1969

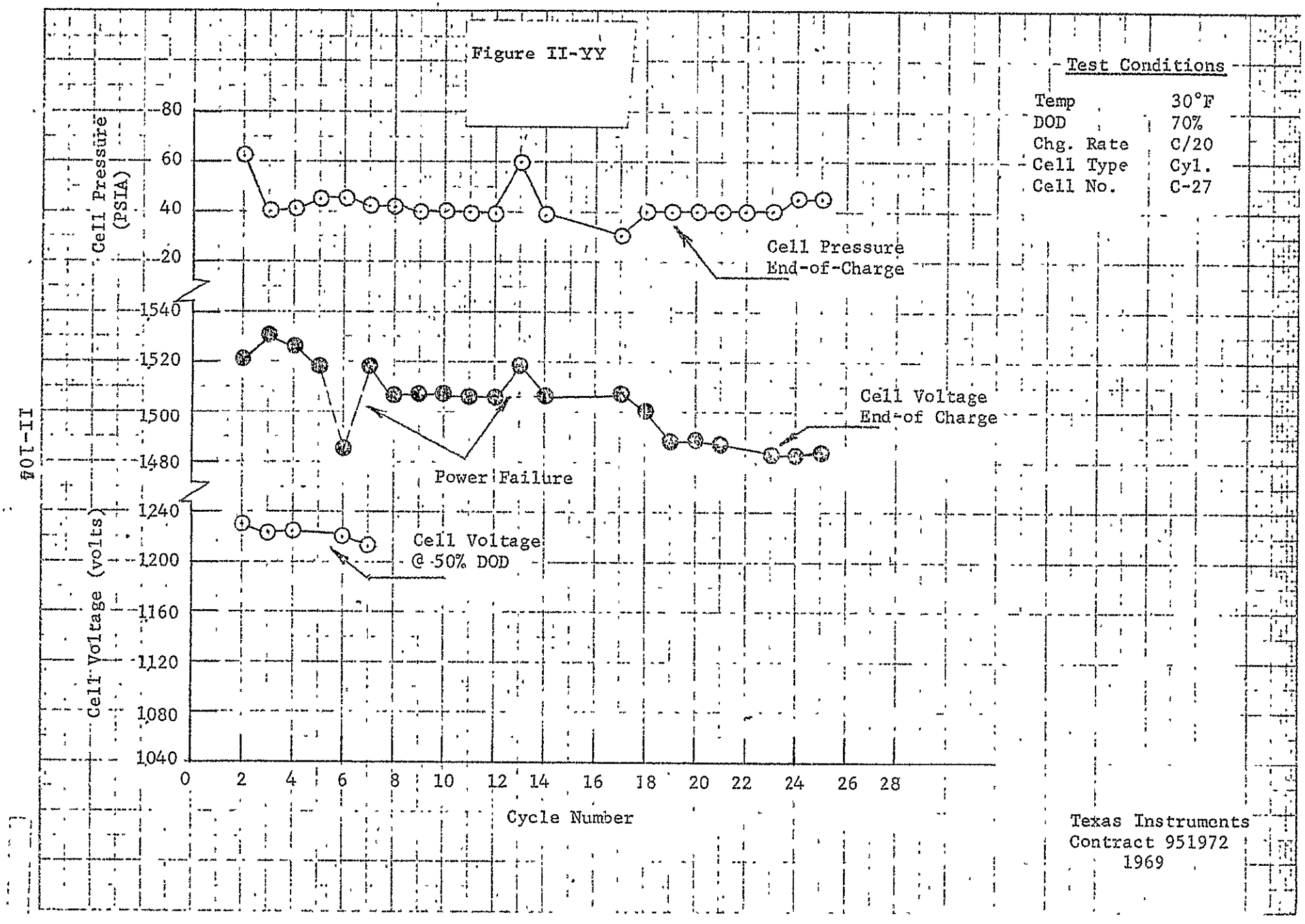
Figure II-YY
Test Conditions
Temp 30°F
DOD 70%
Chg. Rate C/20
Cell Type Cyl.
Cell No. C-27
Cell Pressure (PSIA)
80
60
40
20
Cell Pressure End-of-Charge
1540
1520
1500
1480
Cell Voltage End-of Charge
Power Failure
Cell Voltage (volts)
1240
1200
1160
1120
1080
1040
Cell Voltage @ 50% DOD
0 2 4 6 8 10 12 14 16 18 20 22 24 26 28
Cycle Number
Texas Instruments
Contract 951972
1969

Figure II-ZZ

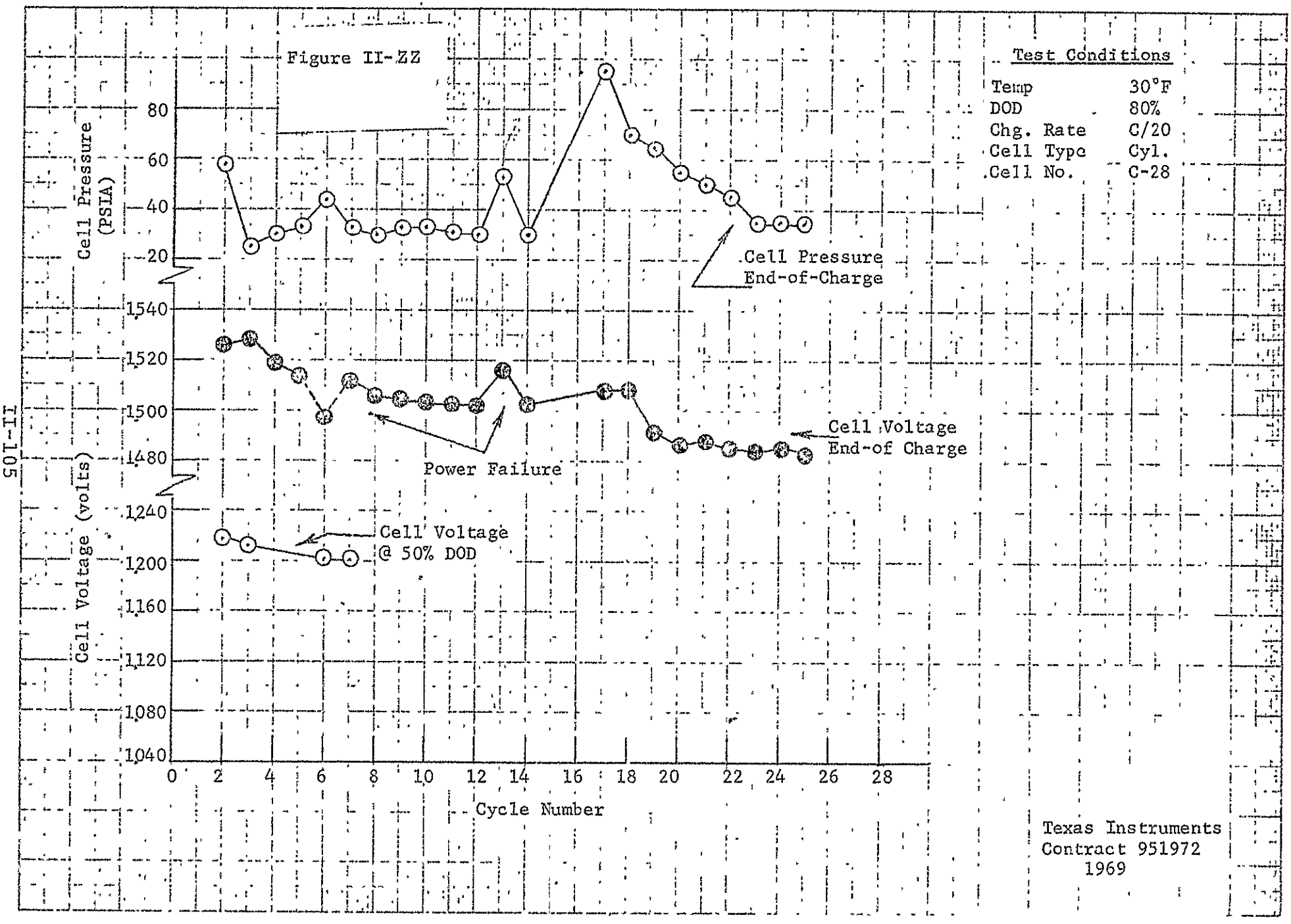
Test Conditions
Temp 30°F
DOD 80%
Chg. Rate C/20
Cell Type Cyl.
Cell No. C-28
Cell Pressure End-of-Charge
Cell Voltage End-of Charge
Power Failure
Cell Voltage @ 50% DOD
Cell Pressure (PSIA)
Cell Voltage (volts)
Cycle Number
80
60
40
20
1540
1520
1500
1480
1240
1200
1160
1120
1080
1040
0 2 4 6 8 10 12 14 16 18 20 22 24 26 28
Texas Instruments
Contract 951972
1969

TEXAS INSTRUMENTS
INCORPORATED
METALLURGICAL MATERIALS DIVISION
ATTLEBORO, MASSACHUSETTS U.S A

5-MMD-19528 2/69

U.S. DEPARTMENT OF COMMERCE - NATIONAL TECHNICAL INFORMATION SERVICE

ARCHIVE FILE CHARGE OUT

N70-34013

ACCESSION NUMBER

DATE OUT	WITHDRAWN BY SIGNATURE	DATE RETURNED	DATE OUT	WITHDRAWN BY SIGNATURE	DATE RETURNED	DATE OUT	WITHDRAWN BY SIGNATURE	DATE RETURNED
3-4	KENYON, NASA	3/15						

FORM NTIS-75 (10-70)

USCOMM-DC 40413-P71

CASE FILE DOCUMENT WITHDRAWAL

DOCUMENT NUMBER

DATE OUT	WITHDRAWN BY SIGNATURE	DATE RETURNED	DATE OUT	WITHDRAWN BY SIGNATURE	DATE RETURNED	DATE OUT	WITHDRAWN BY SIGNATURE	DATE RETURNED

USCOMM-DC 40413-P71